IOWA STATE UNIVERSITY
Digital Repository

Graduate Theses and Dissertations | Graduate College

2016

Modification of flow structures associated with broadband trailing edge noise

Hephzibah Clemons
Iowa State University

Follow this and additional works at: http://lib.dr.iastate.edu/etd

Part of the Aerospace Engineering Commons

Recommended Citation
Clemons, Hephzibah, "Modification of flow structures associated with broadband trailing edge noise" (2016). *Graduate Theses and Dissertations*. 15116.
http://lib.dr.iastate.edu/etd/15116

This Dissertation is brought to you for free and open access by the Graduate College at Iowa State University Digital Repository. It has been accepted for inclusion in Graduate Theses and Dissertations by an authorized administrator of Iowa State University Digital Repository. For more information, please contact digirep@iastate.edu.

المنارة للاستشارات

www.manaraa.com

Modification of flow structures associated with broadband trailing edge noise

by

Hephzibah Clemons

A dissertation submitted to the graduate faculty

in partial fulfillment of the requirements for the degree of

DOCTOR OF PHILOSOPHY

Major: Aerospace Engineering

Program of Study Committee:
Richard Wlezien, Major Professor
Alric Paul Rothmayer
Hui Hu
Anupam Sharma
Sivalingam Sritharan

Iowa State University

Ames, Iowa

2016

Copyright ©Hephzibah Clemons, 2016. All rights reserved.

المنارة للاستشارات

www.manaraa.com

TABLE OF CONTENTS

Page

LIST OF FIGURES iv

LIST OF TABLES x

NOMENCLATURE xi

ACKNOWLEDGMENTS xiv

ABSTRACT xv

CHAPTER 1 INTRODUCTION 1

1.1 Background 2
1.1.1 Trailing edge noise 2
1.1.2 Trailing edge noise reduction 6
1.1.3 Flow instability 9
1.2 Objectives 11

CHAPTER 2 EXPERIMENT DESCRIPTION 12

2.1 Coordinate system 12
2.2 Hardware description 14
2.2.1 Airfoil model 14
2.2.2 Trailing edge modifiers 15
2.2.3 Low turbulence wind tunnel 20
2.2.4 Linear traverse system 21
2.2.5 Instrumentation 23
2.2.6 Probe vibration 25
2.3 Hot-wire measurements 26
2.3.1 Calibration procedure 26
2.3.2 Boundary layer profile measurement 29
2.3.3 Two-point velocity measurement 30
2.4 Data analysis 34
2.5 Turbulent boundary layer development 36

CHAPTER 3 RESULTS 41

3.1 Turbulent boundary layer near the trailing edge at $\alpha = 0^{o}$ 41
3.1.1 Spanwise correlation and coherence of structures 41

المنارة للاستشارات
www.manaraa.com

3.1.2 Contour correlation data with respect to structures in O_t and I_t 44
3.1.3 Streamwise correlation of structures in O_t and I_t 47
3.2 Reference trailing edge configuration at $\alpha = 5^o$ 49
3.2.1 Spanwise correlation of structures in the turbulent wake near the trailing edge 50
3.2.2 Contour correlation data with respect to structures in O_t, I_t and I_b 52
3.2.3 Streamwise correlation of structures in O_t, I_t and I_b 56
3.3 Effect of serrations on boundary layer development and flow structures near the trailing edge 57
3.4 Effect of trailing edge thickness on flow structures 63
3.5 Effect of length of a serrated trailing edge on flow structures 67
3.6 Effect of width of a serrated trailing edge on flow structures 76

CHAPTER 4 SUMMARY AND CONCLUSIONS 86

4.1 Summary 86
4.2 Conclusions 92
4.2 Future work 93

REFERENCES 94

APPENDIX A FIGURES 99

APPENDIX B ERROR ANALYSIS 108

المنارة للاستشارات
www.manaraa.com

LIST OF FIGURES

		Page
Figure 1(a)	Illustration of trailing edge noise and its directivity pattern	3
Figure 1(b)	Turbulent flow over an airfoil with a serrated trailing edge. Picture taken from Howe ("Aerodynamic noise of")	6
Figure 2	Coordinate system.....	13
Figure 3	Airfoil model mounted in the test section.....	14
Figure 4	Blunt thickness modifier	15
Figure 5	Flat extended TE modifier F1 attached to Sh.....	16
Figure 6(a)	Sketch of serrated TE modifier attached to Sh	17
Figure 6(b)	Serrated TE as mounted in the test section	17
Figure 7	Effective serration	17
Figure 8	Dimensions of serrated TE modifiers.....	18
Figure 9	Low turbulence wind tunnel	21
Figure 10	Linear traverse system mounted in the test section	23
Figure 11	Accelerometer mounted on probe holder	25
Figure 12	Minimization of probe vibration	26
Figure 13	Calibration of hot-wire	29
Figure 14	Minimum separation between S and T.....	32
Figure 15	Derivatives of mean velocity with respect to voltage	34
Figure 16	Optimization of Reynold's number at x/C = 0.5	37
Figure 17	Turbulent boundary layer development over the chord at Re of 850000 and $\alpha = 0°$ with BL tripping.....	38
Figure 18(a)	Turbulent boundary layer development in δ^*, θ	39

المنارة للاستشارات
www.manaraa.com

Figure 18(b) Turbulent boundary layer development in wall units 39

Figure 19 Turbulent wake development at Re of 850000 and $\alpha = 0°$ with BL tripping..... 40

Figure 20 Three regions of interest in the turbulent boundary layer from spanwise correlation data at x/C = 0.986. $\alpha = 0°$ 43

Figure 21 Three regions of interest shown in the TBL profile at x/C = 0.986, 1. $\alpha = 0°$..... 43

Figure 22 Spanwise coherence of structures in O_t and I_t at x/C = 0.986. $\alpha = 0°$..... 44

Figure 23(a) Evolution of structures in O_t along the spanwise plane. S is located at x/C = 0.986 and $\Delta t = 0.00016$ s. $\alpha = 0°$ 45

Figure 23(b) Evolution of structures in I_t along the spanwise plane. S is located at x/C = 0.986 and $\Delta t = 0.00016$ s. $\alpha = 0°$ 45

Figure 23(c) Evolution of structures in O_t along the streamwise plane. S is located at x/C = 0.986 and $\Delta t = 0.00016$ s. $\alpha = 0°$ 46

Figure 23(d) Evolution of structures in I_t along the streamwise plane. S is located at x/C = 0.986 and $\Delta t = 0.00016$ s. $\alpha = 0°$ 46

Figure 24(a) Streamwise correlation of structures in I_t. S is at x/C = 0.986. $\alpha = 0°$..... 48

Figure 24(b) Streamwise correlation of structures in O_t. S is at x/C = 0.986. $\alpha = 0°$..... 48

Figure 24(c) XT plot with respect to structures in O_t. S is at x/C = 0.986. $\alpha = 0°$..... 48

Figure 25(a) Wake profiles for Sh and B at x/C = 1, $\alpha = 5°$ 50

Figure 25(b) Normalized power spectral densities at I_b (pressure side) and I_t (suction side) for Sh and B at x/C = 1, $\alpha = 5°$..... 50

Figure 26 Regions of interest in the turbulent boundary layer (wake) from spanwise correlation data at x/C = 1, $\alpha = 5°$ 50

Figure 27(a) Evolution of structures in O_t along the spanwise plane. S is located at x/C = 1 and $\Delta t = 0.00016$ s. $\alpha = 5°$ 53

المنارة للاستشارات

www.manaraa.com

Figure 27(b) Evolution of structures in I_t along the spanwise plane. S is located at x/C = 1 and Δt = 0.00016 s. α = 5° 53

Figure 27(c) Evolution of structures in I_b along the spanwise plane. S is located at x/C = 1 and Δt = 0.00016 s. α = 5° 54

Figure 27(d) Evolution of structures in O_t along the streamwise plane. S is located at x/C = 1 and Δt = 0.00016 s. α = 5° 54

Figure 27(e) Evolution of structures in I_t along the streamwise plane. S is located at x/C = 1 and Δt = 0.00016 s. α = 5° 55

Figure 27(f) Evolution of structures in I_b along the streamwise plane. S is located at x/C = 1 and Δt = 0.00016 s. α = 5° 55

Figure 28 Streamwise correlation of structures in O_t, I_t and I_b. S is at x/C = 1. α = 5° 56

Figure 29 Turbulent boundary layer and wake development near the serration L2W4 58

Figure 30(a) Evolution of structures in O_t along the spanwise plane. S is located at the root and Δt = 0.00016 s. 60

Figure 30(b) Evolution of structures in I_t along the spanwise plane. S is located at the root and Δt = 0.00016 s. 60

Figure 30(c) Evolution of structures in O_t along the streamwise plane. S is located at the root and Δt = 0.00016 s. 61

Figure 30(d) Evolution of structures in I_t along the streamwise plane. S is located at the root and Δt = 0.00016 s. 61

Figure 31(a) Evolution of structures in I_t along the spanwise plane. S is located at r_s-tip and Δt = 0.00016 s. 62

Figure 31(b) Evolution of structures in I_t along the streamwise plane. S is located at r_s-tip and Δt = 0.00016 s. 62

Figure 32 Wake profiles measured at flat trailing edges of various thicknesses 64

Figure 33 Evolution of structures in I_t near the trailing edge in the streamwise direction (F1 and F2) 64

المنارة للاستشارات

www.manaraa.com

Figure 34 Effect of trailing edge thickness on structures in I_t near the trailing edge 66

Figure 35 Spanwise correlation of structures in I_t and O_t at trailing edges of flat edged configurations..... 67

Figure 36 Wake profiles measured at r_s-tip of serrations of different lengths..... 68

Figure 37(a) Effect of length of serrations on convective speeds of structures in I_t near the root 69

Figure 37(b) Effect of length of serrations on convective speeds of structures in I_t near r_s-tip..... 70

Figure 37(c) Effect of length of serrations on convective speeds of structures in I_t near the tip..... 70

Figure 38 Difference in convective speeds of structures in I_t at r_s-tip and tip positions for serrations of different lengths 71

Figure 39 Evolution of structures in the streamwise direction in I_t near the tip, r_s-tip of L3W1 and trailing edge of B 72

Figure 40 Evolution of structures in the spanwise direction in O_t near r_s-tip of L1W2, L3W1 and trailing edge of B..... 73

Figure 41(a) Spanwise correlation and half width of structures in I_t and O_t at the root (varying 2h) 74

Figure 41(b) Spanwise correlation and half width of structures in I_t and O_t at the r_s-tip position (varying 2h)..... 74

Figure 41(c) Spanwise correlation and half width of structures in I_t and O_t at the tip (varying 2h) 75

Figure 42 Wake profiles measured at r_s-tip of serrations of different widths..... 77

Figure 43(a) Effect of width of serrations on convective speeds of structures in I_t near the root 78

Figure 43(b) Effect of width of serrations on convective speeds of structures in I_t near the r_s-tip position..... 78

Figure 43(c) Effect of width of serrations on convective speeds of structures in I_t near the tip..... 79

المنارة للاستشارات

www.manaraa.com

Figure 44 Difference in convective speeds of structures in I_t at r_s-tip and tip positions for serrations of different widths 80

Figure 45(a) Spanwise correlation and half width of structures in I_t and O_t at the root (varying λ) 81

Figure 45(b) Spanwise correlation and half width of structures in I_t and O_t at the r_s-tip position (varying λ) 81

Figure 45(c) Spanwise correlation and half width of structures in I_t and O_t at the tip (varying λ) 82

Figure 46(a) Half width of structures in O_t at the r_s-tip and tip positions respectively 84

Figure 46(b) Difference in convective speeds of structures in I_t at the r_s-tip and tip positions 84

Figure a1 Streamwise correlation of structures in O_t. S is at x/C = 1, Δt = 0.00016 s, α = 0° 99

Figure a2 Streamwise correlation of structures in I_t. S is at x/C = 1, Δt = 0.00016 s, α = 0° 100

Figure a3 Spanwise correlation of structures in O_t and I_t. S is at x/C = 1, Δt = 0.00016 s, α = 0° 101

Figure a4 XT plot of structures in O_t at trailing edge of flat edged configurations 102

Figure a5 XT plot of structures in O_t at r_s-tip of serrations of different lengths 102

Figure a6 XT plot of structures in O_t at r_s-tip, tip of serrations of different lengths 104

Figure a7 XT plot of structures in O_t at r_s-tip of serrations of different widths 103

Figure a8 XT plot of structures in O_t at tip of serrations of different widths 104

Figure a9(a) Boundary layer profiles at root of all serrated TE configurations 104

Figure a9(b) Wake profiles at r_s-tip of all serrated TE configurations 105

المنارة للاستشارات

www.manaraa.com

Figure a9(c) Wake profiles at tip of all serrated TE configurations 105

Figure a10(a) Convective speed of structures in I_t (region 1 and 2) near root for all serrated TE configurations compared with flat TE configurations 106

Figure a10(b) Convective speed of structures in I_t (region 1 and 2) near r_s-tip for all serrated TE configurations compared with flat TE configurations 106

Figure a10(c) Convective speed of structures in I_t (region 1 and 2) near tip for all serrated TE configurations compared with flat TE configurations 106

Figure a11(a) Half width of structures in O_t near root for all serrated TE configurations..... 107

Figure a11(b) Half width of structures in I_t near r_s-tip for all serrated TE configurations..... 107

Figure a11(c) Half width of structures in I_t near tip for all serrated TE configurations..... 107

المنارة للاستشارات

www.manaraa.com

LIST OF TABLES

Page

Table 1 List of TE modifiers 19

المنارة للاستشارات

www.manaraa.com

NOMENCLATURE

BL	boundary layer
TBL	turbulent boundary layer
TE	trailing edge
S, T	stationary and traversing hot-wires respectively
X, Y, Z	global orthogonal coordinate system. Streamwise, normal and span-wise directions respectively
α	angle of attack
x, y, z	variables in (X, Y, Z) respectively
Δx, Δy, Δz	distance between S and T in (X, Y, Z) respectively
y_s	distance from the surface of the airfoil along the y-direction at a given x/C
$\boldsymbol{U}$	unsteady velocity along the x-direction
U	mean velocity along the x-direction
u’	fluctuating component of velocity along the x-direction
u'_{rms}	root mean square of u’
U_∞	free-stream velocity along x-direction
U_c	eddy convective velocity along x-direction
u'_{max}	maximum u’ in the local boundary layer
U_e	Velocity along the x-direction at the edge of the local boundary layer
δ, δ_b	local boundary layer thickness on the suction and pressure side respectively

المنارة للاستشارات
www.manaraa.com

δ^*, δ^*_b	local displacement thickness of the boundary layer on the suction and pressure side respectively
θ	local momentum thickness of the boundary layer
δ, δ_b	suction and pressure side boundary layer thicknesses respectively at the trailing edge of the reference airfoil at α of interest
$\delta_{0.986}$	boundary layer thickness on the suction side of the reference airfoil at x/C = 0.986 at α of interest
δ^*, δ^*_b	suction and pressure side boundary layer displacement thicknesses respectively at the trailing edge at α of interest
C	chord length
M	subsonic Mach number
t	trailing edge thickness
2h	length of a serration from root to tip measured along the x-direction
λ	width of a serration - distance between two roots or tips measured along the z-direction
r_s,t_s	root and tip z-positions respectively of serrations projected onto any y-z plane
φ	angle of serration - $\tan^{-1}(\lambda/4h)$
ρ	cross correlation coefficient
γ^2	coherence
S_{SS} ,S_{TT}	auto-spectral densities of S and T respectively
S_{TS}	cross-spectral density of S and T
t	time

المنارة للاستشارات
www.manaraa.com

τ	time delay between signals from S and T
f	frequency
k	wave number
ω	angular frequency (rad/s)

المنارة للاستشارات
www.manaraa.com

ACKNOWLEDGMENTS

First, I would like to thank God almighty without whom nothing good would be possible. All glory and honor be to him alone.

I am very deeply indebted to many people who have contributed to my work. I thank my major professor and mentor Prof. Richard Wlezien who has guided me patiently through this whole process for the last 5 years. He has been extremely supporting and has taught me so much more than just to do with my research. I am truly honored to have had him as my guide.

I would like to thank Dr. Rothmayer, Dr. Hu, Dr. Sharma and Dr. Sritharan for their valuable input to my research and for being on my committee. I also thank the department staff who made the last few years very memorable. Special thanks to our research team Lucas Clemons, Anil Jairam, Julie Bothell and Eli Shellabarger for all the help, day or night given to me in the laboratory. I also thank Edgardo Diaz and other undergraduates who helped with my research. In addition, I would like to thank the Department of Aerospace Engineering at Iowa State University for the wonderful experience and opportunities I have had.

My deepest gratitude goes to my parents, the inspiration for my doctoral program. I thank my sister and family for their prayers, my parents-in law for their support and all my family and friends for helping me complete my degree. Lastly and most importantly, I thank my husband, colleague and dear friend Lucas Clemons for standing through it all with me.

المنارة للاستشارات

www.manaraa.com

ABSTRACT

Trailing edge (TE) noise due to the interaction between a turbulent boundary layer (TBL) and an airfoil trailing edge is a major source of airfoil self-noise. This broadband noise source generates sound from a few 100 Hz well into the KHz range (~ 15,000 Hz). Wind turbine blades and other subsonic airfoils generate significant TE noise. Improvements such as serrations added to the trailing edge have shown to decrease the far-field noise generated without compromising the aerodynamic performance. A number of aeroacoustic TE noise theories have long been used as the basis for noise-reduction mechanisms. It is well known that they over-predict noise generation and reduction. Serrated trailing edges with different geometries are also known to decrease noise in certain frequency ranges and increase noise in others. In light of these discrepancies, recent work has been focused on understanding the flow mechanisms that cause noise and, by extension, the mechanisms that reduce noise.

In the present research, a NACA 0012 airfoil at a chord Reynold's number of ~850,000 and Mach number of 0.1 was chosen as a baseline configuration to study broadband noise generating flow mechanisms near the trailing edge. The results from the airfoil with a modified blunt trailing edge and 5° angle of attack were used as the baseline. Hot-wire anemometry with two traversing hot-wires were used as the main sensor for unsteady velocity measurements. Spanwise and streamwise correlations were obtained at different depths in the fully turbulent BL near the trailing edge of the baseline configuration to characterize flow structures. From these data, two regions having weak absolute and convective disturbances in the streamwise direction were isolated: the inner log region and the outer region respectively.

المنارة للاستشارات
www.manaraa.com

Correlation and BL profile data near trailing edges of varied thicknesses were compared and it was found that a decrease in thickness and wake deficit near the trailing edge corresponded to an increase in the convective speed of flow structures in the inner region. Sharpness transitions an unsteady wake to an unsteady mixing layer. It has been experimentally proven by other studies that an increase in TE noise occurs with an increase in its thickness. This follows that the interaction of weak absolute disturbances in the inner region with the trailing edge could be a major mechanism of noise generation.

Various serrated TE modifiers whose dimensions λ and 2h (λ is the width between two tips or roots and 2h is the length of a serration from root to tip) were scaled to the TBL thickness at the trailing edge of the baseline configuration were used as flow modifiers. The serrations formed a three dimensional flow structure with different convection speeds along the span. The effect of increasing the length of serrations was to transition the inner region of the turbulent boundary layer near the serration from weak absolute to convective disturbances and to decrease the spanwise correlation of flow structures near the tip. Results suggest that for a given serration width there exists a maximum length that corresponds to the greatest decrease in TE noise. This maximum length has been independently verified by other studies. It was also found that for a given large serration length there exists a minimum width that corresponds to an optimum convective speed of flow structures in the inner region near the serration. Evidence suggests that this width organizes the three dimensional flow structure most desirably to obtain the highest spanwise decay rate of flow-structures near the tip resulting in the maximum reduction of TE noise. Thus, the complex interaction of flow structures near the serration sheds light into the noise reduction mechanism of serrated trailing edges.

المنارة للاستشارات
www.manaraa.com

CHAPTER 1

INTRODUCTION

Airfoil self-noise is caused by the interaction of an airfoil with the turbulence produced in its boundary layer and near wake. Turbulent boundary layer–trailing edge (TBL-TE) interaction noise is one of the major sources of airfoil self-noise and has a unique cardioid shaped directivity. It scales effectively as M^5. It is broadband in nature and exists from a few 100 Hz well into the KHz range (~ 15,000 Hz). Wind turbine blades and other subsonic airfoils generate significant TE noise that can be a source of discomfort to those nearby. As the name suggests, it is very dependent on the property of the trailing edge and the turbulent boundary layer in its vicinity. Hence, changes made to either one of these components should affect TE noise. Improvements such as serrations added to the trailing edge have shown to decrease the far-field noise generated without compromising the aerodynamic performance (Tanner, M (1972), Nedić, J and Vassilicos, J. C (2015)) A number of aeroacoustic TE noise theories have long been used as the basis for noise-reduction mechanisms. It is well known that they over-predict noise generation and reduction. Serrated trailing edges with different geometries are also known to decrease noise in certain frequency ranges and increase noise in others. These discrepancies suggest the need to further understand how the flat and serrated trailing edges interact with the turbulent boundary layer nearby. Recent work has been focused on understanding these flow mechanisms that cause noise and, by extension, the mechanisms that reduce noise. This could potentially help in designing better systems for TE noise control.

المنارة للاستشارات
www.manaraa.com

1.1 Background

1.1.1 Trailing edge noise

Aerodynamic noise associated with an airfoil can be classified into inflow turbulence noise and airfoil self-noise. Inflow turbulence noise is caused by the interaction of turbulence in the atmosphere with the leading edge. The unsteady lift generates a dipole like source and the noise it produces is in the broadband low frequency range. Airfoil self-noise is due to the interaction between an airfoil and the turbulence produced in its own boundary layer near the wake. It is the total noise produced when an airfoil encounters laminar flow. The interest in airfoil self-noise is many fold. It occurs commonly as helicopter rotor, wind turbine and airframe noise. It can be further classified into five self-noise mechanisms (Brooks, T. F et al. (1989)): turbulent boundary layer-trailing edge noise (TBL-TE), laminar boundary layer-vortex shedding noise (LBL-VS), separation stall noise, tip vortex formation noise and trailing edge bluntness-vortex shedding noise. Of these, TBL-TE was found to be the hardest to predict and control. It is a major contributor to broadband noise from the low to high frequency range and is of particular interest in low-speed flow regimes like a wind turbine. Many studies for the past few decades have been dedicated to the study of trailing edge noise. Figure 1 illustrates TE noise: the scattering of pressure waves caused by the interaction of the trailing edge with turbulent eddies in the boundary layer. The cardioid shaped directivity pattern of TE noise is shown beside. In a cambered airfoil or an airfoil at a finite angle of attack, the far-field tonal noise is usually associated with the high energy eddies on the pressure side while the turbulence on the suction side contributes solely to broadband noise.

المنارة للاستشارات
www.manaraa.com

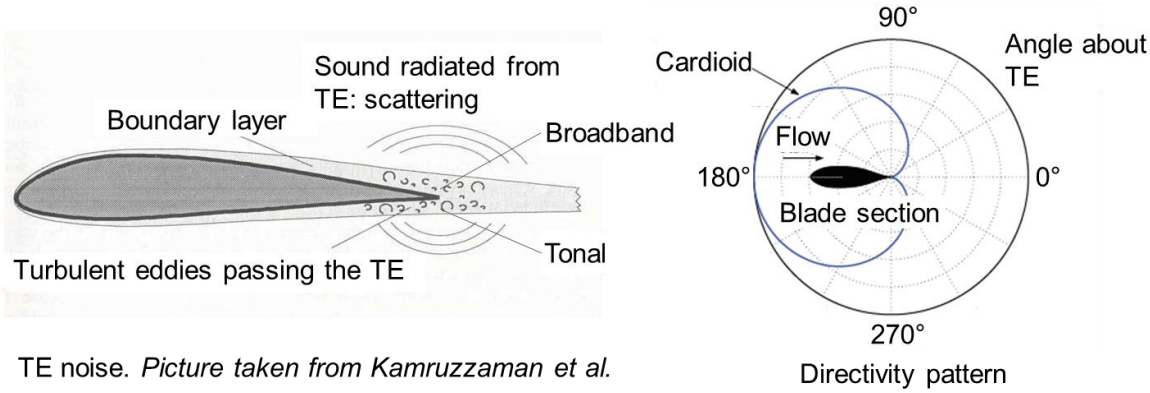

Figure 1(a). Illustration of trailing edge noise and its directivity pattern

Lighthill (1952, 1954) in his theory of aerodynamic sound, modelled the problem of sound generation by turbulence using an exact analogy where sound was radiated by a volume distribution of acoustic quadrupoles in an ideal acoustic medium. The strength of the quadrupoles in Lighthill's stress tensor used in his theory are the unsteady components of the Reynold's stress at low Mach numbers. Curle (1955) showed how the presence of boundary surfaces could be accounted for by adding dipole and monopole sources. A dimensional analysis of the equations showed that the intensity of sound generated by free turbulence (quadrupoles) scales as the eighth power of a typical flow velocity while that induced by unsteady surface forces (dipoles) scales as velocity to the power six. Some of the earliest studies on trailing edge noise were performed by Ffowcs Williams and Hall (1970), Chase (1972) and Amiet (1975 and 1976). Ffowcs Williams and Hall (1970) stated that it was necessary to consider the details of the potential field in the vicinity of a sharp edge of a body that acts as a scattering center. In such a case, dimensional analysis showed that the sound generated is dominated by edge scattering and the resulting noise scales more effectively than a quadrupole or a dipole. The intensity scales as typical flow velocity (U_c) to the power five and is given by $\langle p^2 \rangle \propto \rho_0^2 U_c^5 \left({L l \overline{D}}/{c_0 r^2} \right)$, where p is the far-field acoustic pressure, ρ_0 is the medium density, c_0 is the speed of sound, r is the distance from the trailing edge to the

المنارة للاستشارات
www.manaraa.com

observer, $\overline{D}$ is a directivity constant that equals 1 for observers normal to the surface from the trailing edge, L is the spanwise trailing edge length wetted by the flow and l is a characteristic turbulence correlation scale. The effect of an eddy on trailing edge noise was calculated to be substantially higher when near the edge, within a hydrodynamic wavelength. He also showed the occurrence of cardioid shape directivity ($\sin^2(\underline{\theta}/2)$, $\underline{\theta}$ is the angle made about the TE as shown in figure 1) associated with trailing edge noise. This particular U_c^5 scaling was independently observed in other studies performed by Chase (1972), Howe (1978) and in acoustic experiments performed by Brooks and Hodgson (1981) among others. Chase (1972) related the far-field pressure spectrum to hydrodynamic pressure fluctuations on or near the trailing edge in the presence of a turbulent wall jet. He used measurable properties on the boundary layer upstream of the trailing edge in his theory. He also assumed that the turbulent eddy convected past the trailing edge without interacting with it (evanescent wave). Amiet (1975, 1976) theoretically related the far-field acoustic spectrum to the spanwise correlation length of vertical velocity fluctuation and surface pressure spectrum near the trailing edge. These theories were compared to experimental results and the results did not match as expected. They were limited by the right use of turbulence spectrum, surface pressure spectrum and so on. The theories themselves made considerable assumptions like the evanescent wave mentioned above, absence of mean flow, average value of eddy convective velocity and so on.

Howe (1978) formulated his theory on trailing edge noise. He made modifications from the earlier theories: he accounted for varying convective speeds of turbulent eddies with respect to vertical distance from the trailing edge ($U_c(y)$), forward flight motion and lack of significant correlation between eddies of different mean convection velocities. His results

المنارة للاستشارات
www.manaraa.com

showed the predicted noise is proportional to turbulence wetting length *L*, spanwise correlation length of eddies *l* and eddy convection velocity U_c to the power five. They agreed with previous findings. The most important contribution was the application of the Kutta condition at the trailing edge to account for finite pressure and velocities at trailing edge (as opposed to the evanescent wave theory). His theory showed that the application of Kutta condition under-predicted the far-field noise generated by about 10 dB when compared to results without the use of Kutta condition. Howe explained this discrepancy by the use of a correction factor $(1- (W/U_c(y))^{-2}$, where, W is the speed of shed vortex in the near wake in the y = 0 plane and takes values from 0 to $U_c(y)$ based on the problem being analyzed. Other authors (Brooks, T. F and Hodgson, T. H (1981), Rienstra, S. W (1981)) went on to suggest that the truth in practicality lies somewhere in between, very likely through the application of viscosity in the closer regions to the trailing edge. They did not observe any vortex shedding as a result of the Kutta condition in their experiments (or theory). Lutz et al. (2007) and Kamruzzaman, M et al. (2011) showed the importance of using correlation length of vertical velocity fluctuating components in the vertical direction and mean shear of the turbulent boundary layer while theoretically predicting wall pressure fluctuations that inevitably contribute to far-field noise as stated by previous authors. All the above work is limited to high frequency trailing edge noise where the associated wavelengths are considerably smaller than the chord length of the airfoil. From this review, the need to further explore the effect of turbulence and its interaction with the trailing edge is apparent.

In recent years, many aeroacoustic computational studies have been performed on specific problems, example: computational aeroacoustic analysis of a high lift configuration by Singer et al. (2000) and its corresponding experimental study by Choudhari et al. (2002),

المنارة للاستشارات
www.manaraa.com

convective effects and the role of quadrupole sources for airfoil aeroacoustics by Wolf et al. (2012). The results of vortex shedding by Singer were compared with experiments performed in their group and were found to be agreement. Few results from the computations on a NACA 0012 airfoil performed by Wolf were in agreement with experimental data by Brooks (1981,1989). Discrepancies were still observed at complex flow configurations.

1.1.2 Trailing edge noise reduction

In light of the trailing edge noise problem, many studies have been performed to mitigate it. Some of the earliest ones stem from Howe's theoretical work on serrated trailing edges (1991) in a low Mach number flow. He suggested the use of passive devices: serrated trailing edges of serration angle (figure 1(b)) $\varphi < 45^{o}$ would reduce noise by up to 8 dB at high frequencies ($f\delta/U_{\infty} > 0.16$, $fh/U_{\infty} >> 1$, where δ is the boundary layer thickness of the trailing edge and 2h is the length of the serration as shown in figure 1(b)).

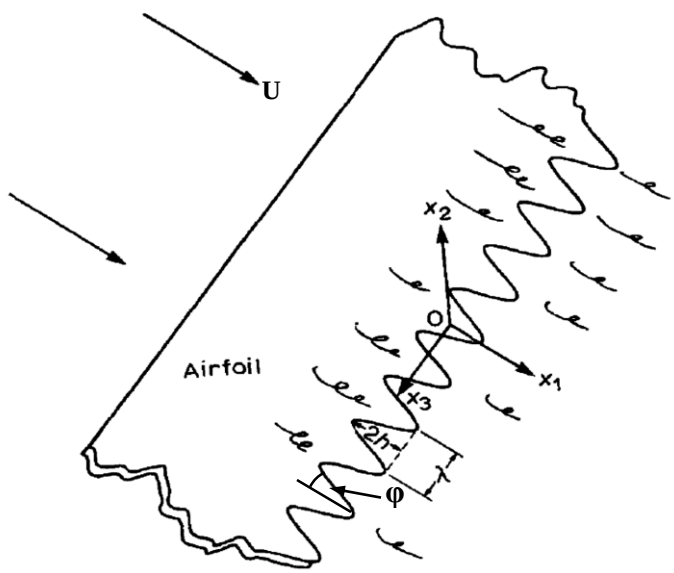

Figure 1(b). Turbulent flow over an airfoil with a serrated trailing edge. Picture taken from Howe ("Aerodynamic noise of")

المنارة للاستشارات
www.manaraa.com

Howe explained that as noise is understood to be directly proportional to the effective wetting length of convective eddies arriving normal to the trailing edge, any method to reduce the effective wetting length could potentially reduce noise. He over predicted noise reduction and this was experimentally shown by many authors including Gruber et al. (2010, 2011). Gruber showed that at some frequency $f\delta/U_\infty \approx 1$, the noise generated by sawtooth serrations of all dimensions (2h and λ – figure 1(b)) increases. He also showed that serrations are most efficient in the length range $1 < 2h/\delta \leq 4$. In addition, noise reduction improves when λ decreases. He attributed the increase in noise to jets forming in between the serrations. He observed that where noise was reduced, it occurred over low to mid frequencies by 1 to 7 dB respectively. Noise increase of over 3 dB occurred at high frequencies. He could not establish a trend between h and λ even though he observed that they depended on each other with respect to noise reduction. Few others showed that the same serration dimension that worked at a given frequency range at high Reynold's numbers caused an increase in noise at low Reynold's numbers signifying a dependence of effectiveness of serrations on flow dynamics near the trailing edge. It has also been shown that serrations do not affect the aerodynamic performance of the airfoil, in fact, they can improve it (Tanner, M (1972), Nedić, J and Vassilicos, J. C (2015)).

Oerlemans et al. (2001) showed that modifying the shape of the airfoil and adding serrations could reduce noise by 4 to 7 dB. Dassen et al. (1996) showed that misaligned teeth of ≈ 15º with respect to the chord plane increases noise. Finez et al. (2010) used polypropylene fibers at the trailing edge and noticed a reduction of ≈ 3 dB noise. This was attributed to the coherent decay of structures in the spanwise and transverse direction of the trailing edge. Herr (2005, 2007) also experimentally studied flexible and rigid brushes/combs

المنارة للاستشارات
www.manaraa.com

as trailing edge noise treatments and found noise reduction of 2 to 10 dB over a wide frequency range. He attributed this to viscous damping of turbulent flow pressure amplitudes in the comb area. In general, it was observed that noise reduction depended on length, width, spacing and flexibility of the brushes through their effect on local flow structures near the trailing edge.

Khorrami and Choudhari (2003) computationally applied passive porous treatments to slat trailing edge noise. They found potential reduction of about 20 dB across frequency regions of interest accompanied by a secondary effect of an upward shift in shedding frequency to a frequency band of reduced auditory sensitivity in full-scale applications. Wolf et al. (2015) used active noise reducers (wall normal suction) to alter the boundary layer characteristics responsible for trailing edge noise. He showed that steady suction had a positive effect on the trailing edge noise (reduction by 3.5 dB) by reducing boundary layer thickness and the integral length scales of eddies in the boundary layer. Jaworski and Peake (2013) mathematically studied the effect of porosity and elasticity of a scattering edge. They showed that it might be possible to reduce noise scattering from a rigid edge from U_c^5 to U_c^6 and U_c^7 respectively by the appropriate use of porosity and elasticity as in an owl's wing. Following this, Clark et al. (2014, 2015) tested passive bio-inspired rough surfaces and canopies to modify the turbulence features before they scatter into trailing edge noise. They had considerable success over a wide frequency range (10 dB attenuation) and dependence on modifier geometries is being studied. Again, an increase in noise at high frequencies was observed for a few TE treatments and could not be explained. These modifiers were a combination of rough surfaces, porous and flexible materials.

المنارة للاستشارات
www.manaraa.com

Much effort has been dedicated towards the progress of trailing edge noise reduction. The presence of turbulent features near the trailing edge and their interaction with the trailing edge, with or without the use of modifiers is the underlying problem behind most of this research and there is work yet to be done in this particular field of research. In this study, we make use of known sawtooth serrations to better understand some of these basic flow problems involved in trailing edge noise.

1.1.3 Flow instability

In the course of this research, it was found that absolute and convective disturbances affect the nature of trailing edge noise to varying degrees. This section gives a brief introduction to the concept of these two instabilities. Huerre and Monkewitz (1990) in their review of local and global instabilities in spatially developing flows explained the concepts of classical linear stability theory concerned with the development in space and time of infinitesimal perturbations around a basic parallel flow U(y; R) where R (example: Reynold's number) is the sole control parameter that defines the character of U in the local x-position. Fluctuations are typically decomposed into elementary instability waves $\underline{\phi}(y; k)e^{\{i(kx - \omega t)\}}$ of complex wave number k and complex frequency ω. $\underline{\phi}(y; k)$ is shown in most cases to satisfy an ordinary differential equation of Orr-Sommerfeld type. After enforcing boundary conditions, it leads to an eigenvalue problem where eigenfunctions $\phi(y; k)$ exist only if k, ω satisfy a dispersion relation of the form given in equation 1.1.

$$D[k, \omega; R] = 0 \tag{1.1}$$

It is possible to ignore variations in the y-direction and consider the spatio-temporal evolution of instability waves in the (x, t)-plane without losing any of the important

المنارة للاستشارات
www.manaraa.com

characteristics of stability. A differential operator D[$-i(\partial/\partial x)$, $i(\partial/\partial t)$; R] in physical space (x, t) is associated with the dispersion relation (in spectral space) in equation 1.1 such that the fluctuations ψ(x,t) satisfy equation 1.2.

$$D\left[-i\frac{\partial}{\partial x}, i\frac{\partial}{\partial t}; R\right]\psi(x,t) = 0 \tag{1.2}$$

The impulse function G(x,t) (Green's function) of the flow in question is given by equation 1.3.

$$D\left[-i\frac{\partial}{\partial x}, i\frac{\partial}{\partial t}; R\right]G(x,t) = \underline{\delta}(x)\underline{\delta}(t) \tag{1.3}$$

where $\underline{\delta}$ is the Dirac delta function.

The basic flow is then said to be linearly stable if

$$\lim_{t\to\infty} G(x,t) = 0 \text{ along all rays } x/t = \text{constant}, \tag{1.4}$$

and it is linearly unstable if

$$\lim_{t\to\infty} G(x,t) = \infty \text{ along at least one ray } x/t = \text{constant}. \tag{1.5}$$

Among linearly unstable flows, the basic flow is convectively unstable if

$$\lim_{t\to\infty} G(x,t) = 0 \text{ along the ray } x/t = 0, \tag{1.6}$$

and it is absolutely unstable if

$$\lim_{t\to\infty} G(x,t) = \infty \text{ along the ray } x/t = 0. \tag{1.7}$$

In general, convective disturbances vary in space and absolute disturbances vary in time. Given a parallel flow approximation, at a local streamwise station, if localized disturbances spread upstream and downstream and affect the entire parallel flow, the velocity profile is said to be locally absolutely unstable. If the disturbances are swept away from the source, it is said to be locally convectively unstable. The implication of a locally absolute flow often is that it results in globally instability. The spatial evolution of unsteady flows that

المنارة للاستشارات
www.manaraa.com

are locally convectively unstable everywhere (example: mixing layers) is in large determined by the amplitude or frequency content of the excitation of the control. They are in essence "noise amplifiers". On the other hand, shear flows with regions of absolute instabilities of sufficiently large size (example: bluff-body wake) behave as "oscillators" where fluid particles are advected downstream, but temporally growing global modes may be present. The evolution of vortices does not rely on spatial amplification of external perturbations but on the growth of initial disturbances in time.

1.2 Objective

The objective of this research is to understand the basic flow mechanism involved in the generation of broadband TE noise. Given the discrepancies between theories associated with TE noise, the goal is to find the common denominator flow physics that could better explain it. By contrasting the flow structures and their interaction with flat trailing edges with the flow structures and their interaction with known independently verified "good" and "bad" serrated trailing edge noise reducing modifiers, we want to investigate flow mechanisms that generate and reduce noise. Through this process, we intend to expand the design space for practical and effective trailing edge noise reducing modifiers.

المنارة للاستشارات
www.manaraa.com

CHAPTER 2

EXPERIMENT DESCRIPTION

A NACA 0012 airfoil was chosen for study because it is a simple airfoil and many aeroacoustic and experimental fluid studies have used it before. It has become a good standard for comparison in basic flow problems. Research by Brooks, T. F et.al (1989) and Brooks, T. F and Hodgson, T. H (1981) are a few well-known studies that have used the given airfoil in their experiments to measure and predict TE noise. In more recent years, Wolf, W. R et al. (2012) performed compressible large eddy simulations on a NACA 0012 airfoil with a rounded edge to study the effects of mean-flow and quadrupole sources on TE noise. This airfoil is optimally thick to provide a turbulent boundary layer at the trailing edge as often is the case in low speed airfoils (eg: wind turbines). It is a symmetric airfoil and therefore the broadband flow problem can be de-coupled from the tonal component at high Reynold's numbers, for a sharp trailing edge and at zero degrees angle of attack. Knowledge of this broadband flow structure is used for the main part of this research where the broadband flow structures modified near the trailing edge at $\alpha = 5°$ is explored. The turbulent boundary layer generated near the trailing edge at this angle of attack is optimal for this study as it can be compared to what happens in practicality.

2.1 Coordinate system

The schematic diagram of the orthogonal coordinate system used in this study is shown in figure 2.

المنارة للاستشارات
www.manaraa.com

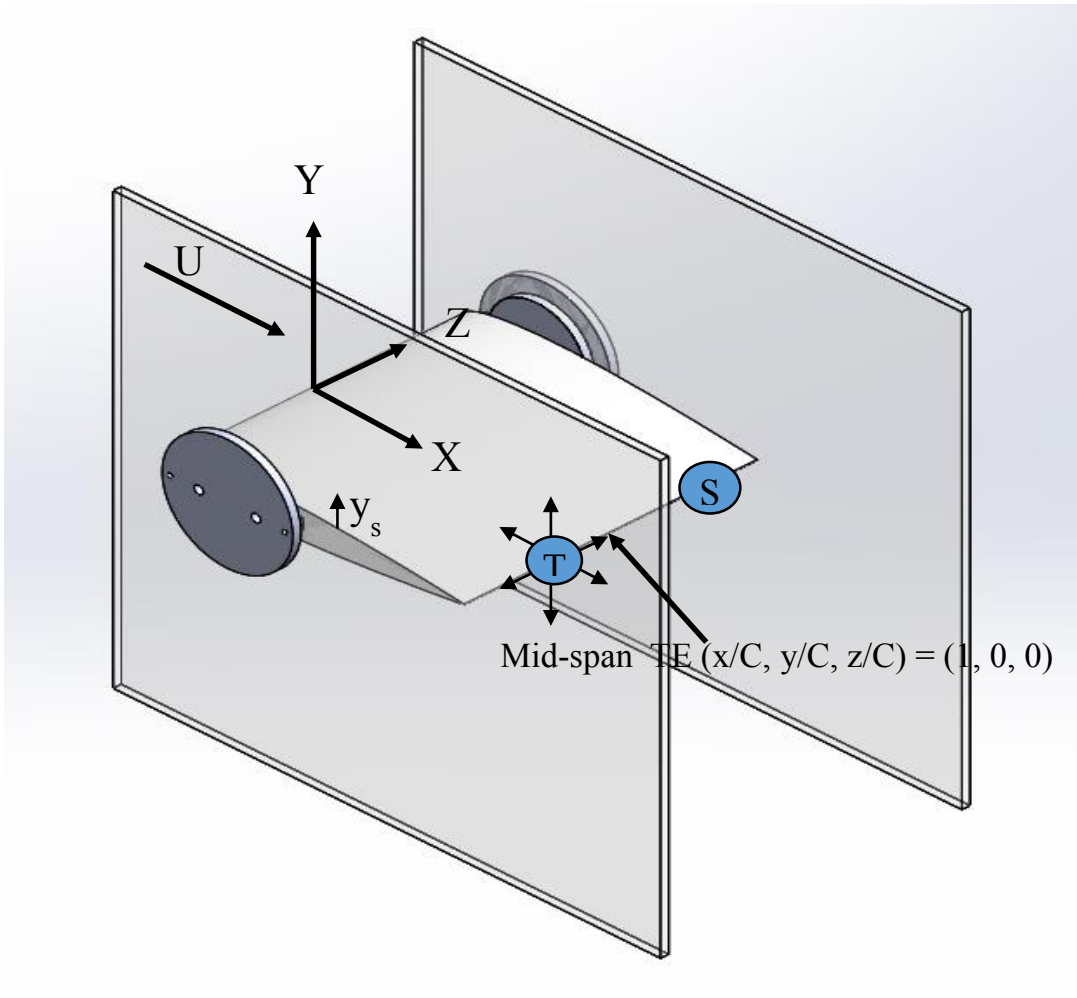

Figure 2. Coordinate system

Figure 2 shows the airfoil model mounted to the side panels of the wind tunnel at α = 0°. The X-axis is along the streamwise direction. The Z–axis is in the spanwise direction and the Y-axis is in the normal direction. The mid-span of the trailing edge is taken as the point of reference at any angle of attack and takes the value (x/C, y/C, z/C) = (1, 0, 0). The distance from the surface of the airfoil measured along the y-direction is given by y_s. In the wake, y_s = 0 is the point that has the least streamwise velocity U. S and T are the stationary and traversing hot-wires respectively.

المنارة للاستشارات
www.manaraa.com

2.2 Hardware description

2.2.1 Airfoil model

The NACA 0012 airfoil model used has a chord length C = 18 in. The experimental setup was designed to run at a Reynolds number of ≈ 850000 and Mach number of 0.1. The airfoil model was machined out of one solid piece of RenShape 440, a medium-low density polyurethane board. It was sanded, painted and finally sanded again with a 2000 grit sandpaper. The CNC machine used to machine the model has a tolerance of ≈ ± 0.0005 in. The trailing edge is rounded and has a radius of curvature of ≈ 0.025 in ($t \approx 0.05$ in or 0.003C). To develop a turbulent boundary layer at the trailing edge, the boundary layer was tripped at 10% chord by a roughness of ≈ 0.0007C. The roughness consists of glass beads of size 60 grit (≈ 0.01 in) stuck to the model at 10% chord by a ¼ in, 0.002 in thick double sided adhesive tape. The glass beads were tightly packed and randomly distributed on the double sided adhesive. Figure 3 shows the airfoil model as mounted in the wind tunnel.

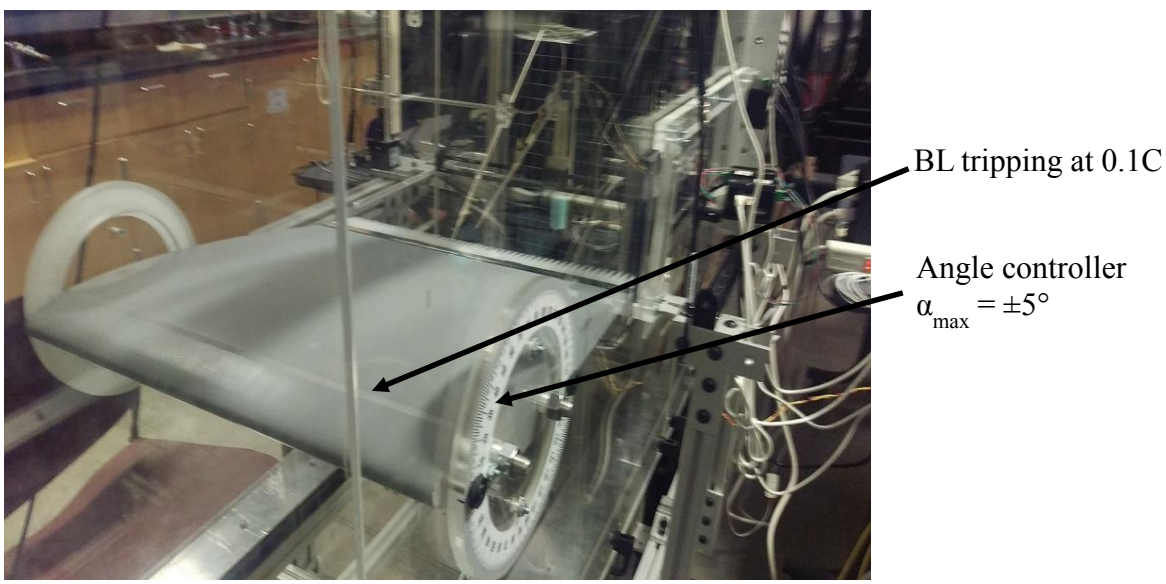

Figure 3. Airfoil model mounted in the test section

المنارة للاستشارات
www.manaraa.com

A manual angle control attached to both the sides of the model and the test section was used to control the angle of attack of the incoming airflow with respect to the chord. The maximum angle that could be set with the controller is $\alpha_{max} = 5°$. The airfoil was mounted such that it could be rotated about 0.25C.

2.2.2 Trailing edge modifiers

All modifiers were rapid prototyped from UV cured VeroWhite+. They were attached to the airfoil with Mylar tape of thickness ≈ 0.002 in. A total of 12 TE modifiers were used. The first modifier was a bluntness or thickness modifier. Figure 4 schematically shows the blunt thickness modifier attached to the original "sharp" trailing edge - Sh. The resulting trailing edge was named as "blunt" trailing edge - B and was used as the reference configuration at $\alpha = 5°$. The reasons for these choices, names and the effect of the Mylar tape on the turbulent boundary layer are described later in the results section. The effective thickness for the blunt trailing edge, taking the Mylar tape into account is $t \approx 0.09$ in.

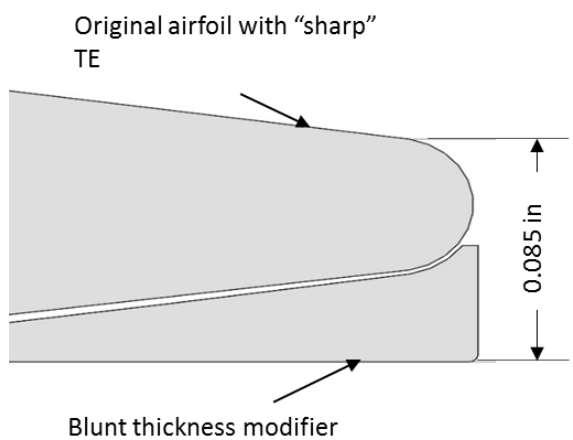

Figure 4. Blunt thickness modifier

For the purpose of our study, it is undesirable for the modification geometry and not the serrations to alter the flow structures near the trailing edge. For this reason, 2

المنارة للاستشارات
www.manaraa.com

modifications F1 and F2 were added to the original trailing edge. They differ from the serrations in that they do not have serrations (they are flat) and they extend the chord of the airfoil over ≈ 1.2 in. These modifiers followed the profile of the airfoil near the trailing edge but have different rounded TE thicknesses (t = 0.05 in and 0.16 in respectively). Figure 5 schematically shows the first of these flat extended trailing edges F1 attached to Sh. Mylar tape of thickness ≈ 0.002 in was used to attach the lip of modifiers to the suction and pressure sides of the original airfoil. F1 and F2 were also used to study the effect of TE thickness on the flow structures in the turbulent boundary layer near the trailing edge. The effect the lip of the modifier/ Mylar tape on the turbulent boundary layer is insignificant near the new extended trailing edge (displaced downstream of the original TE) as are discussed later in the results.

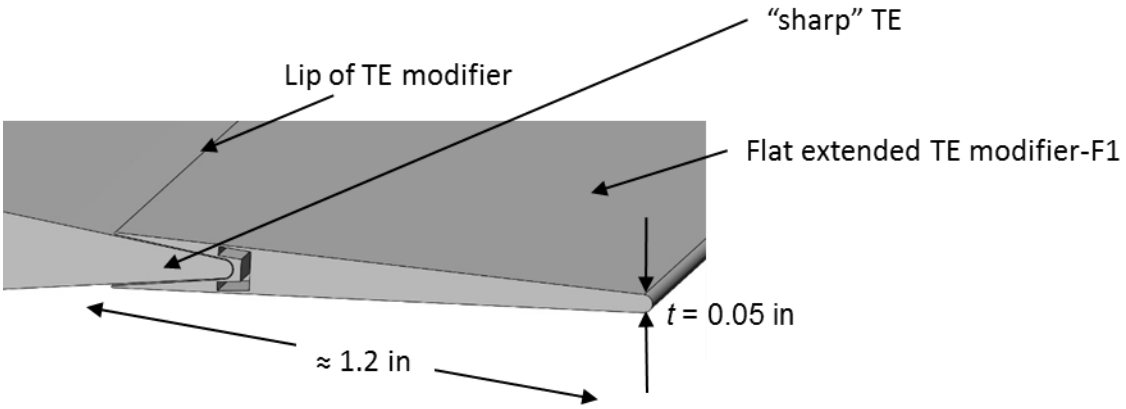

Figure 5. Flat extended TE modifier F1 attached to Sh

Nine serrated TE modifiers were used in this study. They were attached to the original airfoil in the same way as F1 and F2, as described above. Figure 6(a) shows a sketch of a serrated TE modifier attached to the original airfoil and figure 6(b) shows the serrated trailing edge as mounted in the wind tunnel.

المنارة للاستشارات
www.manaraa.com

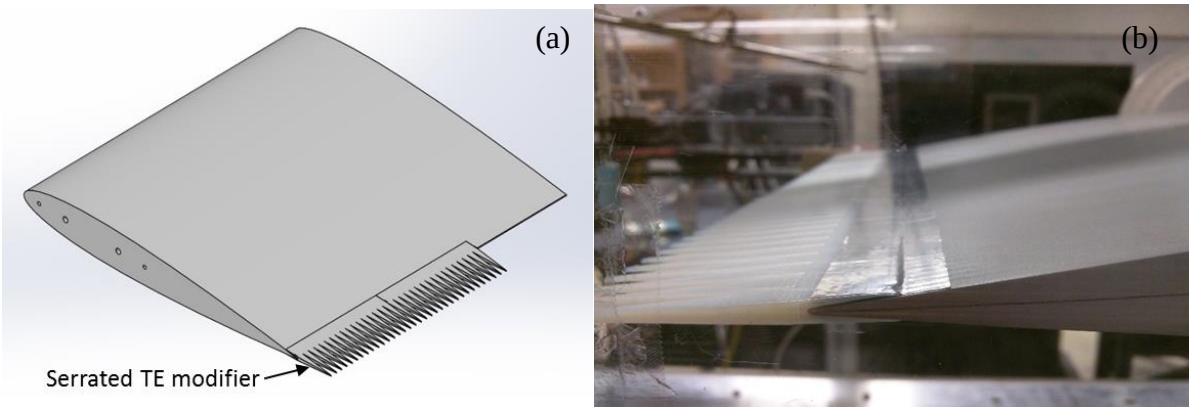

Figure 6. (a) Sketch of serrated TE modifier attached to Sh. (b) Serrated TE as mounted in the test section

Previous analytic and experimental work (Howe, M. S (1991) and Gruber, M et al. (2011)) show that serrations need to be scaled with respect to the boundary layer at the trailing edge for them to be effective at noise reduction. Figure 7 shows a schematic diagram of an effective serrated trailing edge with important notations that are used in this study.

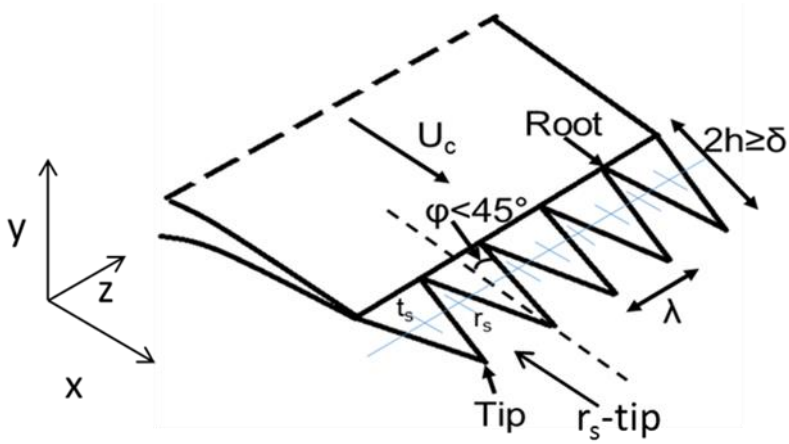

Figure 7. Effective serration

Following this, the dimensions of the serrated TE modifiers used were scaled to the boundary layer thickness at the trailing edge of the reference configuration (B) at α = 5° (δ = 0.72 in) and are shown in figure 8. The findings from Gruber, M et al. (2011) and Howe, M. S (1991) were used as a reference to pick the dimensions of serrations. Gruber, M et al.

المنارة للاستشارات
www.manaraa.com

(2011) experimentally showed that a serration is most effective at $1 < 2h/\delta \leq 4$ and for smaller values of λ. He could not establish a consistent trend between 2h and λ for effective noise reduction. In our study we picked a range of values of 2h (length) and λ (width) to reach our goals. Some of these serrations (example: L2W4) were shown to reduce noise by Gruber, M et al. (2011) while others (example: L1W1) are expected to be poor noise reducers. Such a choice could make a comparison of the flow structures around the baseline TE configuration to those around serrations of "good" and "bad" serrated trailing edges meaningful i.e., they could point out the flow mechanism that actually helps in noise reduction. Table 1 shows a list of all the modifiers used alongside their configuration names, relevant dimensions and color coding that will be used throughout this study.

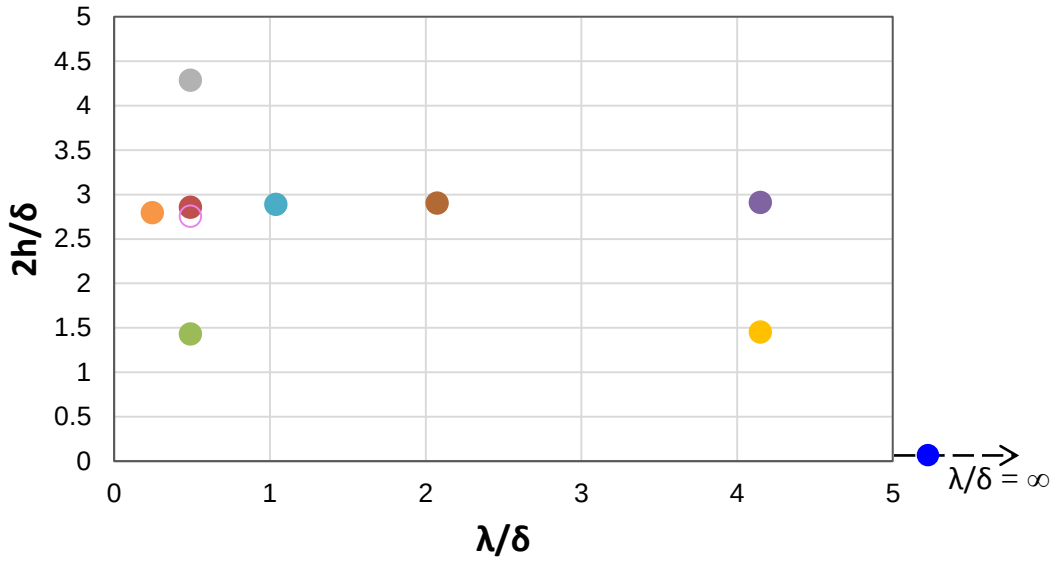

Figure 8. Dimensions of serrated TE modifiers

المنارة للاستشارات
www.manaraa.com

Table 1. List of TE modifiers

TE configuration name	Pictographic representation and color code	2h/δ	λ/δ	*t*	
				Tip/ TE (in)	Root (in)
Sh	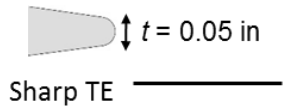	0	∞	0.05	N/A
B	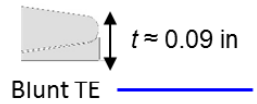	0	∞	≈ 0.09	N/A
F1	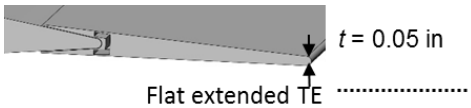	0	∞	0.05	N/A
F2	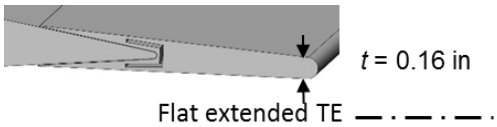	0	∞	0.16	N/A
L1W1		1.5	4.1	0.05	0.19
L1W2		1.4	0.5	0.05	0.19
L2W1		2.9	4.1	0.05	0.19
L2W2		2.9	2.1	0.05	0.19
L2W3	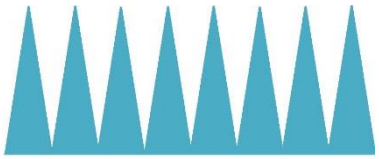	2.9	1.0	0.05	0.19
All serrations are drawn to scale:			δ (= 0.72 in)		

المنارة للاستشارات
www.manaraa.com

Table 1. continued

L2W4		2.9	0.5	0.05	0.19
L2W5		2.8	0.2	0.05	0.19
L2P2	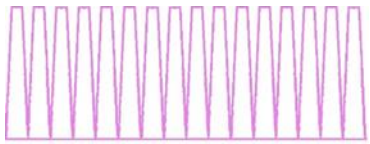	2.8	0.5	0.05	0.19
L3W1	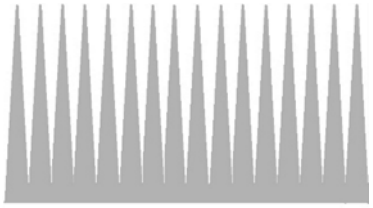	4.3	0.5	0.05	0.19
All serrations are drawn to scale:			δ (= 0.72 in)		

The configuration L2P2 was designed such that the plan-wise effective porosity of the serrated trailing edge would be 25% as opposed to the standard 50% porosity that all triangular (sawtooth) serrated trailing edges will have.

2.2.3 Low turbulence wind tunnel

The experiment was performed in the low turbulence wind tunnel at the aerospace engineering department of Iowa State University. It is a closed loop wind tunnel with a test section– 60 in x 24 in x 18 in (length x height x width). A proportional integral controller connected to its cooling system regulates the temperature in the tunnel to an accuracy of ± 2.5 °C. A differential pressure transducer connected to entrance of the test section and the contraction section respectively measures the free-stream velocity (U_∞) at the entrance of the

المنارة للاستشارات
www.manaraa.com

test section. The maximum U_∞ that can be achieved is 42 m/s. The free-stream turbulence intensity ($(u'_{rms}/U_\infty)*100$) measured using a single probe hot-wire at various locations in the test section ranges from 0.01% to 0.05%. The lower turbulence intensity corresponds to low wind speeds. Flow conditioning consists of a honey comb section made of tightly packed drinking straws and several steel meshes upstream of the contraction section. The contraction chamber has a ratio of 6.75:1. Its shape is a fifth order polynomial and is designed to minimize flow separation. Figure 9 is a picture of the wind tunnel as seen in the laboratory.

Figure 9. Low turbulence wind tunnel

2.2.4 Linear traverse system

The stationary S and traversing T hot-wires were both mounted on high resolution linear traverses by Hayden Kerk motion solutions. T is capable of traversing in the x, y and z directions and S can traverse only in the y-direction. The linear traverses that mount T have a resolution of (0.0002/64) in (along x, y and z) and S is mounted on a traverse that has a resolution of (0.0005/64) in. Optical position encoders connected to the shaft of the linear traverses are capable of resolving the physical position to a precision of (0.0002/8) in. All the

المنارة للاستشارات
www.manaraa.com

traverses were controlled via programmable stepper drives. The hot-wire position files were loaded to a LabVIEW program written in house that communicates with the drive. The setup makes it possible to automate the process of moving the hot-wires to desired positions in the test section and obtaining instantaneous velocity data. In an effort to minimize flow blockage in the test section the following was done: most of the traverse system was kept outside the wind-tunnel, part of the z-traverse and the y-traverse that mounted T were in the test section at a minimum distance of 9 in downstream of the trailing edge for all velocity measurements made around the trailing edge. The linear traverses were sturdy and sleek. Fairings were added to the parts of the traverse system that were directly exposed to the flow. All hardware mounted near and in the tunnel used suitable damping material at all joints to minimize vibration. An external sliding wall was created and mounted on the traverse system on the outside of the tunnel. This ensured sealing the tunnel as the traverse moved in the x-direction. Figure 10 shows S and T as mounted on linear traverses in the tunnel. The hot-wires were mounted using hollow stainless steel rods of length 1 ft and external diameter 5/16 in (probe holders). The x and z positions of S were adjusted manually using a sliding and rotating mechanism of probe holders. The probe holder for T was mounted to the linear traverse at angles of 5° to 25° to free-stream flow. The smallest angle was used to make BL measurements close to the leading edge of the airfoil. As this requires the use of long probe holders, carbon fiber reinforced carbon tubes of similar external diameters were specially made and used to reduce probe vibration. For all correlation data, the probe holder for T was mounted at 15° or 25° and used 1 ft long stainless steel hollow rods. The probe holder for S was mounted at angles ranging from 25° to 45°. Irrespective of the angle of the probe holder

المنارة للاستشارات
www.manaraa.com

of S and T, the hot-wire sensor itself remained perpendicular to U_∞ (the yaw angle between the wire-normal plane and U_∞ is zero).

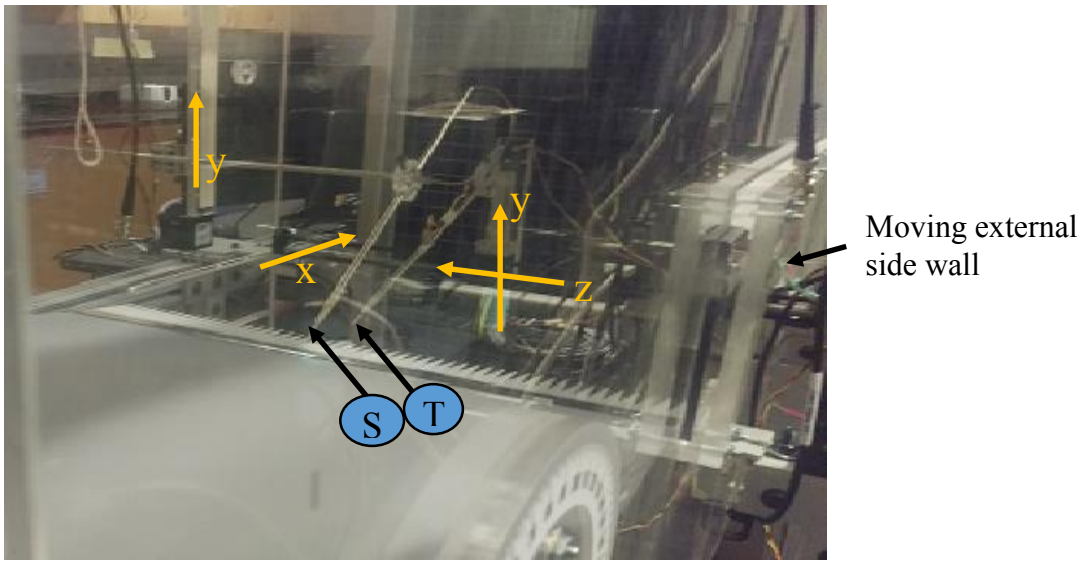

Figure 10. Linear traverse system mounted in the test section

2.2.5 Instrumentation

The tunnel temperature was constantly monitored for all BL profile and correlation data by an RTD placed at the end of the test section. The RTD used is a 3-wire Pt3851 sensor with resistance at 0°C, $R_0 = 100\ \Omega$. For the calibration of hot-wires, a differential pressure transducer by Setra capable of measuring 0 to 5 in WC was connected to entrance of the test section and the contraction section respectively. The density of air in the test section was constantly updated using the temperature sensor and a barometric pressure transducer by Omega (model PX2760) with pressure ratings of 0 to 20 psia. The updated density along with the difference in pressure was used to calculate U_∞.

The main instrument used in the measurement of unsteady velocity (all BL profile and correlation data) was the constant temperature anemometer (CTA) with antialiasing filter and amplifier –AN-1003 from AA lab systems. A 1:10 bridge ratio was used for all hot-

المنارة للاستشارات
www.manaraa.com

wires. The hot-wire probes used were single wire Dantec probes (model 55P11) with a tungsten wire of length 1.25 mm and 5μm diameter. The wires were soldered to the prongs in house and calibrated in the same low speed wind tunnel as required.

A single axis accelerometer was surface mounted to the probe holder of T to monitor the hot-wire vibrations for both BL profile and correlation data. The accelerometer used is a model 805M1 miniature adhesive mount voltage output accelerometer by Measurement specialties. It measures an acceleration of ± 20 g. It has a sensitivity of 100 mV/g and has a three wire interface. It gives an analog voltage output that can be recorded by a data acquisition system.

The data acquisition system consists of NI-CDAQ 9712 chassis that mounts NI-9215, NI-9217 and NI-9239. The voltage signals from the hot-wire anemometer were sent to the NI-9215 analog to digital converter (ADC). It has a measurement range of ± 10 V and a 16 bit resolution. The signals from S and T were synchronized using this ADC. The voltage signals from the differential pressure transducer, the barometer and the accelerometer were connected to NI-9239. NI-9239 has a measurement range of ± 10 V and a 24 bit resolution. It also has an inbuilt antialiasing filter that was made use of. The RTD was internally excited with 1 mA current from NI-9217. NI-9217 has an ADC resolution of 24 bits and is capable of handling commonly used RTDs. It converts the signals directly into temperature as required. The NI-CDAQ 9712 chassis is capable of synchronizing signals from all three ADCs mounted on it. Initial measurements were made from all instruments using the data acquisition system and steps were taken to ensure that electronic noise was not generated via ground loops. LabVIEW was used as the program for data acquisition and handling.

المنارة للاستشارات
www.manaraa.com

2.2.6 Probe vibration

The hot-wire holders experienced vibration that was unavoidable. The longer the probe holder, the larger the vibration. The vibration affected the unsteady velocity measurements. For this reason an accelerometer was mounted on the holder of the traversing hot-wire (T). Measurements were taken to quantify the error generated due to vibration in unsteady velocity signals. Figure 11 shows the accelerometer mounted on T's holder.

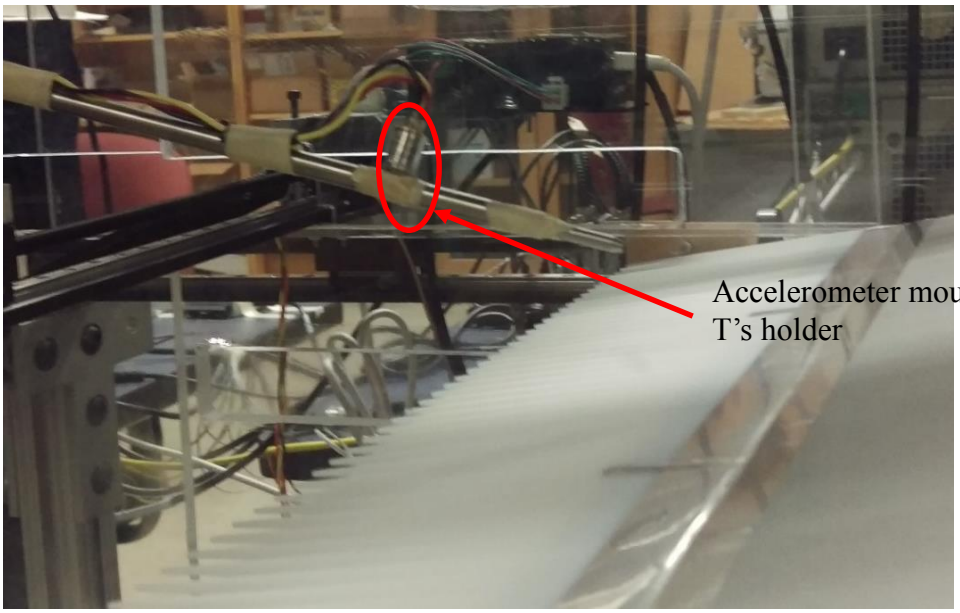

Figure 11. Accelerometer mounted on probe holder

Figure 12 shows the coherence between unsteady time varying signals obtained from T (unsteady velocity) and accelerometer (voltage as a function of acceleration). There is a noticeable peak around 20 and 30 Hz that correspond to probe vibration. As this could adversely affect the unsteady velocity data, the probe was stiffened until the coherence between these two signals dropped below ≈ 0.15. This can be seen in the red curve in figure 12. Thus the error due to the probe vibration is minimized.

المنارة للاستشارات
www.manaraa.com

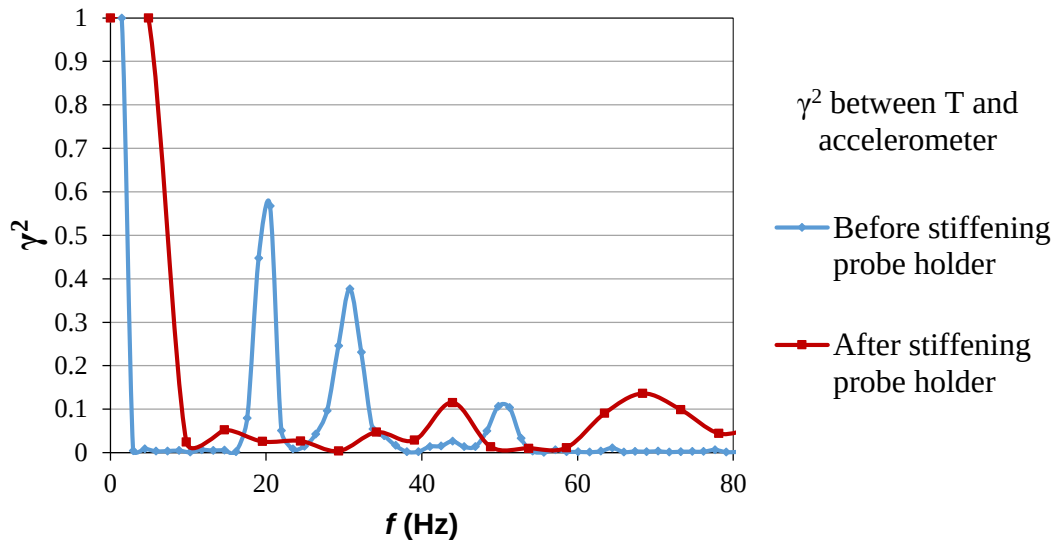

Figure 12. Minimization of probe vibration

2.3 Hot-wire measurements

Time series signals of unsteady velocity ***U*** obtained from S and T were the main data used in this study. The voltage signals from the hot-wire anemometer were temperature corrected and converted to unsteady velocity using a calibration curve specific to every hot-wire used. Boundary layer velocity profile data were first obtained for various x/C locations on the airfoil using T. Based on the preliminary results from BL profile data, 2-point correlation data between unsteady velocity signals from S and T were obtained and analyzed.

2.3.1 Calibration procedure

The difference in pressure between the entrance of the contraction section and the test section was obtained from the differential pressure transducer, the barometer gave the atmospheric pressure and the RTD provided the ambient temperature in the test section of the wind tunnel. All these data were in the form of time series voltage signals that were

المنارة للاستشارات
www.manaraa.com

converted to pressure and temperature values respectively with the use of ADCs and calibration charts of instruments. The free-stream velocity U_∞ was calculated from these pressure and temperature data using Bernoulli's equation and mass conservation between the entrance of the contraction section and the test section as shown in equation 2.1.

$$U_\infty^2 = \frac{\Delta P}{\rho/2\left[1-\left(\frac{A_t}{A_c}\right)^2\right]} \tag{2.1}$$

ΔP is the positive difference in pressure between the entrance of the contraction section and the test section. A_t is the area at the test section and A_c at the entrance of the contraction section. ρ is the density given by equation 2.2.

$$\rho = \frac{P_{atm}}{RT} \tag{2.2}$$

R is the universal gas constant, P_{atm} is the atmospheric pressure obtained from the barometer and T is the temperature from the RTD.

The sampling of voltage signal by the ADC from the hot-wire anemometer was synchronized with those obtained from the above mentioned instruments used to calculate U_∞. The sampling frequency used for the calibration procedure was 5000 Hz. 50 ensemble averages were performed with 1024 samples per average. The two pole antialiasing filter of the hot-wire anemometer was set to a cut-off frequency of 3.8 KHz. The voltage signal was filtered and amplified at the anemometer before sending it to the ADC.

During calibration, the hot-wire was appropriately placed in the test section of the tunnel such that it experienced U_∞. First, the resistance of cable was zeroed out using a shorting probe. The cold resistance of the hot-wire and its ambient temperature were noted as R_{ac}, T_{ac}. It was then heated such that the desirable over heat ratio (OHR) of 1.8 was attained. The new heated resistance of the wire to be maintained during measurements is R_w = OHR×R_{ac}. Next, the frequency response of the wire was tuned by applying a known pulse to

المنارة للاستشارات
www.manaraa.com

the unit. The anemometer response was viewed on an oscilloscope, and the gain and bridge reactance were adjusted until the desired response was obtained.

The tunnel was run at 39 different speeds starting at the lowest speed (1 m/s) and continuing to the highest speed (42 m/s). Calibration points were clustered near the lower speeds to ensure good accuracy at the low speeds since the sensitivity of the wire increases at lower velocities. The tunnel velocity was allowed to settle at each speed for at least 10 seconds before the data were acquired.

Temperature compensation was applied to the raw voltages using the linear correction formula reported by Kanevce, G and Oka, S (1973) and Rahman, A. A et al. (1987):

$$e = e_m \times \sqrt{\frac{T_w - T_{ac}}{T_w - T_{am}}} \tag{2.3}$$

e is the temperature corrected voltage. e_m is the amplified raw bridge voltage from the anemometer. T_w is the heated temperature of the wire and is given by equation 2.4. T_{am} is the temperature in the test section from the RTD at the time of measurement.

$$T_w = \frac{(\mathrm{OHR}-1)+\alpha_{20}T_{ac}}{\alpha_{20}} \tag{2.4}$$

α_{20} is the temperature coefficient of tungsten at 20 °C. α_{20} = 0.0045 (1/°C). OHR is set to 1.8 while heating the hot-wire to T_w. A 4th order polynomial of the form,

$$U = A + Be^2 + Ce^4 \tag{2.5}$$

was used to obtain a relation between U_∞ and the corrected wire voltage e. The values of A, B and C were numerically obtained by fitting a curve using the method of least squares to the calibration data. Figure 13 shows an example of the curve fit.

المنارة للاستشارات
www.manaraa.com

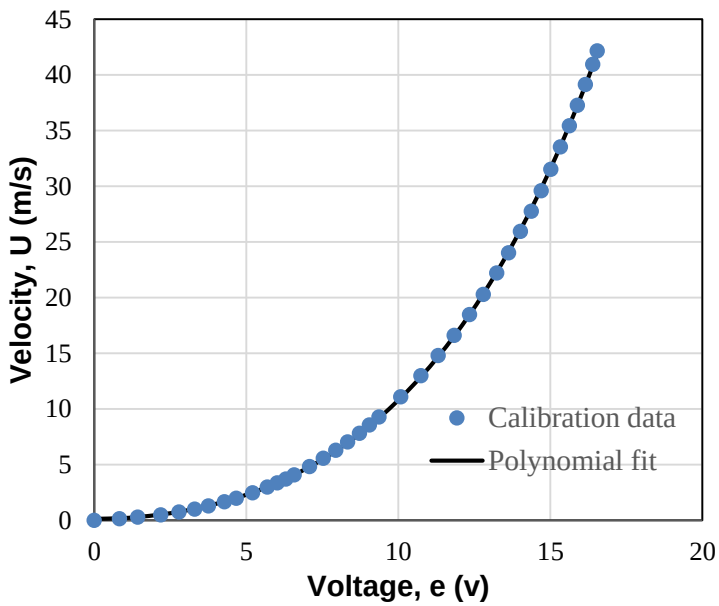

Figure 13. Calibration of hot-wire

2.3.2 Boundary layer profile measurement

The traversing single sensor hot-wire T was used to obtain boundary layer profile data. The assumption is that the measured flow is dominated by velocity components in the x direction. Even though cross-flow is expected near trailing edges and serrations, the direction of the wire is aligned such that it does not respond to the fluctuating component of velocity in the z-direction. Hence measurements are made only of wire-normal mean and fluctuating components of velocity. The spacing of measurements points for the BL profile was optimized such that it is much tighter close to the surface $y_s = 0$. The finest spacing that was used is 0.0012 in. This value lies well within the accuracy level of the y-traverse. The y position of the traverse is often zeroed to the surface (or TE/ tip of serration) at the x/C of interest to minimize position bias errors. The surface of the airfoil is located by tracking the instantaneous mean velocity of T as it is lowered to the surface. When the sensor gets too close to the surface ($y+ \approx 5$) it starts measuring a spurious velocity as a result of the heat

المنارة للاستشارات
www.manaraa.com

conduction to the surface. The traverse is stopped at the point where this effect shows up. It is also worth noting that the airfoil model is made of poly-urethane that has poor heat conduction properties unlike metal. It is later revealed that the region of interest in this study occurs well away from this region of wall conduction. In general, during a measurement sweep, the traverse moves the hot- wire to a given position and waits for about 2 seconds before acquiring data.

For all wake measurements, starting at the trailing edge (x/C = 1), the true position of the hot-wire was maintained at about 0.1 in downstream of the recorded value. For example, x/C = 1.014 refers to a true position in the experiment of ≈ 0.352 in (and not 0.252 in) downstream of the trailing edge. This downstream displacement was maintained consistently through the study.

All BL profile data were taken with a sampling frequency of 5000 Hz, 50 ensemble averages with 1024 samples per average per point. The antialiasing filter of the hot-wire anemometer was set to a cut-off frequency of 3.8 KHz. These values were optimized for speed in measurement and data resolution. The mean velocity U, turbulent intensity u'_{rms}/U_e and power spectral density (PSD) were estimated for all points in the BL profile at different streamwise locations at the mid-span of the airfoil. Various spanwise BL profile measurements were made to ensure the two dimensional nature of the flow. The results from the BL profile data were useful in planning the two-point velocity correlation measurements.

2.3.3 Two-point velocity measurement

All two-point unsteady velocity measurements between S and T were taken with a sampling frequency of 6250 Hz, 50 to 100 ensemble averages with 1024 samples per average

المنارة للاستشارات
www.manaraa.com

per point. The antialiasing filter of the hot-wire anemometer was set to a cut-off frequency of 3.8 KHz. The cross correlation coefficient ρ of unsteady velocity ***U***(t) between S and T and other time and frequency dependent variables with respect to ***U*** were estimated at each location combination of the hot-wires.

z-correlation data

Spanwise correlation data between S and T at various y_s positions in the turbulent boundary layer near the trailing edge (and serrations) were obtained. S was kept stationary at a given location of x/C, y_s/C (or y/C) and z/C. T traversed only in the z-direction (x/C and y_s/C (or y/C) values were kept constant and approximately equal to that of S). The spacing (grid) along the spanwise direction was optimized such that the points were clustered close together when the separation along z between S and T was small. The hot-wire positions were often zeroed for all two-point velocity measurements to minimize bias error in position. The results from BL profile data made it possible to optimize spacing along y_s. The minimum separation between S and T that could be achieved in the y and z-directions are ≈ 0.02 in and 0.075 in respectively. Figure 14 shows S and T with minimum separation in the y-direction. For all z-correlation data taken in the first half of this study, T was placed below S (Δy_{min} = 0.02 in) at $\Delta z = 0$. In this case the value ρ will not be 1 at $\Delta z = 0$. For the second half of the study where S and T were placed beside each other with $\Delta y = 0$ and Δz_{min} = 0.075 in, ρ takes the value 1 at $\Delta z = 0$ as cross-correlation is being performed with the same signal: S with S or T with T. The difference between these two configurations is very minimal but when comparing correlation results obtained from various TE modifiers, the same configuration of S and T with respect to each other was consistently maintained.

المنارة للاستشارات
www.manaraa.com

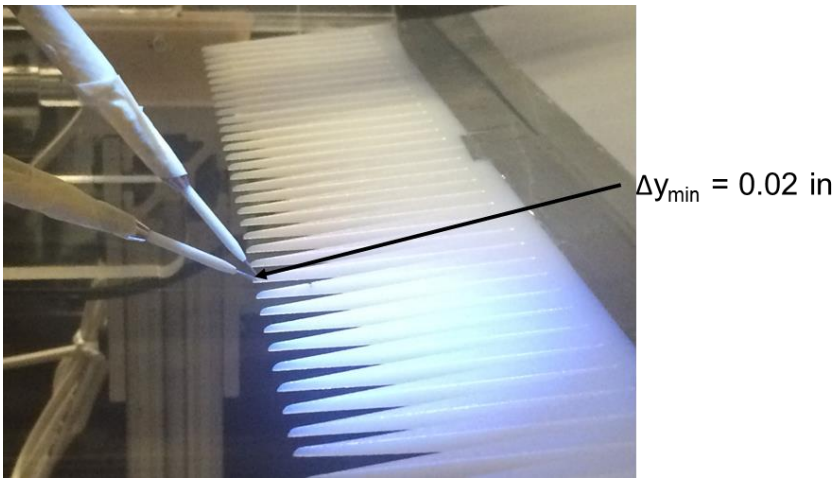

Figure 14. Minimum separation between S and T

x–correlation data

Streamwise correlation data between S and T at two isolated regions of interest (discussed in the results section) in the turbulent boundary layer near the trailing edge and serrations were obtained. S was kept stationary at a given location of x/C, y_s/C (or y/C) and z/C. T traversed only in the x-direction (z/C and y_s/C (or y/C) values were kept constant and approximately equal to that of S). The process is very similar to the z-direction correlation. The spacing along the streamwise direction was optimized such that the points were relatively close even when the separation along x between S and T was large. Early in the study S and T were placed beside each other with $\Delta y = 0$ and $\Delta z \approx 0.1$ in at $\Delta x = 0$. The value of ρ is never 1 as there is always a distance Δz between S and T. At $\Delta x = 0$, ρ should be close to 1 but as $\Delta z \approx 0.1$ in it was noticed that ρ took significantly smaller values (≈ 0.2 to 0.3) in the inner regions of the BL. To fix this problem, later in the study Δz was maintained at ≈ 0.075 in (Δz_{min}) at $\Delta x = 0$. The value of ρ increased to more acceptable values (≈ 0.3 to 0.5) and the percentage error associated with these numbers was decreased. Similar to the z-direction, when comparing correlation results obtained from various TE modifiers, the same configuration of S and T with respect to each other was consistently maintained. Convection

المنارة للاستشارات
www.manaraa.com

(XT) plots were generated by tracking the peak of the cross-correlation coefficient curves for increasing time delay (τ) between S and T. The slope of the XT plot gave the speed of the convecting eddy. Gaussian curves were fit to the correlation curves at increasing τ and their peaks (Gauss center) were methodologically tracked using a LabVIEW code. Spanwise variation of XT – data was observed in the far wake regions of the flat trailing edges. This was taken into account while formulating conclusions. The spanwise variation was minimal for serrated trailing edges.

Contour data

Similar to the streamwise and spanwise correlation data, contour data were acquired with S fixed in two identified regions of interest (discussed in the results section) in the turbulent boundary layer near the flat trailing edge and one of the serrations (L2W4). T traversed in the y-z plane (spanwise plane) and the x-y plane (streamwise plane) for each fixed location of S. The grid was optimized such that the points clustered together when S and T were close to each other along the z-direction. Along the x-direction, the spacing of points remained small even when the distance between S and T were large. Contour plots were generated using the Tecplot software.

For the yz-contours of flat trailing edges, the actual location of S along the z-direction was not considered significant due to the two dimensional nature of the flow. For serrated trailing edges, the root, tip and r_s-tip positions were considered and not the actual position of S along the Z-axis. The same can be said for the xy-contours of serrated trailing edges. In the case of xy-contours of flat trailing edges, small spanwise variations were observed in the far wake regions but the trend that contributed towards the results remained the same. All these details were taken into account while formulating conclusions.

المنارة للاستشارات
www.manaraa.com

2.4 Data analysis

The unsteady velocity ***U***(t) was estimated using the hot-wire calibration curves after temperature correction. The nature of flow turbulence lets us assume ***U*** to be wide sense stationary over the time span of the entire data set (i.e., over 50 (or 100) × 1024 samples acquired). Therefore, all final results were reported as an ensemble average over 50 to 100 sets. The mean velocity U was estimated as the ensemble average of the unsteady velocity time series signal ***U***. The instantaneous fluctuating velocity u'(t) was estimated after as ***U*** – U. This turned out to be similar to u' estimated from equation 2.6. Figure 15 shows the variation of slope dU/de and d^2U/de^2 over the range of e for the same hot-wire used in figure 13. It can be seen that it is possible to ignore the higher order term d^2U/de^2 in the estimation of u'. The results turn out to be well within tolerance limits.

$$u' = e' \times \frac{dU}{de} \tag{2.6}$$

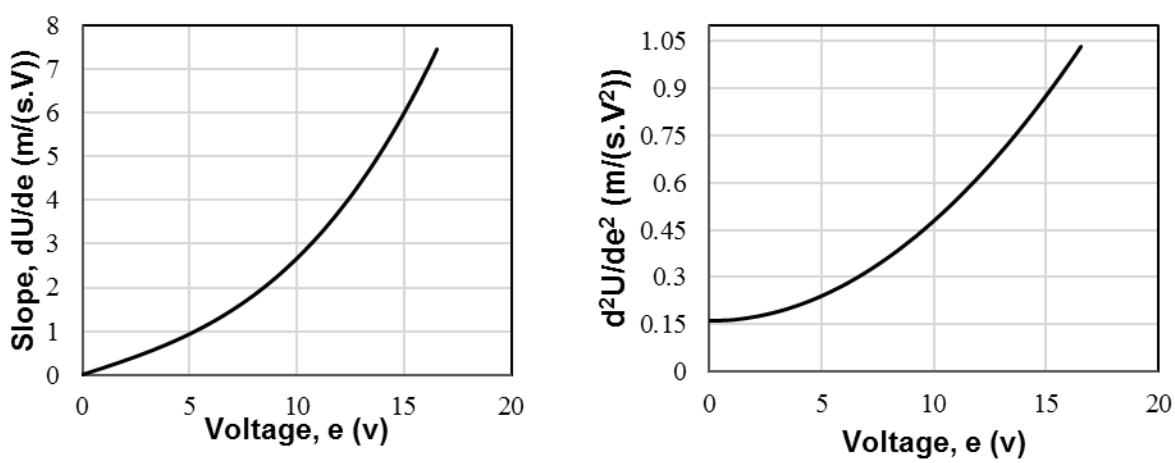

Figure 15. Derivatives of mean velocity with respect to voltage

The turbulence intensity in the boundary layer is given by equation 2.7. U_e is the velocity at the edge of the local boundary layer. The power spectral densities ($S_{TT}(f)$ and $S_{SS}(f)$) of an unsteady velocity signal ***U***(t) from T and S were computed after applying a Hamming window for every data set (1024 samples). With the given sampling rate (6250 Hz)

المنارة للاستشارات
www.manaraa.com

and number of samples (1024), the frequency resolution obtained was ≈ 6 Hz (6250/1024). The coherence $\gamma^2(f)$ given by equation 2.8 is computed from the auto and cross-spectral densities $S_{TT}(f)$, $S_{SS}(f)$ and $S_{TS}(f)$. The signals from S and T are perfectly coherent at a given frequency if γ^2 at that frequency is equal to 1. When they are unrelated, γ^2 takes the value 0.

$$\text{Turbulence intensity in the boundary layer} = \frac{u'_{rms}}{U_e} \tag{2.7}$$

$$\gamma^2(f) = \frac{|S_{TS}(f)|^2}{S_{TT}(f) \times S_{SS}(f)} \tag{2.8}$$

Cross-correlation coefficient ρ(Δx, Δy, Δz, τ) between u'(t) from T (u'_T) and S (u'_S) respectively is given by equations 2.9. The mean value U is first subtracted from ***U*** for the estimation of ρ.

$$\rho(\Delta x, \Delta y, \Delta z, \tau) = \frac{\int_0^{(N-1)\times\Delta t} (u'_S(x,y,z,t) \times u'_T(x+\Delta x, y+\Delta y, z+\Delta z, t+\tau))dt}{(u'_{rms-S} \times u'_{rms-T})} \tag{2.9}$$

A discretized version of equation 2.9 was used. N is the number of samples per ensemble average (1024). u'_{rsm-s} and u'_{rms-T} are the root mean square values of u' from S and T respectively. With the given sampling rate (6250 Hz) and number of samples N, the finest time resolution or delay ($\tau_{min} = \Delta t$) for correlation data between signals from S and T that can be attained is 0.00016 s. τ takes values of multiples of Δt i.e., $\tau = N \times \Delta t$. The equation takes values (Δx, Δy) = (0,0) for spanwise correlation data, (Δy, Δz) = (0,0) for streamwise correlation data, Δz = 0 for xy-correlation contours and Δx = 0 for yz-correlation contours. When S sees an eddy that is perfectly positively correlated with that measured by T, ρ takes the value 1. When S sees local maximum and opposite in direction to that measured at T, it takes the value -1. Just as γ^2 is a function of *f*, ρ is a function of τ. ρ is the primary variable used in this research. It is a preferred tool to understand how time signals (flow structures) interact with each other over space and time.

المنارة للاستشارات
www.manaraa.com

2.5 Turbulent boundary layer development

The purpose of this research is to examine the flow structures in a turbulent boundary layer associated with TE noise. Therefore, a fully turbulent boundary layer near the trailing edge was deemed essential in this study. Preliminary measurements were made and steps were taken to ensure the same. Boundary layer profile measurements were initially taken at different streamwise locations over the chord of the airfoil (with Sh trailing edge configuration) at $\alpha = 0°$, without BL tripping and at a Reynold's number (Re) of 550000. It was noticed that a fully turbulent boundary layer did not occur at the trailing edge. The boundary layer was then tripped at 0.1C as described in the airfoil model section and BL profile data was obtained at $x/C = 0.5$ for increasing Reynold's number. Figure 16 shows the findings. It can be seen, at Reynold's number of 850000 the flow is as turbulent as 950000. A very high flow velocity is undesirable as it would increase probe vibration errors. A Reynold's number of 850000 was therefore chosen for this study.

المنارة للاستشارات
www.manaraa.com

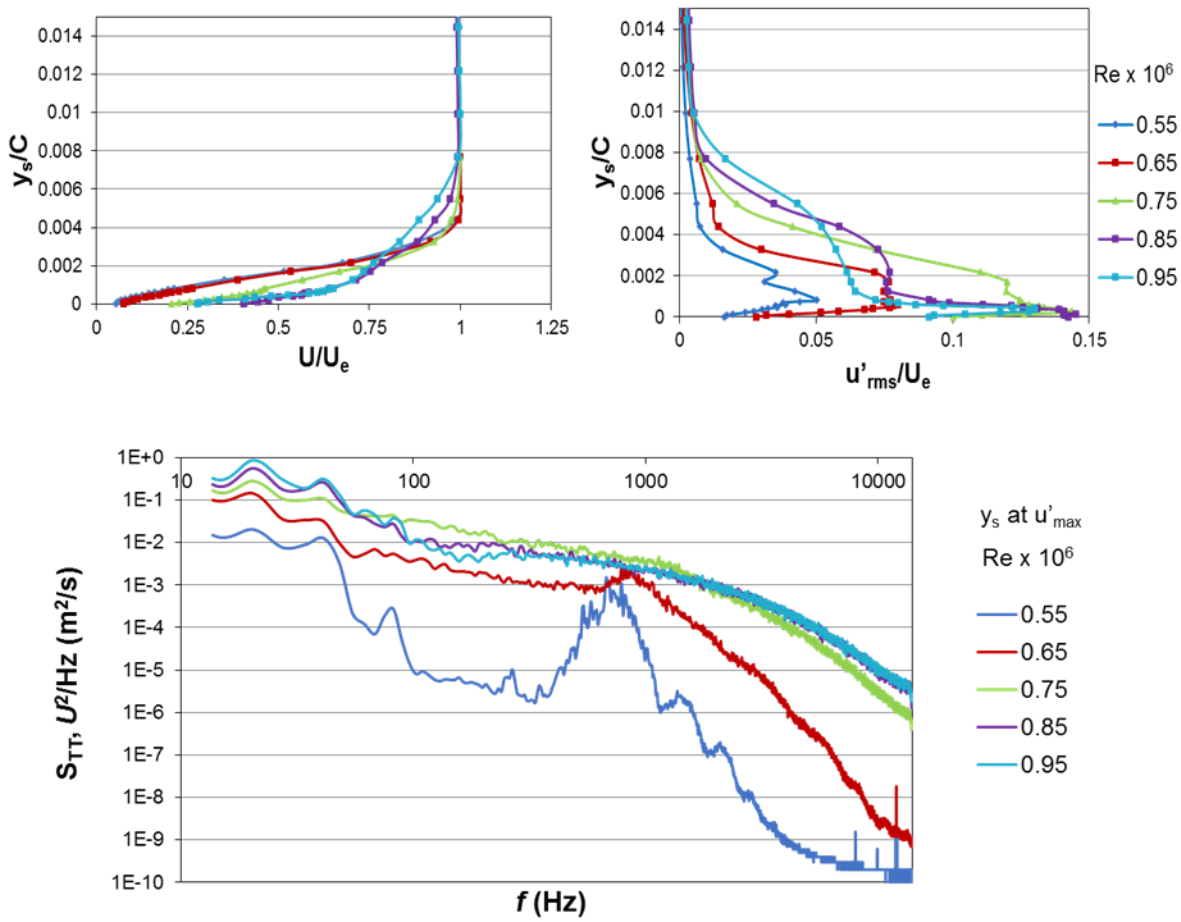

Figure 16. Optimization of Reynold's number at x/C = 0.5

Figure 17 shows the turbulent boundary layer development over the chord of the airfoil at a Reynold's number of 850000 and α = 0°. It shows the presence of a fully turbulent boundary layer towards the trailing edge. Figures 16 and 17 both show the power spectral densities of ***U*** from T at positions in the boundary layer with maximum u'. The spectra towards the trailing edge show typical characteristics of turbulence decay. It also shows an absence of peaks. It is broadband in nature.

المنارة للاستشارات
www.manaraa.com

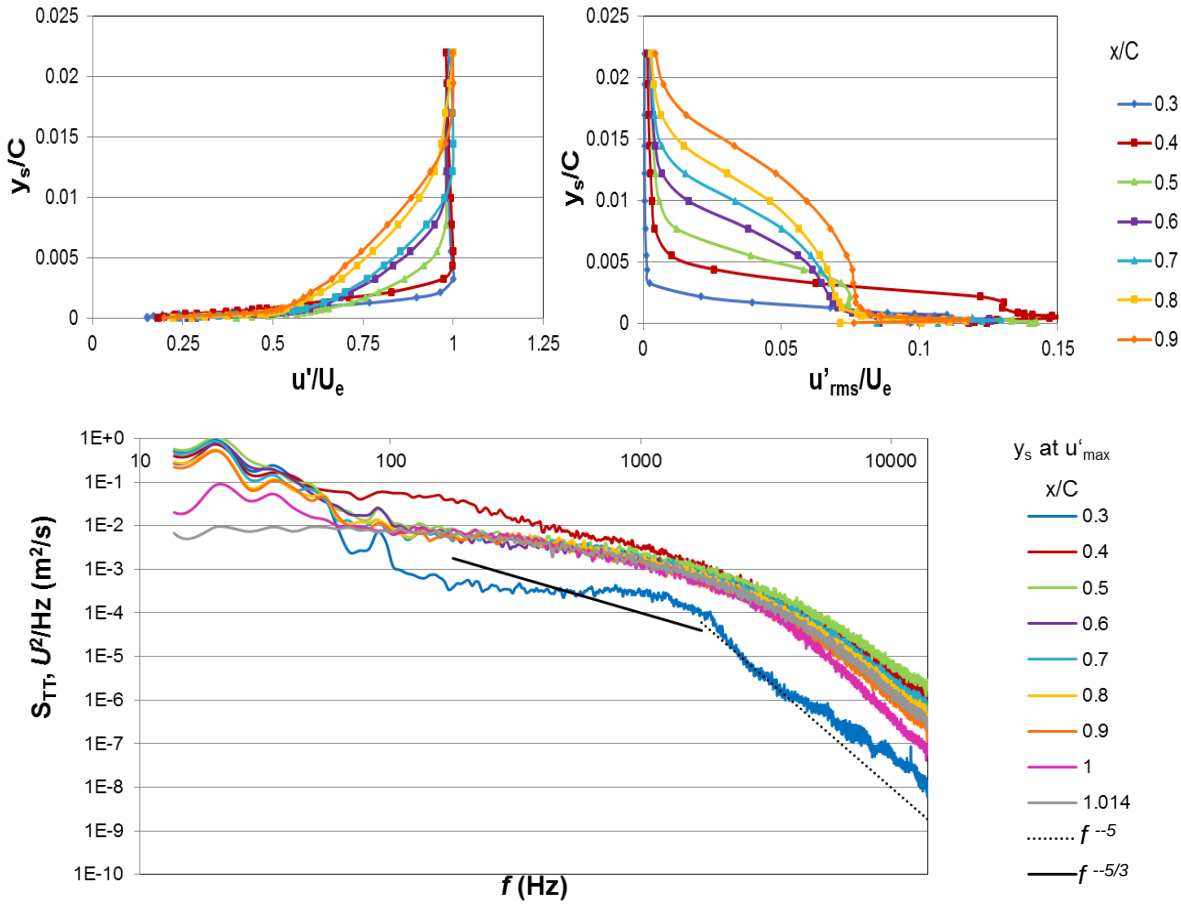

Figure 17. Turbulent boundary layer development over the chord at Re of 850000 and α = 0° with BL tripping

The boundary layer variables - displacement thickness δ^* and momentum thickness θ were estimated at various chord positions. Figure 18(a) shows how the boundary layer transitions to a fully turbulent boundary layer near the trailing edge. These results were compared against existing literature (Sagrado, A.G and Hynes, T (2012), Wolf, W.R et al., (2012)) and showed good comparison. The BL profiles were also plotted using wall units as shown in figure 18(b). Near the trailing edge the viscous sublayer is very small in size. There is a larger log law region that quickly transitions into the outer layer of the turbulent boundary layer. The start of the potential layer can also be seen. These preliminary work

المنارة للاستشارات
www.manaraa.com

ensured the development of a turbulent boundary layer near the trailing edge necessary for the study of broadband TE noise.

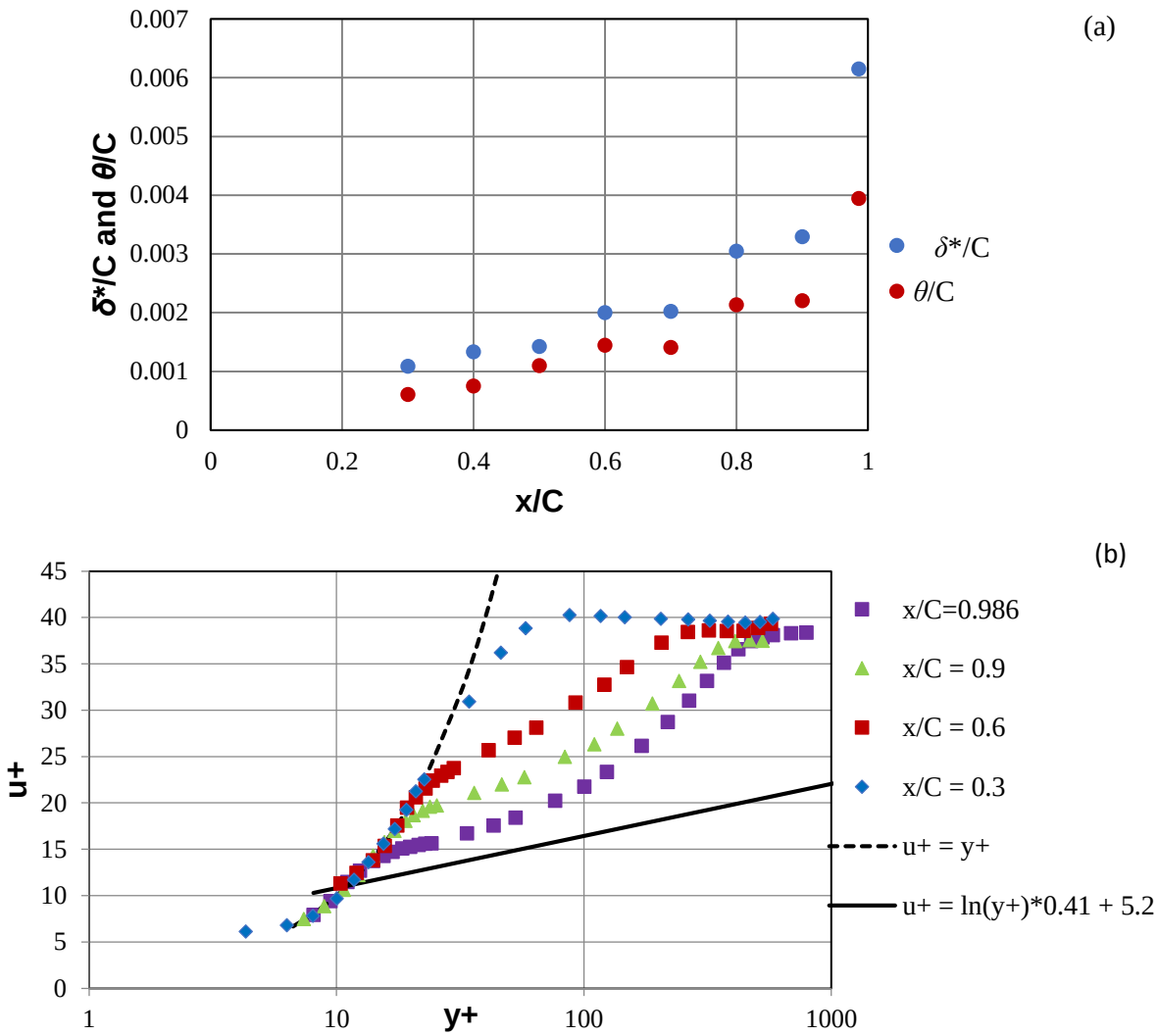

Figure 18. Turbulent boundary layer development in (a) δ*, θ and (b) wall units

Figure 19 shows development of the turbulent wake. The wake deficit decreases as it develops downstream. The asymmetry in the wake is accounted to blockage by the z-traverse downstream of the trailing edge. The traverse was moved as far downstream from the airfoil as possible and centered in the y-direction about the trailing edge. The effect was minimized

المنارة للاستشارات
www.manaraa.com

but was still present. The position of the traverse system was kept a constant while comparing between TE modifiers thus eliminating its effect on our conclusions.

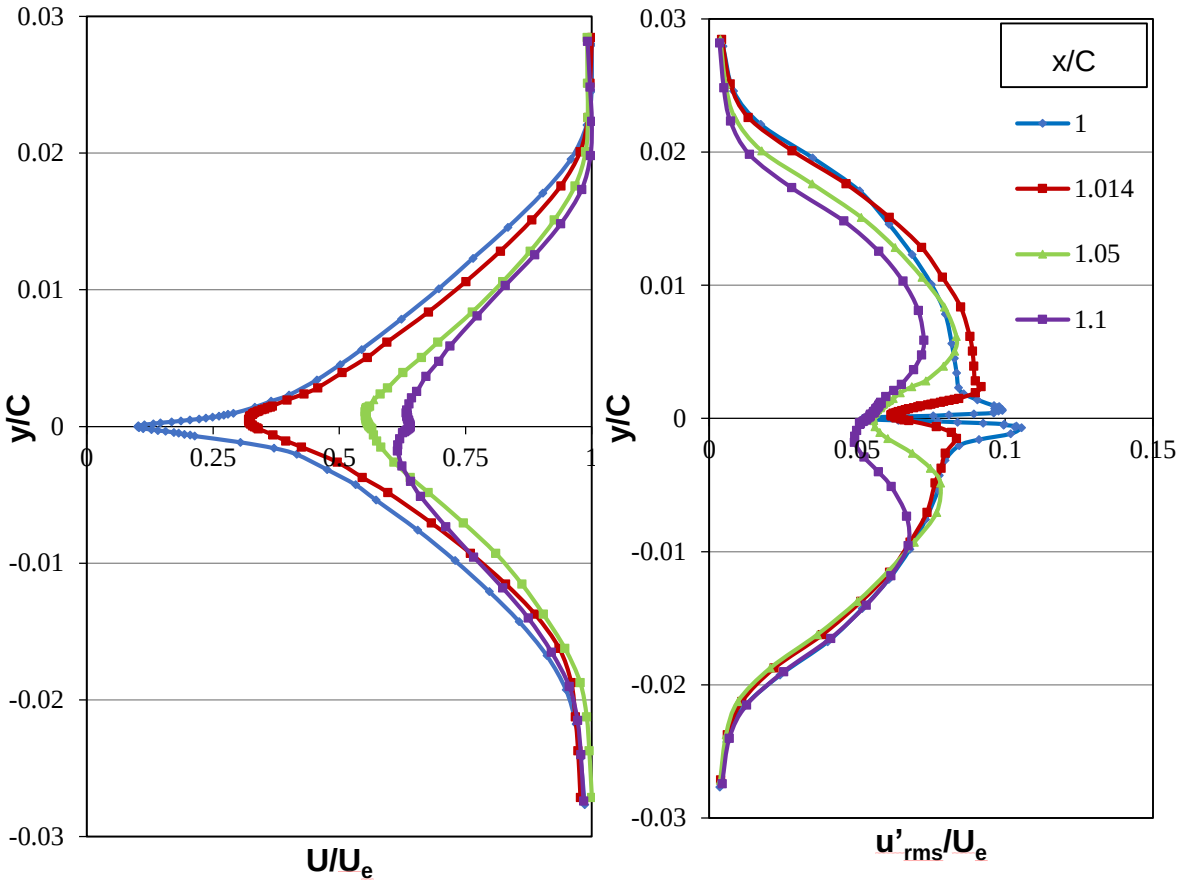

Figure 19. Turbulent wake development at Re of 850000 and α = 0° with BL tripping

المنارة للاستشارات
www.manaraa.com

CHAPTER 3

RESULTS

3.1 Turbulent boundary layer near the trailing edge at α = 0º

3.1.1 Spanwise correlation and coherence of structures

We categorized the turbulent boundary layer near the trailing edge of a flat edged airfoil. The unmodified baseline TE configuration Sh was first used. Work was performed at α = 0º. BL profile and spectral data (figure 17) taken in the near wake of the trailing edge gave us a preliminary idea to expect mainly broadband noise from this configuration. This can be explained by the ratio of the trailing edge thickness of Sh to the displacement thickness at the trailing edge, t/δ^*. It was estimated to be ≈ 0.34. This is towards the lower range of expected vortex shedding (Blake, W (1986)). This condition is a suitable point to start with as there is an absence of interaction with other tonal noise producing features. Therefore, it is possible to isolate the flow features that affect broadband trailing edge noise and establish a baseline in this study. Figure 17 shows the boundary layer profile near the trailing edge. There is a deep region of high turbulence intensity. To start with, spanwise correlation data was obtained at x/C = 0.986 and at various depths in the boundary layer on the suction side of the airfoil. As the boundary layer is symmetric, the results should apply to the pressure side as well. Figure 20 shows these z-correlation data at a time delay τ = 0 between signals from S and T. The spanwise distance between S and T is non-dimensionalized by the local boundary layer δ at x/C = 0.986 (= 0.54 in). Figure 20(b) is an expanded view of 20(a) close to $\Delta z/\delta = 0$. Based on the rate of decay of flow structures, three regions of interest were identified in the boundary layer. The spanwise correlation of

المنارة للاستشارات
www.manaraa.com

structures close to surface drops down quickly and decays within $\Delta z/\delta = 0.6$. These structures lie in the log-law region of the boundary layer and their spanwise correlation curves can be approximated to a strongly damped sinusoid. This region was named inner-top region I_t and occurs at $0 \leq y_s/\delta < 0.8$. A second region with structures that decay as a Gaussian curve at $\Delta z/\delta \approx 5$ and extends from $0.8 \leq y_s/\delta < 1$ was named the outer-top region O_t. It lies in the outer region of the boundary layer. A third region $y_s/\delta \geq 1$ that does not decay even at $\Delta z/\delta$ >10 lies in the potential region outside the boundary layer. It was named P_t. This region was not further investigated in this study as we are focused to structures within the boundary layer and their interaction with the trailing edge even though P_t is relevant in the noise problem. This same process of z-correlation data was repeated at x/C = 1 and similar results were obtained. Figure 21 shows these three regions in the BL profile at x/C = 0.986, 1. Based on these findings, x-correlation and contour correlation data were obtained with hot-wires confined to I_t and O_t.

Figure 22 shows coherence (γ^2) plots corresponding to figure 20. S and T are placed in I_t and O_t and spanwise γ^2 data is shown for increasing frequencies *f*. In the O_t region structures with lower frequencies, decay slowly over $\Delta z/\delta$ while structures with higher frequencies decay fast. In the I_t region, structures of all frequencies decay relatively fast over $\Delta z/\delta$.

المنارة للاستشارات
www.manaraa.com

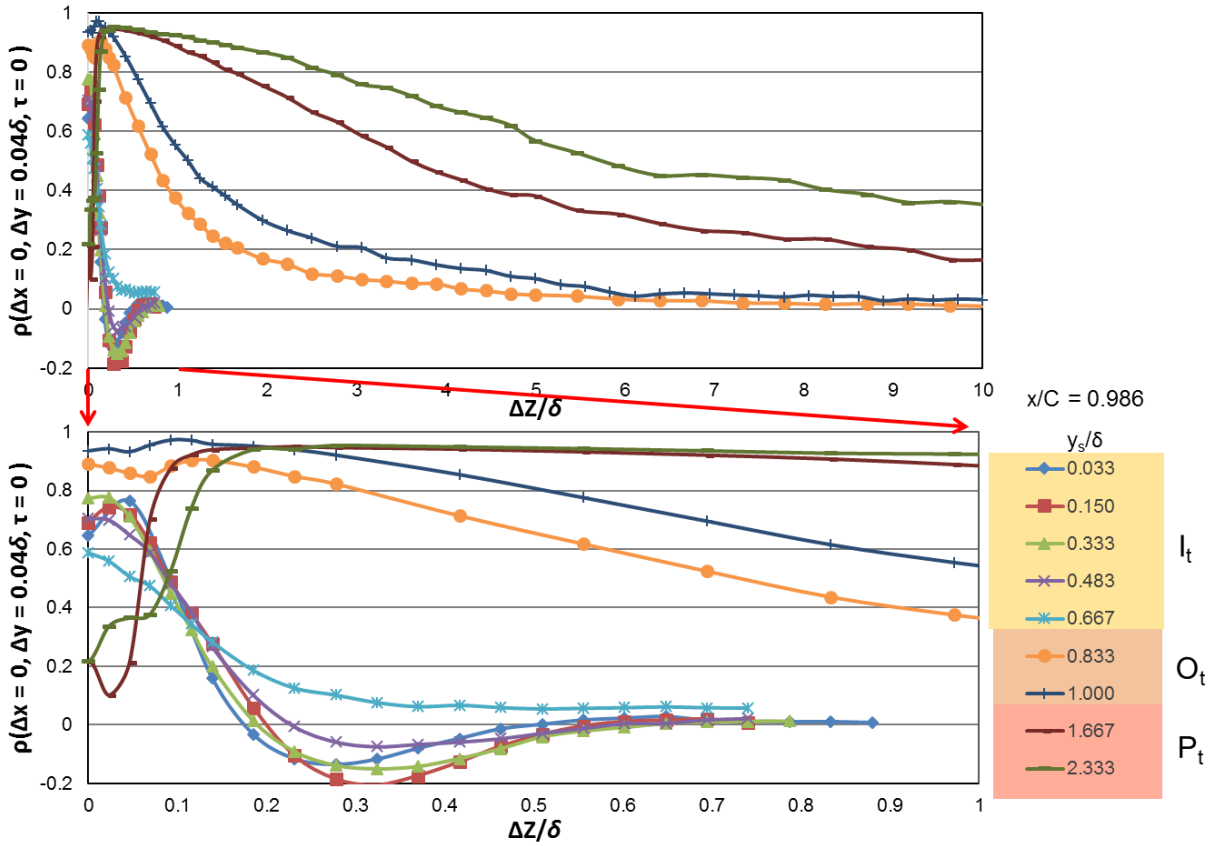

Figure 20. Three regions of interest in the turbulent boundary layer from spanwise correlation data at x/C = 0.986. α = 0°

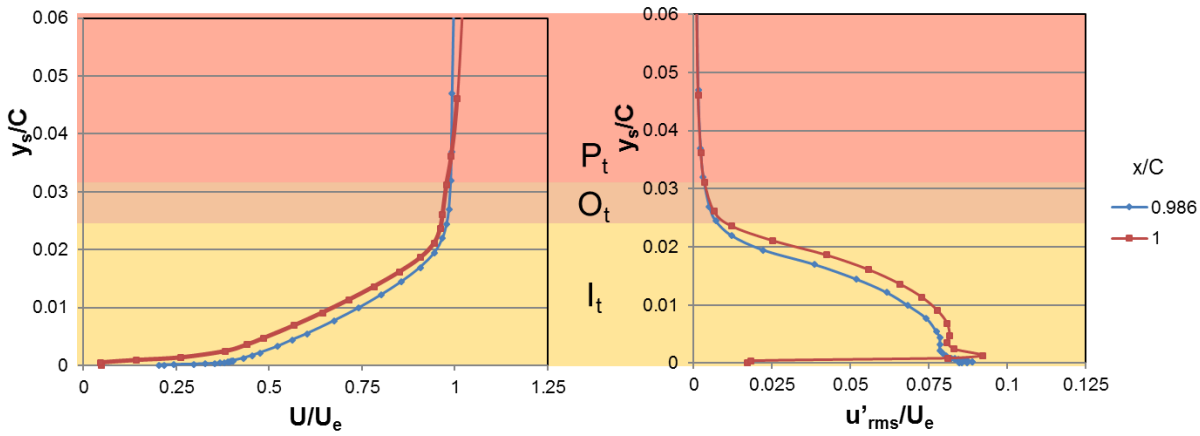

Figure 21. Three regions of interest shown in the TBL profile at x/C = 0.986, 1. α = 0°

المنارة للاستشارات
www.manaraa.com

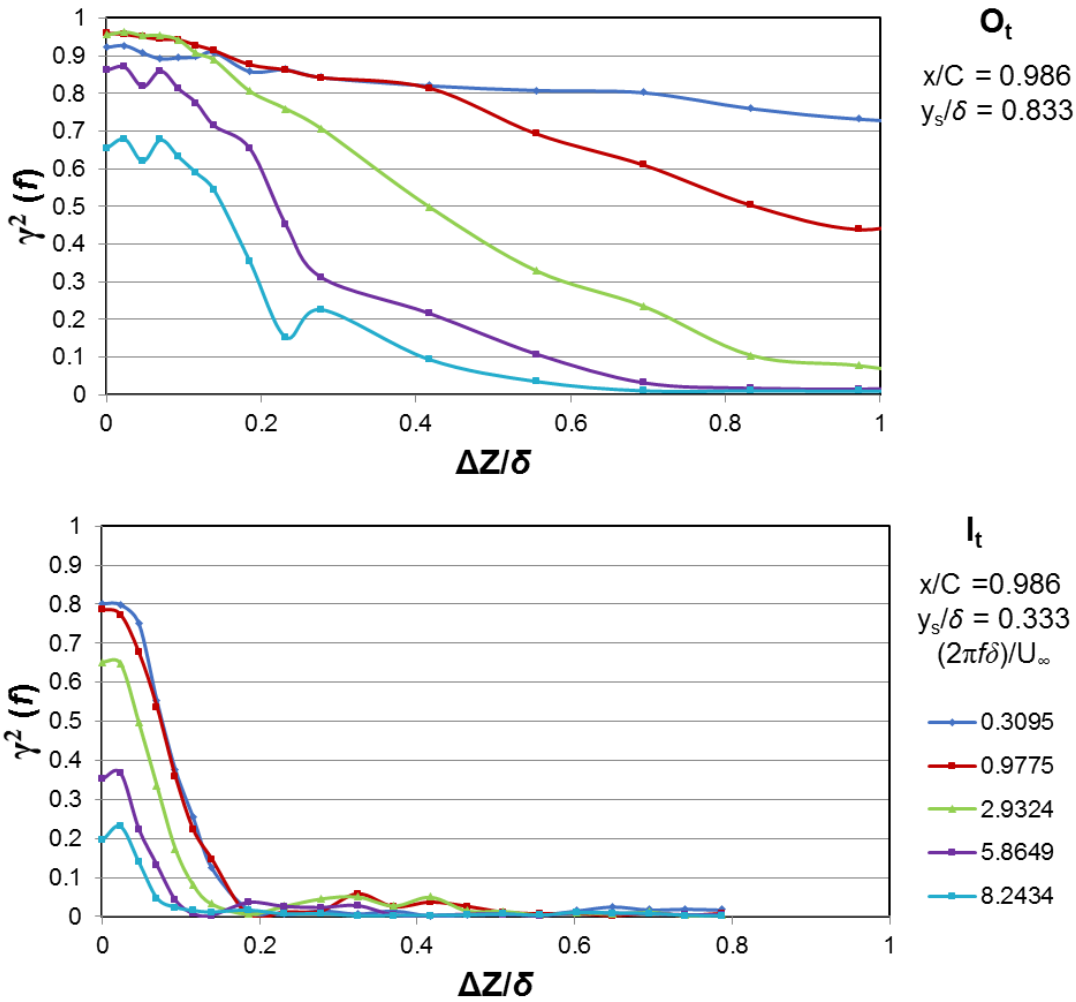

Figure 22. Spanwise coherence of structures in O_t and I_t at x/C = 0.986. α = 0°

3.1.2 Contour correlation data with respect to structures in O_t and I_t

For a broad understanding on how the flow structures in O_t and L_t interact with each other and are affected by the presence of a trailing edge, contour-correlation plots were generated. They show the spatial correlation of structures in these two regions as a function of time delay τ between the signals obtained at S and T. S was placed at a location in O_t (y_s = 0.833δ) and I_t (y_s = 0.333δ) respectively and T traversed along the x-y plane and y-z plane for each location of S, thus generating snap-shots of the evolution of structures in the

المنارة للاستشارات
www.manaraa.com

boundary layer near the trailing edge. Figures 23(a) and 23(b) show the evolution of structures in O_t and I_t respectively in the y-z plane (span). Figures 23(c) and 23(d) show the same along the x-y plane (stream). All these data are taken for S located at x/C = 0.986. The distances y_s, Δz and Δx are non-dimensionalized with respect to the boundary layer thickness ($\delta_{0.986}$ = 0.54 in) at x/C = 0.986 and Δt = 0.00016s.

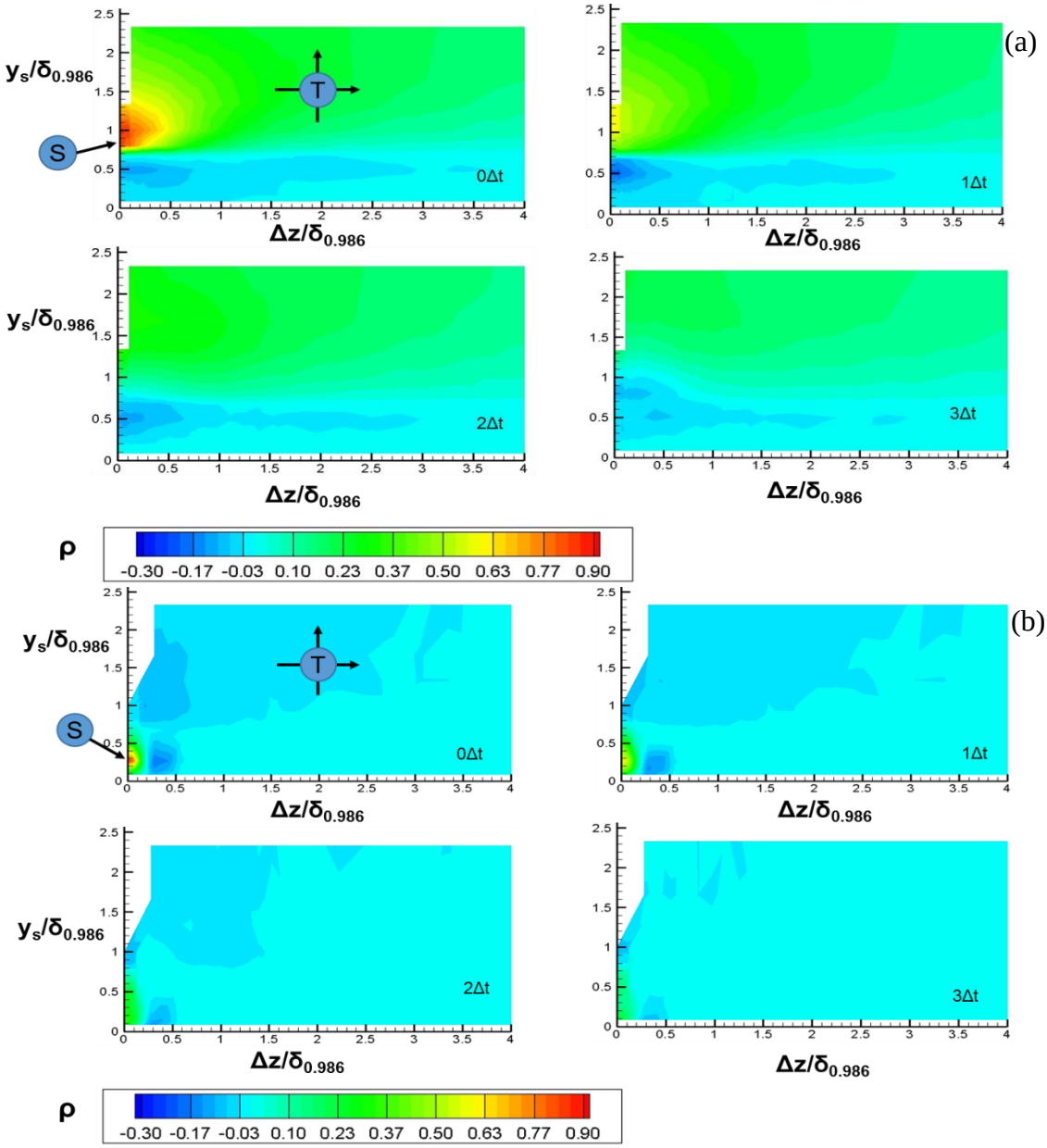

Figures 23(a and b). Evolution of structures in O_t and I_t respectively along the spanwise plane. S is located at x/C = 0.986 and Δt = 0.00016 s. α = 0°

المنارة للاستشارات
www.manaraa.com

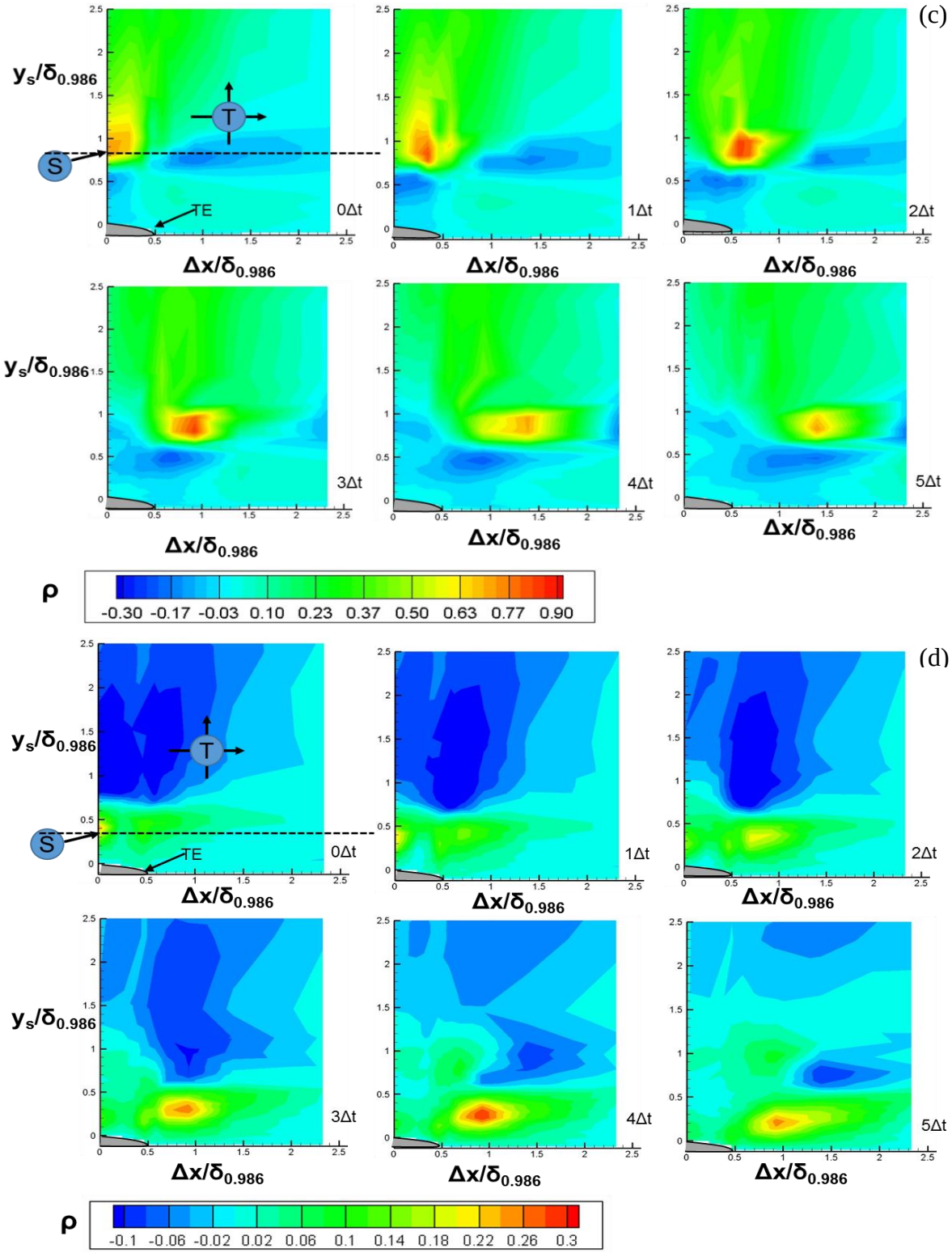

Figures 23(c and d). Evolution of structures in O_t and I_t respectively along the streamwise plane. S is located at x/C = 0.986 and Δt = 0.00016 s. α = 0°

المنارة للاستشارات
www.manaraa.com

Figure 23(a) with yz-correlation contours shows that the structures in O_t are anti-correlated with those in I_t. With the progression of time, they become anti-correlated with structures in O_t itself. This could be an indication of oscillating features that convect with the streamwise flow in this region. In terms of spanwise decay, structures are correlated to greater than $\approx 4\delta_{0.986}$ as seen in the previous section. Structures in I_t (figure 23(b)) are anti-correlated with those in O_t. The correlation magnitude decreases with time evolution as seen in figure 23(a) as well. They quickly decay to negative correlation values along the spanwise direction and level off to zero at $0.6\delta_{0.986}$ as seen before. At any given location (example, $\Delta z/\delta_{0.986} = 0$, $y_s/\delta_{0.986} = 0.2$) and with increase in τ, ρ does not change sign.

Correlation contours along the streamwise plane show that structures in O_t convect in the direction of flow (figure 23(c)). Structures in I_t (figure 23(d)) linger near the trailing edge and then convect at a much slower speed further downstream. To investigate this difference in behavior, cross sections across the x-y plane and at the location of S as shown in the xy-contour plots of figures 23(c) and (d) were taken. They are described in the following section.

3.1.3 Streamwise correlation of structures in O_t and I_t

Cross correlation plots for increasing Δt along the streamwise direction at these cross-sections were generated. Figure 24 shows the same. The streamwise correlation for structures in I_t (figure 24(a)) shows that there exists a combination of flow mechanisms. Close to the trailing edge at $0 \leq \Delta x/\delta_{0.986} < 0.7$, there exists a region where the flow structures do not move. Further downstream at $\Delta x/\delta_{0.986} \geq 0.75$, these eddies convect although at a low speed. Due to reduced grid resolution further downstream, the convecting speed could not be

المنارة للاستشارات
www.manaraa.com

quantified and clear conclusions on this matter cannot be drawn. Further research was done with higher grid spacing and the same was observed. In general, there seemed to be a presence of absolute instabilities superimposed on convective instabilities. This region near the trailing edge was termed to have "weak absolute disturbances". Flow particles here still advect downstream but the flow structure itself does not move. Figure 24(b) shows the streamwise correlation of structures in O_t. The structure clearly convects downstream. This reinforces what was observed in the spanwise contour plots. The peaks of the correlation curves at increasing τ were tracked and the corresponding convection (XT) plot is shown in figure 24(c). The slope of this line gives the speed at which the flow structure convects in O_t. It turned out to be $U_c \approx 0.8U_\infty$. Flow structures in O_t are therefore convective disturbances.

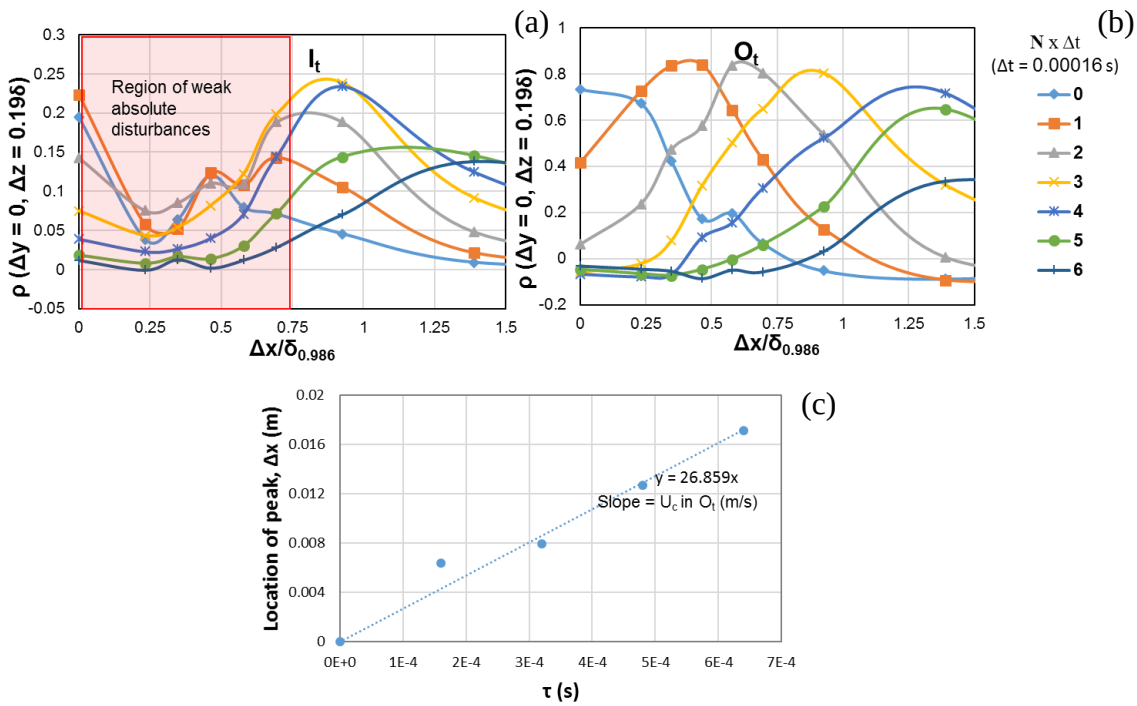

Figure 24. S is at x/C = 0.986. α = 0°. (a and b) Streamwise correlation of structures in I_t and O_t respectively. (c) XT plot with respect to structures in O_t

The same process was repeated with S moved to the trailing edge (x/C = 1). Similar conclusions were obtained. The relevant contour correlation figures are shown in the

المنارة للاستشارات
www.manaraa.com

appendix (a1, a2 and a3). A baseline for the interaction of the broadband flow structures in the turbulent boundary layer near the trailing edge was established. This could help in understanding the flow modifications that might occur with the addition of known working and failed TE noise reducing modifiers.

3.2 Reference trailing edge configuration at $\alpha = 5^{o}$

The main part of this research will explore the flow structures modified near the trailing edge at $\alpha = 5°$. The turbulent boundary layer generated near the trailing edge at this angle of attack is optimal for this study as it can be compared to what happens in practicality. Wake profile measurements taken at the trailing edge of the Sh (sharp TE) configuration were compared with those at the trailing edge of configuration B (blunt TE). They are shown in figure 25(a). Both the wakes are fully turbulent in nature. The effect of the Mylar tape used to fix the modifier to the sharp trailing edge is non-existent. There is no change in turbulence intensity that is usually associated with a surface bump in the very lower regions of the profile near the trailing edge of the airfoil. It can be seen that there is an increase in wake deficit associated with B. The shape of the velocity profile otherwise remains the same. The values of t/δ^* for the suction side of the airfoil for Sh and B are 0.23 and 0.37 respectively. On the pressure sides, t/δ_b^* takes the values 0.85 and 1.14 for Sh and B respectively. The vortex shedding limit of $t/\delta^* > 0.3$ is greatly exceeded on the pressure sides of both configurations. On the suction side, they are close to the limit. Turbulent vortex shedding from the pressure side is observed for both cases. The normalized power spectral density at u'_{max} on the suction (I_t) and pressure (I_b) sides are shown in figure 25(b). There is a wide hump and a peak at I_b for B. For Sh, sharp spikes are noticed without the hump. On the

المنارة للاستشارات
www.manaraa.com

suction side at I_t of both configurations, a broadband spectrum is mostly present. This is more prominent with the configuration B. The spectra are also compared with that from Sh at I_t and at α = 0°. It is to be noted that $t \approx 0.09$ in for the configuration B. It is a better reference than Sh while comparing with results from the serrations that have t ranging from 0.19 in at the root to 0.05 in at the tip. For the above stated reasons, B was chosen as the reference configuration at α = 5°.

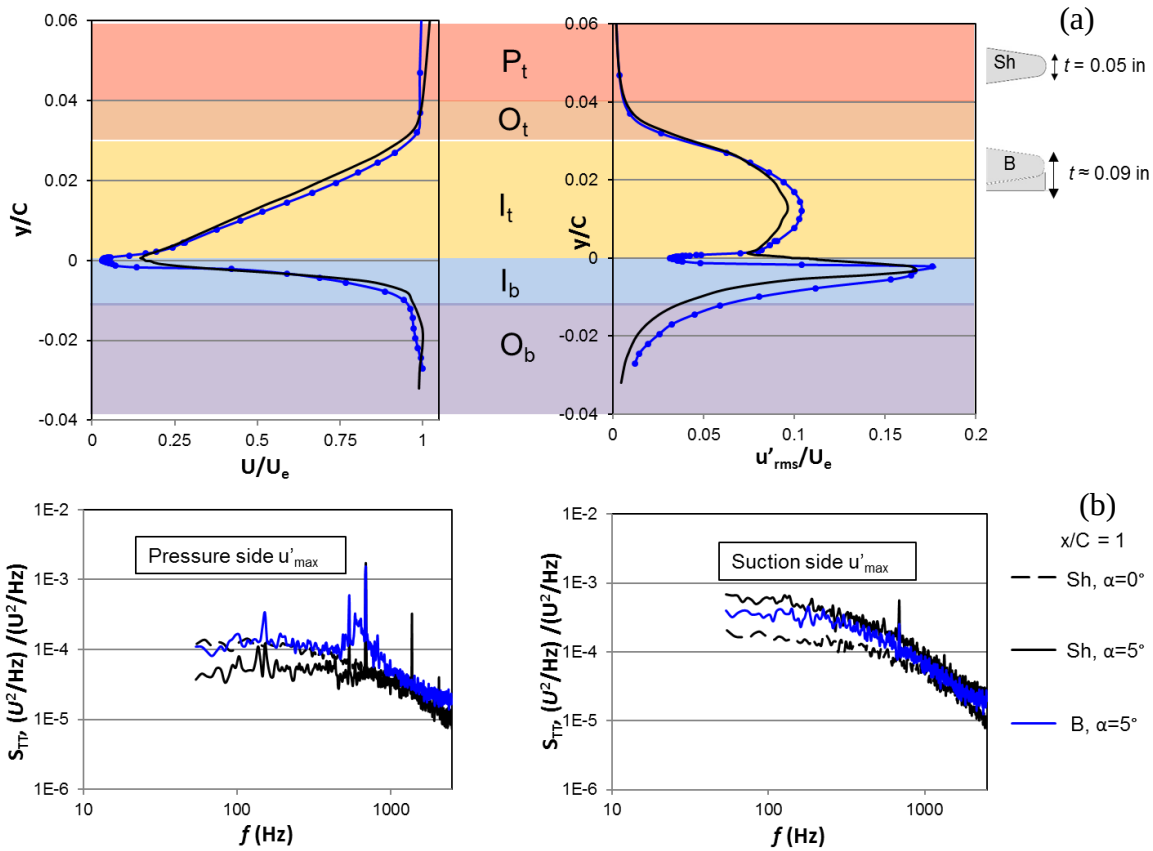

Figure 25. x/C = 1, α = 5°. (a) Wake profiles for Sh and B (b) Normalized power spectral densities at I_b (pressure side) and I_t (suction side) for Sh and B

3.2.1 Spanwise correlation of structures in the turbulent wake near the trailing edge

Similar to the spanwise correlation data near the trailing edge at α = 0°, correlation data was obtained with S and T simultaneously at various y_s location at x/C = 1. With S on

المنارة للاستشارات
www.manaraa.com

the suction side, distances were normalized with respect to BL thickness on the suction side δ at x/C = 1 (δ = 0.72 in). On the pressure side, distance normalization was with respect to BL thickness on the pressure side δ_b at x/C = 1 ($\delta_b \approx 0.54$ in). Figure 26 shows the same.

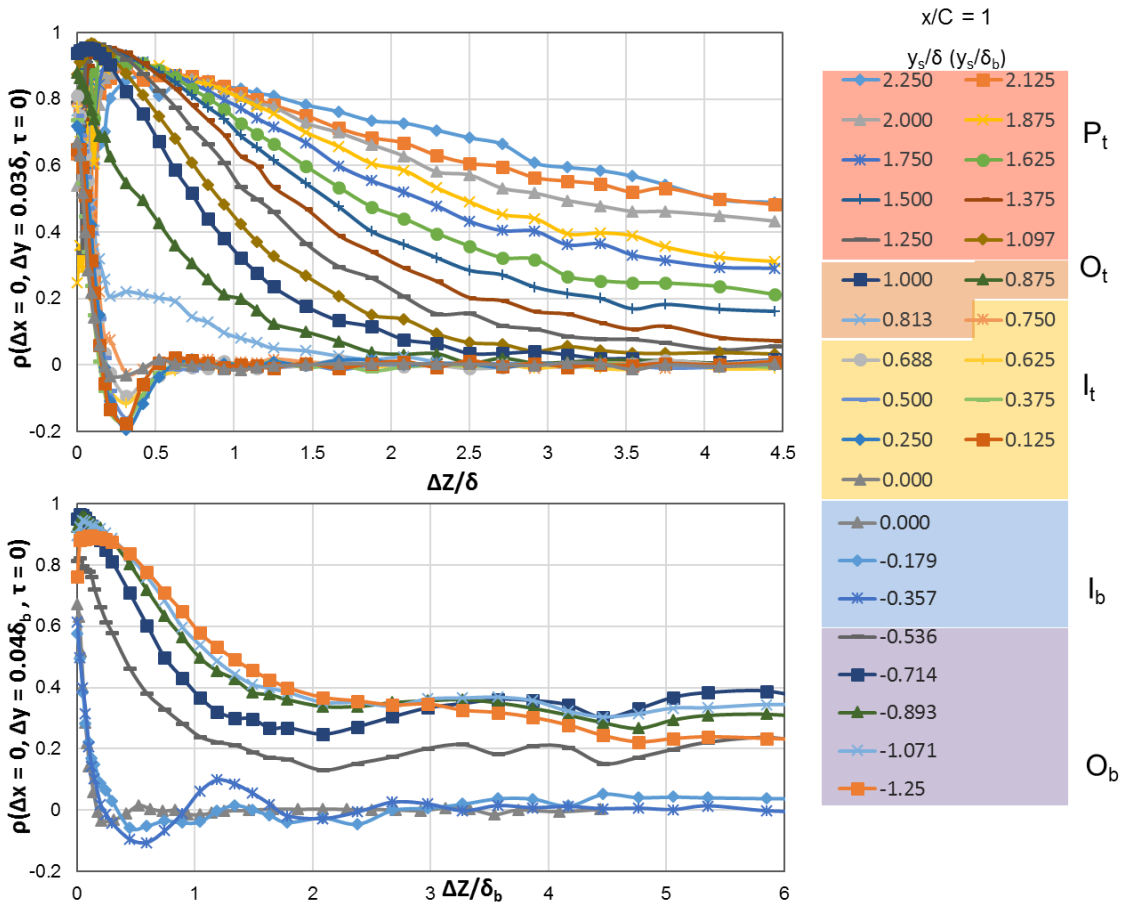

Figure 26. Regions of interest in the turbulent boundary layer (wake) from spanwise correlation data at x/C = 1. α = 5°

Similar to the conditions at α = 0°, three regions of interest I_t, O_t and P_t were identified on the suction side. Structures in I_t decayed within Δz = 0.6δ. Those in O_t decayed within Δz = 2.5δ, faster than their counterparts at α = 0°. Outside the boundary layer in P_t they do not decay even at Δz > 4δ. The transition of decay characteristics from I_t to O_t is very sharp. On the pressure side, two regions of interest were identified: the inner-bottom region I_b and outer-bottom region O_b. The behavior here is quite different from the suction side.

المنارة للاستشارات
www.manaraa.com

Though the structures in I_b decay fast, they generally oscillate in direction about $\rho = 0$ until $\Delta z \approx 1.75\delta_b$ before settling to 0. This is an indication of the high energy correlated structures that generate tonal noise from the pressure side. In the outer region O_b, a similar trend is observed. The structures do not decay to zero even beyond $\Delta z > 6\delta_b$. The oscillating nature of structures along the span can be observed. There was no clear distinction between the O_b layer and any potential layer on the pressure side. Though the basic flow mechanisms causing broadband noise and tonal noise might be similar, we chose to narrow our study to trailing edge broadband noise. Therefore, further study using serrations was limited to the regions of interest on the suction side. For sake of completion, contour correlation data in the spanwise and streamwise planes are provided for the structures in the I_b region of the turbulent boundary layer near the trailing edge. Figure 25 shows the regions of interest in the fully turbulent wake near the trailing edge.

3.2.2 Contour correlation data with respect to structures in O_t, I_t and I_b

Figures 27(a to f) show the evolution of flow structures (using correlation contours) along the spanwise and streamwise planes at each region of interest: O_t, I_t and I_b (S at y = 0.9δ, 0.25δ, $-0.167\delta_b$ respectively). The spanwise evolution of structures in the O_t and I_t region (figures 27(a) and 27(b)) are quite similar to that at $\alpha = 0°$. Structures in the I_b region (figure 27(c)) are of higher energy and are correlated over large distances and time in the y-z plane. This indicates the presence of high energy vortex structures.

Flow structures in O_t (figure 27(d)) convect downstream while being asymmetrically related to regions in the turbulent wake on the pressure side. Flow structures in I_t (figure 27(e)) show the previously stated combined mechanism: they have a near wake region of

المنارة للاستشارات
www.manaraa.com

weak absolute disturbances and a far-wake region of convective disturbances. On first glance, one can say that structures in I_t convect downstream at a much slower speed than those in O_t. The structures in I_b (figure 27(f)) exhibit a region near the trailing edge (starting slightly upstream from the trailing edge) with absolute disturbances. This seems to combine with convecting and shedding structures.

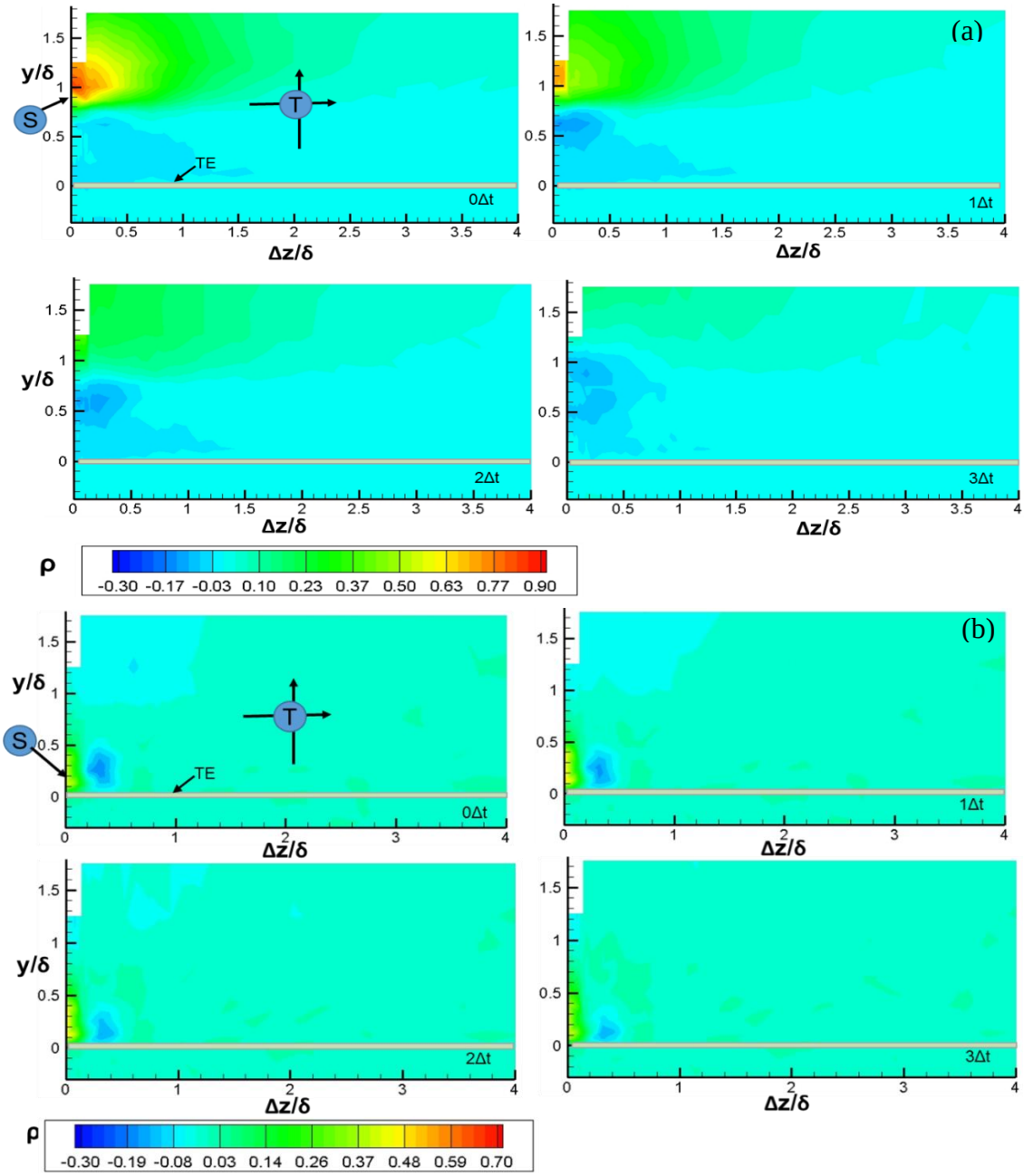

Figures 27(a and b). Evolution of structures in O_t and I_t respectively along the spanwise plane. S is located at x/C = 1 and Δt = 0.00016 s. α = 5°

المنارة للاستشارات
www.manaraa.com

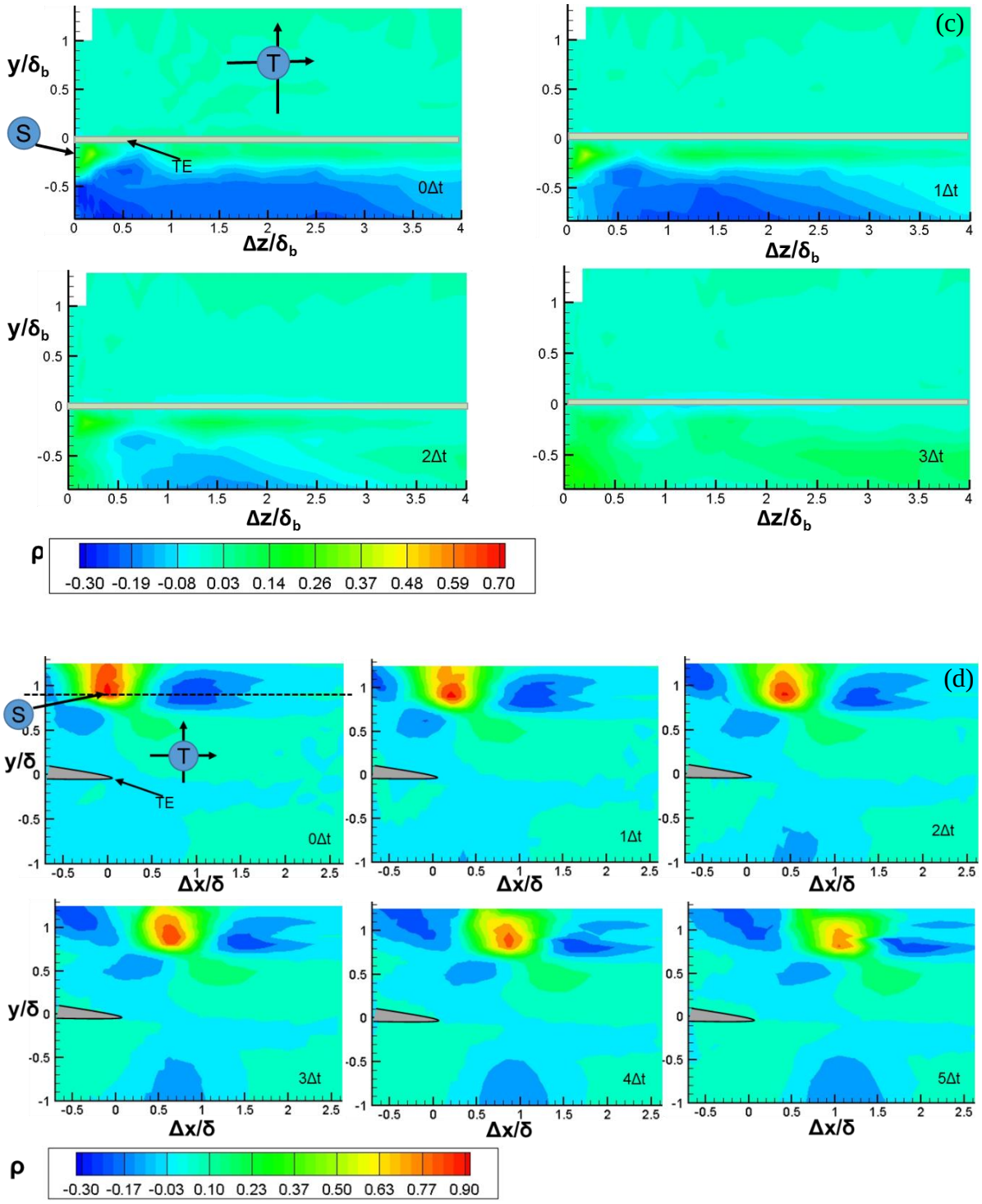

Figures 27(c and d). Evolution of structures in I_b along the spanwise plane and O_t along the streamwise plane respectively. S is located at x/C = 1 and Δt = 0.00016 s. α = 5°

المنارة للاستشارات
www.manaraa.com

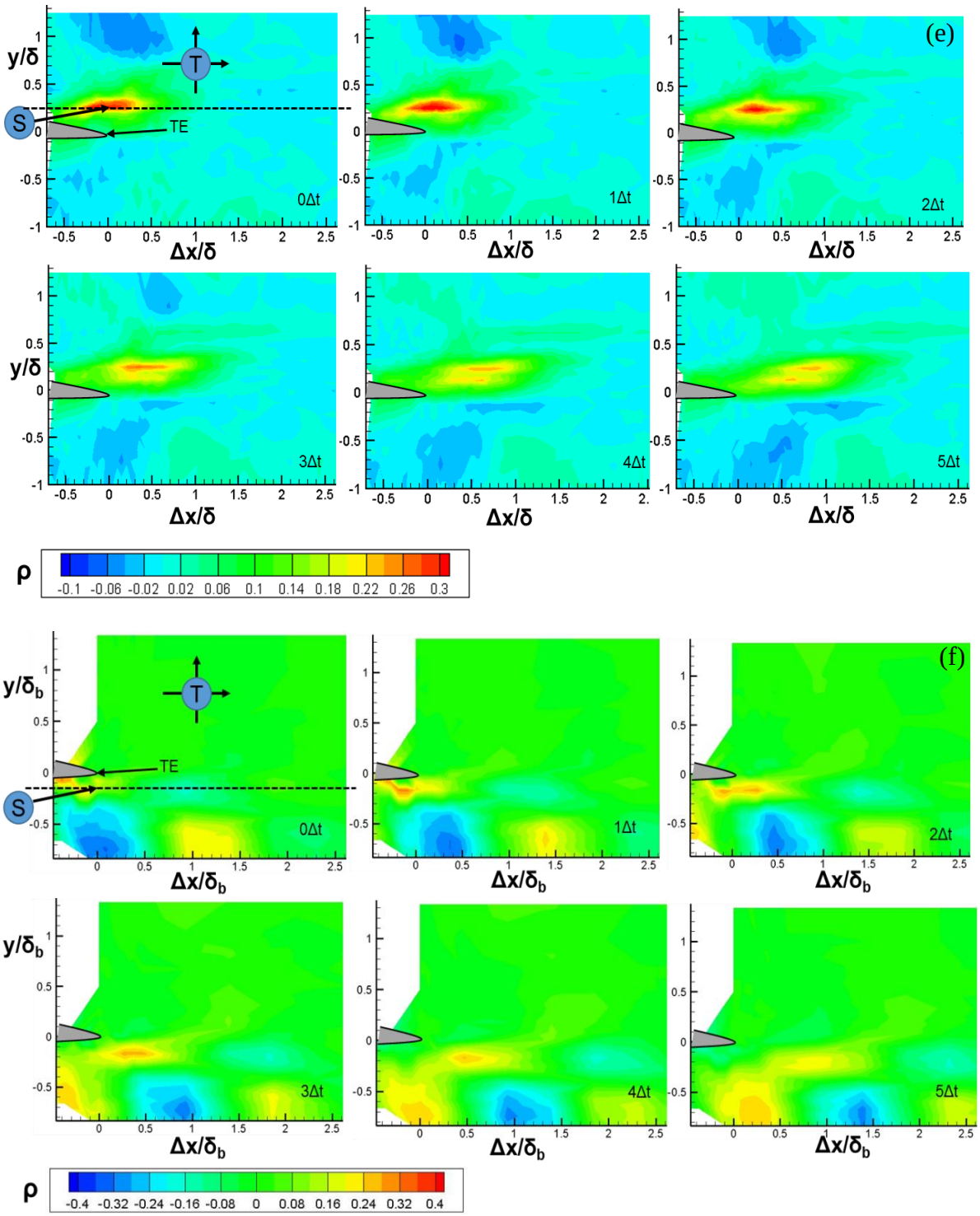

Figures 27(e and f). Evolution of structures in I_t and I_b respectively along the streamwise plane. S is located at x/C = 1 and Δt = 0.00016 s. α = 5°

المنارة للاستشارات
www.manaraa.com

3.2.3 Streamwise correlation of structures in O_t, I_t and I_b

Cross correlation plots for increasing τ along the streamwise direction with respect to structures in O_t, I_t and I_b are shown in figure 28. They are taken at cross-sections marked in figures 27 (d), (e) and (f) respectively. Structures in I_t are weak absolute disturbances near the trailing edge ($-0.5 \leq \Delta x/\delta < 0.5$) and convective disturbances ($U_c \approx 0.65U_\infty$) further downstream ($\Delta x/\delta > 0.9$). The region of weak absolute disturbances seems to have absolute disturbances super-imposed on convecting structures similar to the Sh configuration at $\alpha = 0°$. The structures in O_t convect with a speed $U_c \approx 0.8U_\infty$. The structures in I_b are similar to those in I_t but for the fact that the disturbance that lingers near the trailing edge changes sign with time. This is indicative of a high energy vortex shedding phenomenon. Further downstream, the disturbances are convective in nature.

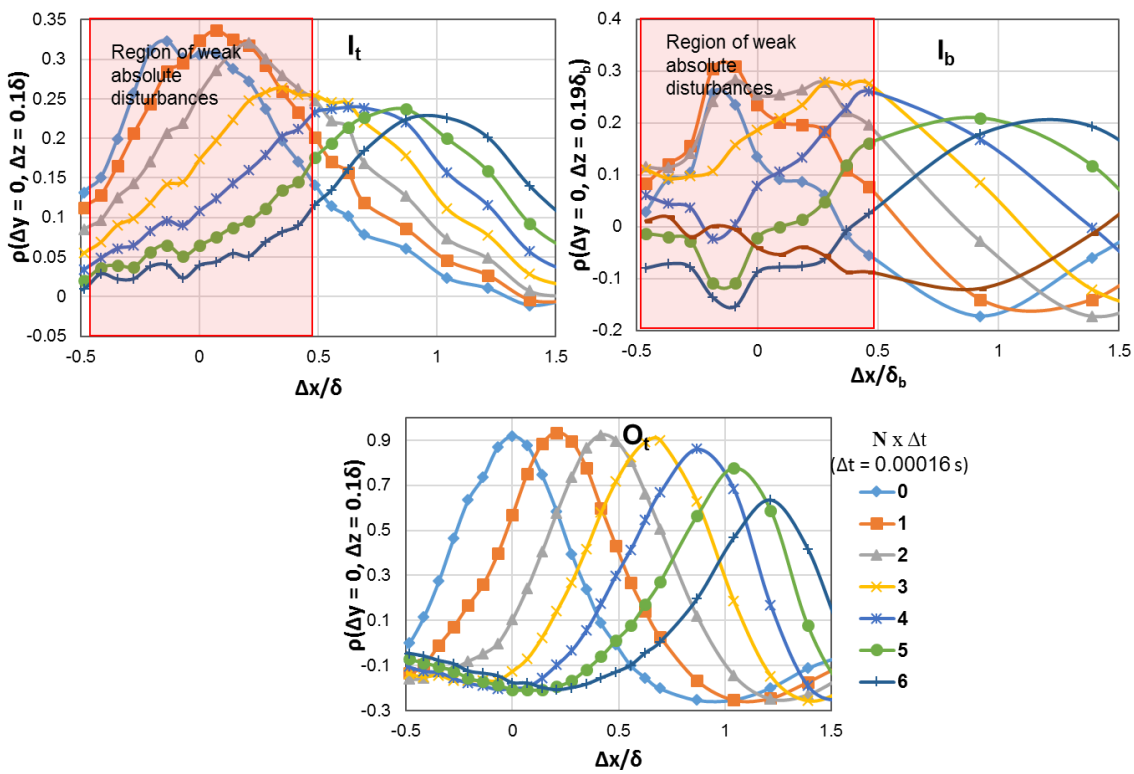

Figure 28. Streamwise correlation of structures in O_t, I_t and I_b. S is at x/C = 1. $\alpha = 5°$

المنارة للاستشارات
www.manaraa.com

Conclusions were made for the reference TE configuration B at $\alpha = 5°$: The flow-structures in the two regions of interest O_t and I_t decay as a Gauss function and approximately as a strongly damped sinusoid respectively in the spanwise direction. In I_t, near the trailing edge, there is a region of weak absolute disturbances followed further downstream by a convective zone of speed $U_c \approx 0.65U_\infty$. The flow structures in O_t are purely convective in nature ($U_c \approx 0.8U_\infty$). These characteristics were established as the baseline for comparison with known serrated TE modifiers.

3.3 Effect of serrations on boundary layer development and flow structures near the trailing edge

The first serrated trailing edge that was installed was L2W4 (refer to table 1 of section 2.2.2 - TE modifiers) with dimensions $2h = 2.9\delta$ and $\lambda = 0.5\delta$ ($\delta = 0.72$ in, measured at trailing edge of reference configuration B at $\alpha = 5°$). Figure 7 in section 2.2.2 shows the serration nomenclature used in the study. All serrated trailing edge measurements were made at $\alpha = 5°$. From previous research (Gruber, M et al. (2011)) a serrated trailing edge with similar dimensions was shown to reduce noise over the low to middle frequency range and increase noise in the high frequency range with a net decrease of TE noise over all measured frequency ranges under similar flow conditions. The changes in flow structures near the trailing edge that occur due to the presence of the added serration could therefore explain the noise reduction mechanism of serrated trailing edges.

Boundary layer and wake profile measurements made near the root, t_s-root, tip and r_s-tip locations of the serrated trailing edge L2W4 (red) are shown in figure 29. They are contrasted with the profiles from B (blue). The color codes used while comparing between trailing edge configurations are specified in table 1 of section 2.2.2. $y_{s\ at\ tip}$ is the local y_s coordinate at the

المنارة للاستشارات
www.manaraa.com

tip ($y_{s\ at\ tip}$ = 0). The mean velocity profiles measured at the root are very similar to that measured at the trailing edge of B. The shape of the turbulence intensity profiles at these locations remains the same but the profile at the root position shrinks in size when compared to that at t_s-root position. The same trend was observed for all serrations. The effect of the lip of the serration modifier (figure 5 of section 2.2.2) at the root and the tip is minimal but still exists as can be seen near $y_s = 0$ in the turbulence intensity plots. This effect is non-existent at the measurement points for correlation data (i.e., I_t and O_t). The wake velocity profiles at the tip and r_s-tip are more developed when compared to that at the trailing edge of B. At r_s-tip, the wake is most developed and rises as a result of mixing with the flow from the pressure side. The turbulence intensity profile at r_s-tip represents this phenomenon better. The difference in u'_{max} between the suction and pressure side at this point is greatly reduced, indicative of energy transfer between the r_s-tip and tip regions, top and bottom sides of the wake. All this preliminary data points to a possible existence of a three dimensional structure near the serration.

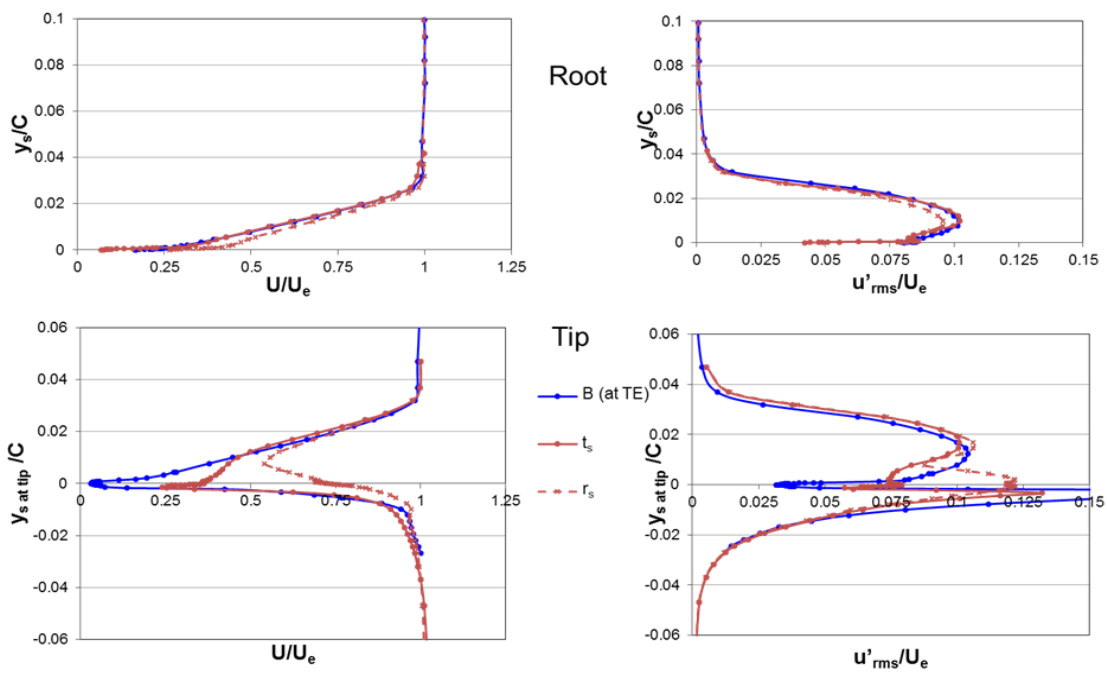

Figure 29. Turbulent boundary layer and wake development near the serration L2W4

المنارة للاستشارات
www.manaraa.com

Contour correlation data in the spanwise and streamwise planes were obtained with respect to flow structures in O_t and I_t regions of the turbulent boundary layer (or wake) at the root and r_s-tip positions. As the wake rises at the r_s-tip position (figure 29), the $y_s = 0$ location shifts up by 0.01C. The corresponding I_t ($\approx 0.25\delta$) and O_t ($\approx 0.9\delta$) locations at r_s-tip were also shifted up by the same value and scaled with respect to the new δ on the suction side. All distances were non-dimensionalized with respect to $\delta = 0.72$ in, measured at the trailing edge of the reference configuration B at $\alpha = 5°$. Figures 30(a) and 30(b) show the correlation of structures in the y-z plane at O_t and I_t respectively near the root. The trend does not vary from the baseline configuration B. Streamwise contour data at O_t (root) shown in figure 30(c) follows a similar trend as B. Structures in I_t (root) seem to convect faster (figure 30(d)) and the region of weak absolute instability might be reduced in size. A closer look at all these changes using correlation data at cross-sections and convection plots showed clear changes in behavior with respect to the baseline flat trailing edge B and are discussed in later sections. Figure 31(a) shows the spanwise evolution of structures in the I_t region at r_s-tip. It is possible to see that there are alternating regions of positive and negative correlation that coincide with the periodic shape of the serration. This is indicative of an organized three dimensional structure with a spanwise length scale similar to the width of the serration. Figure 31(b) shows the structures in I_t (r_s-tip) and in the streamwise plane traveling faster than their counter-parts in configuration B. The presence of the absolute instabilities in I_t near the r_s-tip is now absent. A closer look at these differences is required. Previous studies (Howe, M. S (1978), Amiet, R. K (1975), Howe, M. S (1991)) state that noise is generated by highly correlated structures in the spanwise direction and is proportional to their wetting length of the trailing edge. Researchers (Finez, A et al. (2010), Howe, M. S (1991)) therefore indicate

المنارة للاستشارات
www.manaraa.com

that de-correlating them and/or reducing their effective spanwise wetting length using serrations and other TE modifiers would reduce noise. We suggest that the process is more complicated than simply de-correlating structures near the trailing edge. For one, the absence of a region of absolute instability near the serration seems to play an important factor in noise reduction as will be proven by the use of known “good” and “bad” serrations.

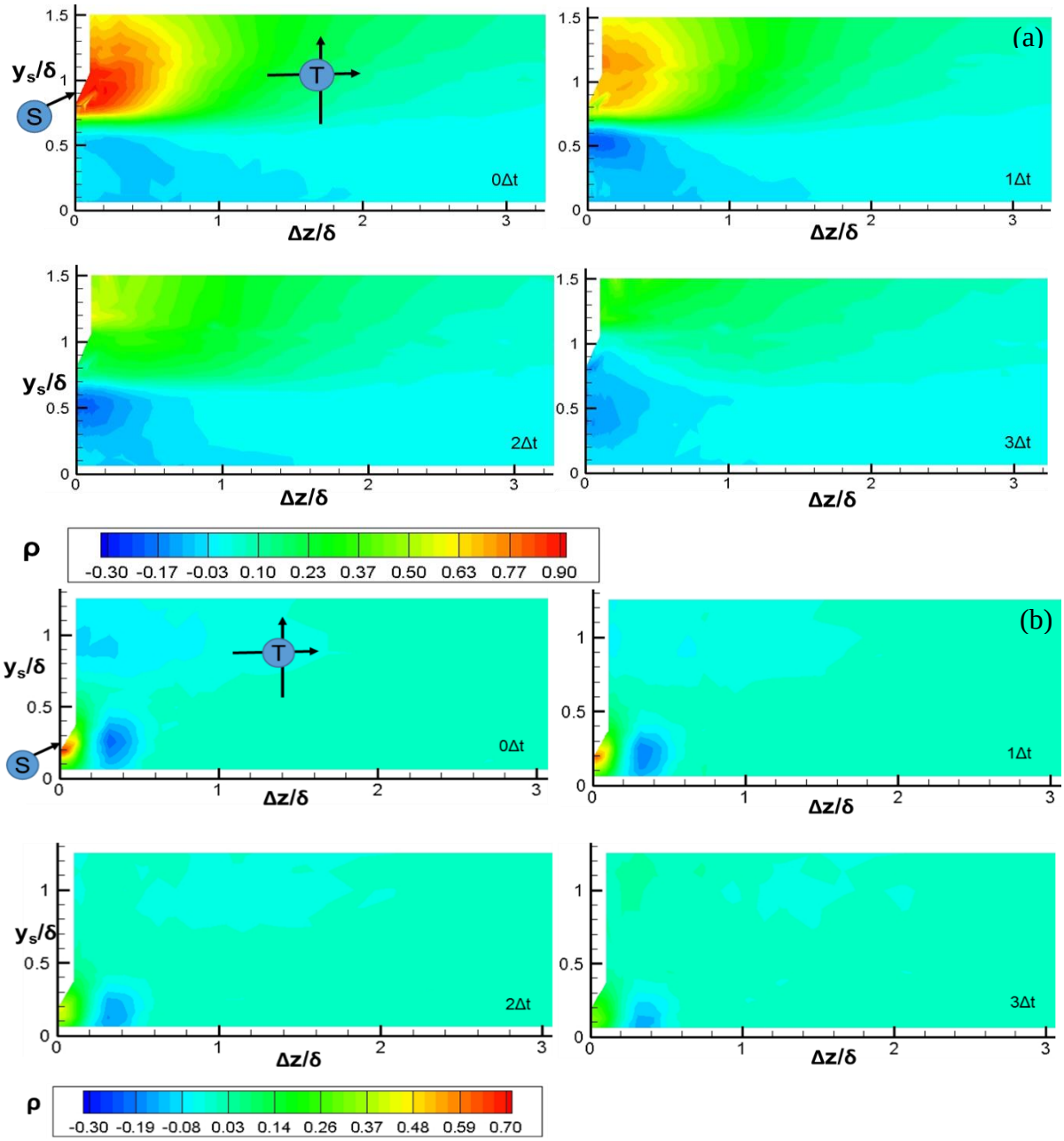

Figures 30(a and b). Evolution of structures in O_t and I_t respectively along the spanwise plane. S is located at the root and $\Delta t = 0.00016$ s

المنارة للاستشارات
www.manaraa.com

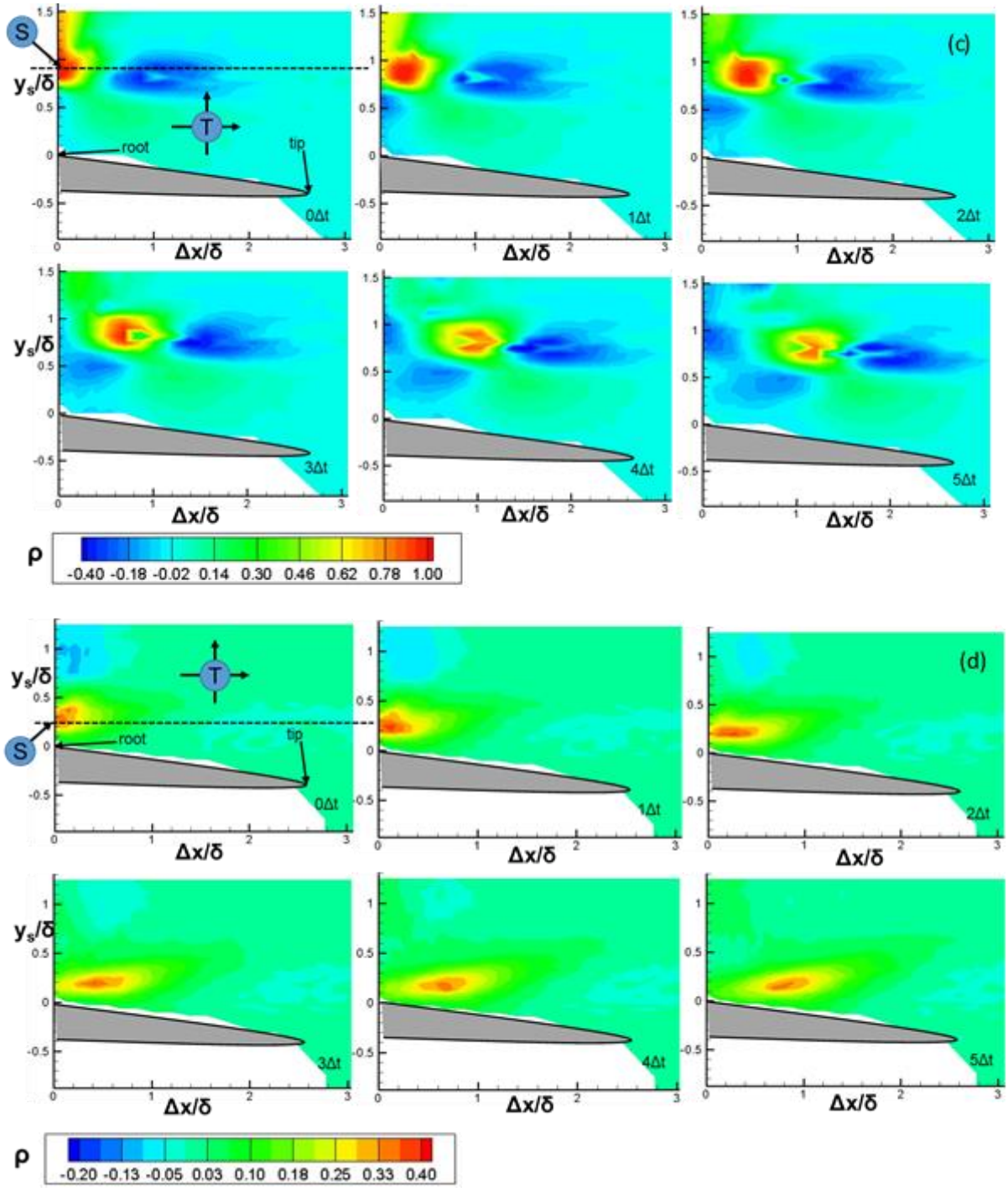

Figures 30(c and d). Evolution of structures in O_t and I_t respectively along the streamwise plane. S is located at the root and $\Delta t = 0.00016$ s

المنارة للاستشارات
www.manaraa.com

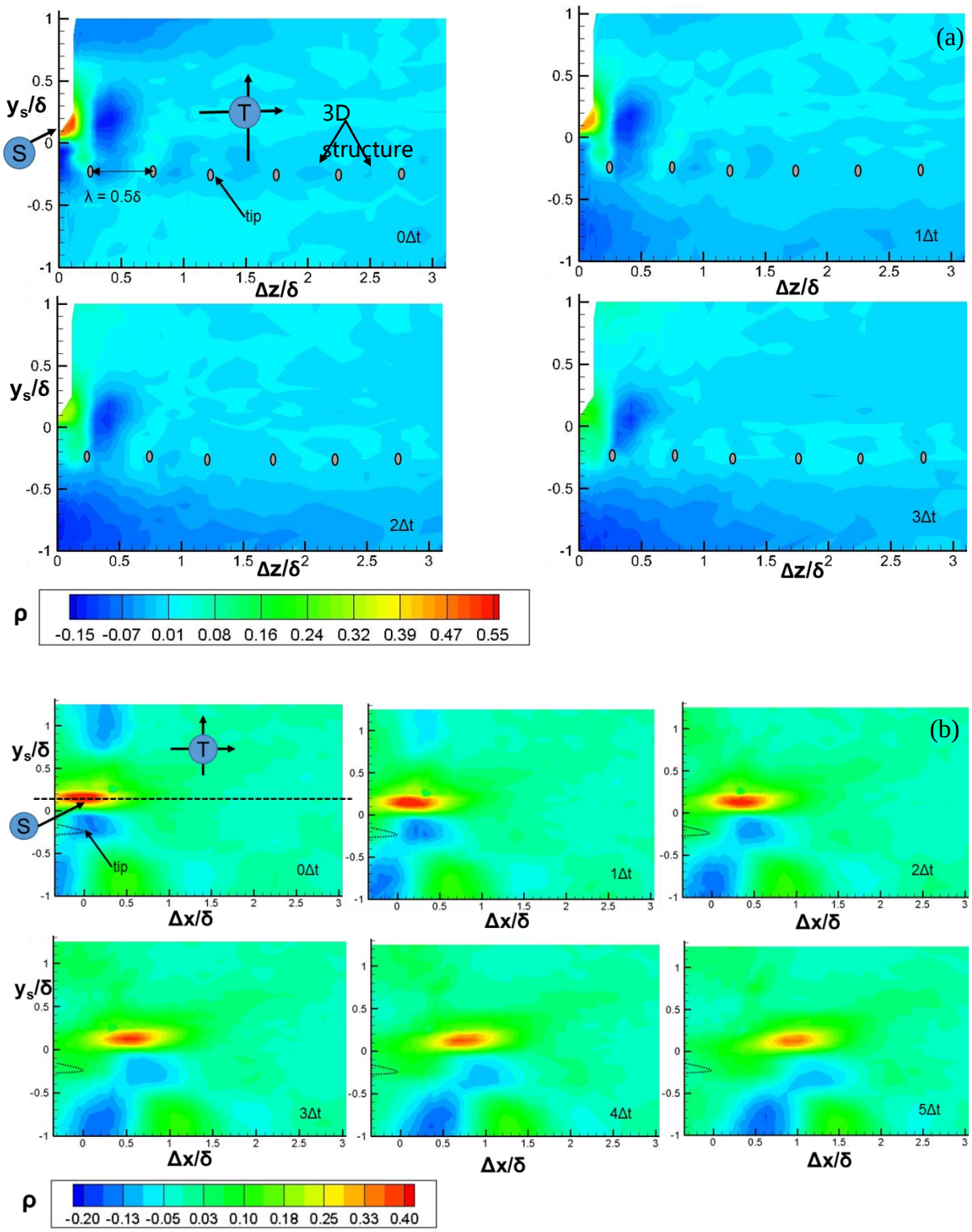

Figure 31(a and b). Evolution of structures in I_t along the spanwise plane and streamwise plane respectively. S is located at r_s-tip and $\Delta t = 0.00016$ s

المنارة للاستشارات
www.manaraa.com

The presence of this new three dimensional structure may affect noise generation, but to what extent is to be explored in further detail.

3.4 Effect of trailing edge thickness on flow structures

For the purpose of our study, it is undesirable for the modification geometry and not the serrations to alter the flow structures near the trailing edge. For this reason, 2 modifications F1 and F2 of various TE thicknesses (*t*) were studied. They differ from the serrations in that they do not have serrations (they are flat) and they extend the chord of the airfoil over ≈ 1.2 in (refer to section 2.2.2 for more details on these modifiers). Previous studies (Henderson, B et al. (2004), Brooks, T. F et al. (1989), Hutcheson, F.V and Brooks, T. F (2004)) show that an increase in trailing edge thickness corresponds to an increase in both broadband and tonal noise. Knowing that sharpness decreases noise, its effect on the weak absolute disturbances near the trailing edge in I_t (as seen in configuration B) needed to be investigated. A total of 4 flat trailing edges (Sh, B, F1 and F2) were used in this study ($\alpha = 5°$). Figure 32 shows the wake profile at the trailing edges of these configurations. Though the general shape remains the same, the blunt trailing edges (B and F2) show the highest wake deficit. The effect of the modifier geometry itself on the wake is minimal. This is more prominent on the suction side. One can conclude that major changes in flow structures that are observed on the suction side near a serrated TE modifier are functions of the serration and the TE thickness alone. The trailing edge Sh and F1 have the same thickness. The wake deficit of F1 is smaller than that of Sh. This can be accounted to the extra 1.2 in of chord that helps in the development of the turbulent boundary layer towards the trailing edge.

المنارة للاستشارات
www.manaraa.com

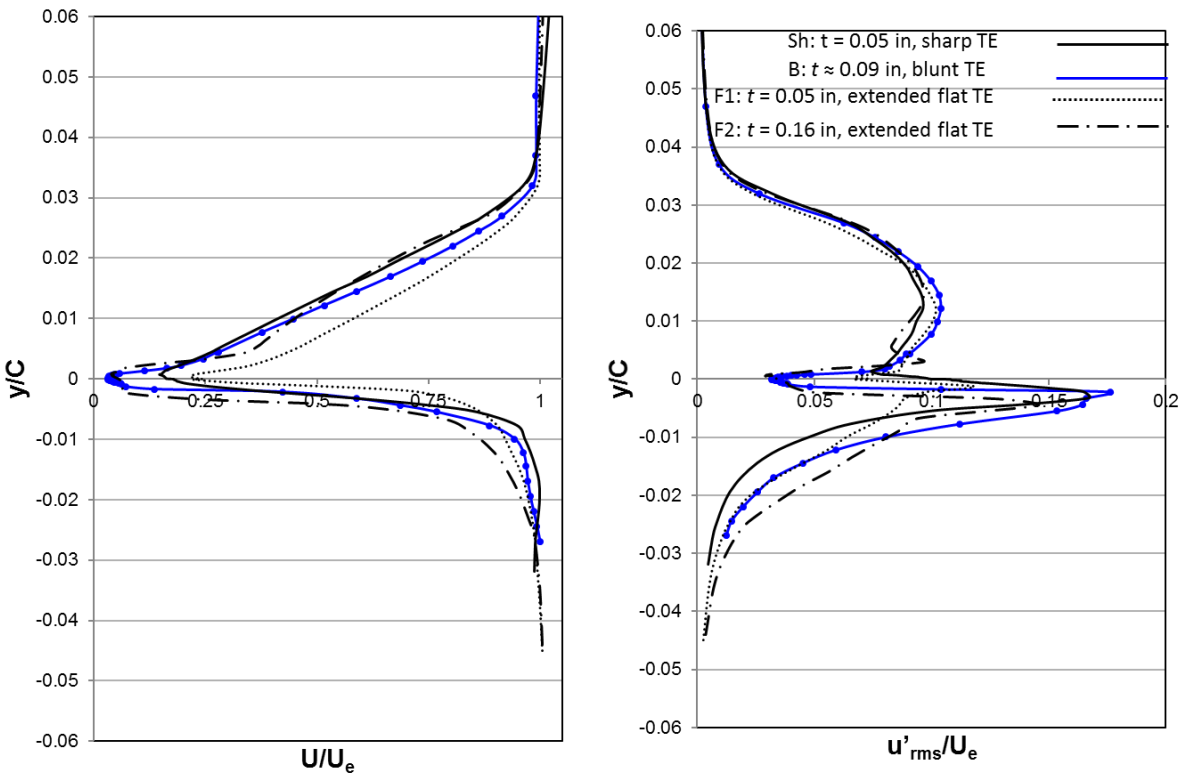

Figure 32. Wake profiles measured at flat trailing edges of various thicknesses

In order to study the effect of trailing edge thickness on the weak absolute disturbances in I_t near the trailing edge, streamwise correlation data were obtained for the four flat TE configurations. Figure 33 shows the correlation of structures in I_t evolving in the streamwise direction over time for configuration F1 (thinnest) and F2 (thickest).

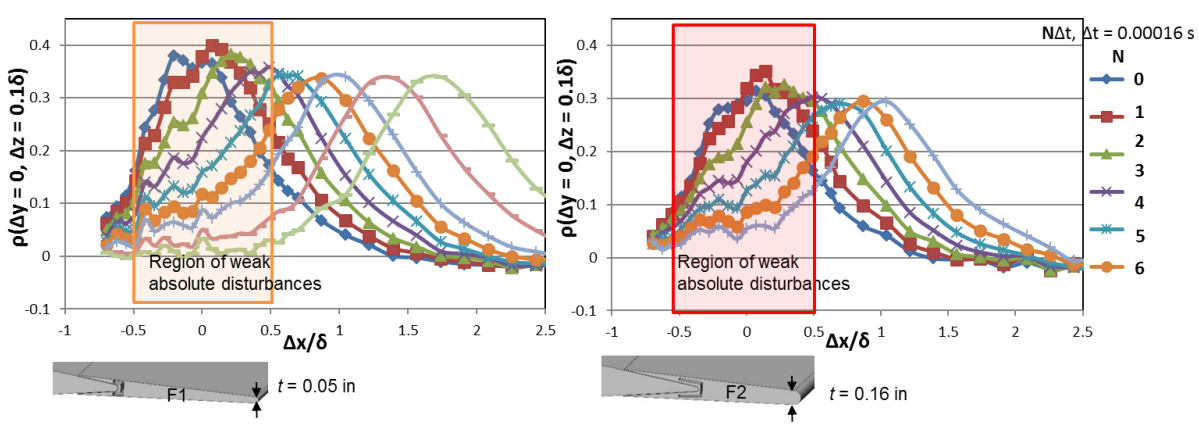

Figure 33. Evolution of structures in I_t near the trailing edge in the streamwise direction (F1 and F2)

المنارة للاستشارات
www.manaraa.com

The region near the trailing edge in both the cases seem to have structures of weak absolute disturbances (figure 33). It can also be seen that the structures associated with F2 are more pronounced and broader in size. To explore this quantitatively, convection plots for all the 4 flat TE configurations were generated. Gaussian curves were fit to the correlation data at increasing τ and the peaks were tracked. The resulting XT curves are shown in Figure 34(a). The x-location of the travelling Gaussian peak with respect to S in I_t is non-dimensionalized with respect to boundary layer thickness δ at the trailing edge of B. The slope of the XT plot gives the convective speed of the structure. The XT plot is divided into 2 regions of interest. The first one is close to the trailing edge that is dominated by weak absolute disturbances and the second is further downstream with convective disturbances. Region 1 is shown in the expanded view in the red box. It can be seen that the slope in the first region is very shallow and the peak shifts downstream of the trailing edge with increasing thickness. There was some spanwise variation with respect to slope in the second region. Even though the slope in the second region was consistently greater than that in the first as a consequence of convective structures, a trend could not be established between the 4 TE configurations as a result of the spanwise variation. This variation was absent with serrations as the three-dimensional structure dominated in the spanwise direction. The wake deficit given by the maximum value of $(U_e - U)/U_e$ along the wake velocity profile for each configuration was plotted against the non-dimensionalized convective speed (U_c/U_∞) in each region (figure 34(b)). It can be seen that there is a definite relation between wake deficit and convective speed of flow structures in region 1. A larger wake deficit is associated with a slow speed indicative of the presence of weak absolute disturbances. Sharpness transitions an

المنارة للاستشارات
www.manaraa.com

unsteady wake into an unsteady mixing layer. Region 2 does not give conclusive results for the above stated reasons.

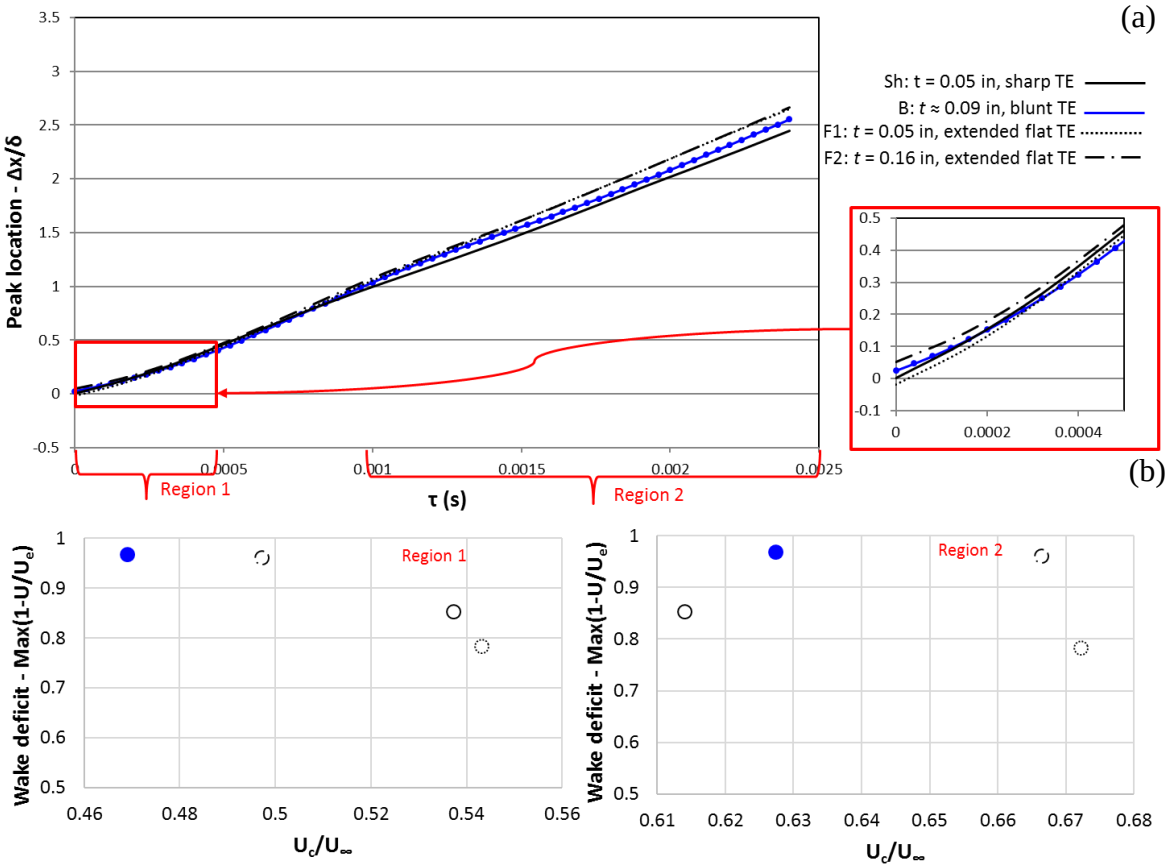

Figures 34(a and b). Effect of trailing edge thickness on structures in I_t near the trailing edge

From these observations, we conclude that absolute disturbances in the I_t region of the turbulent wake near a trailing is one of the major sources of TE noise. Their interaction with the trailing edge could be a major flow mechanism that causes TE noise. It also reinforces the observation made before that the changes associated with these very flow structures in I_t near the trailing edge L2W4 could be one of the noise reducing mechanisms associated with serrated TE modifiers. Further research with serrations we know to be effective ("good") and bad with respect to noise-reduction was performed and a better understanding into this relation between noise reduction and convective flow structures was obtained.

المنارة للاستشارات
www.manaraa.com

Convection plots were generated for structures in O_t near the trailing edge for the various flat TE configurations. There was no noticeable trend between the configurations in this region. They convected with an average speed $U_c \approx 0.75U_\infty$ to $0.8U_\infty$. The figure is shown in the appendix (a4).

The spanwise correlation curves were obtained for structures in I_t and O_t. They are shown in figure 35. The spanwise correlation in I_t is the same for all configurations. In O_t, though quite similar, the thickest trailing edge F2 shows a slightly higher decay rate.

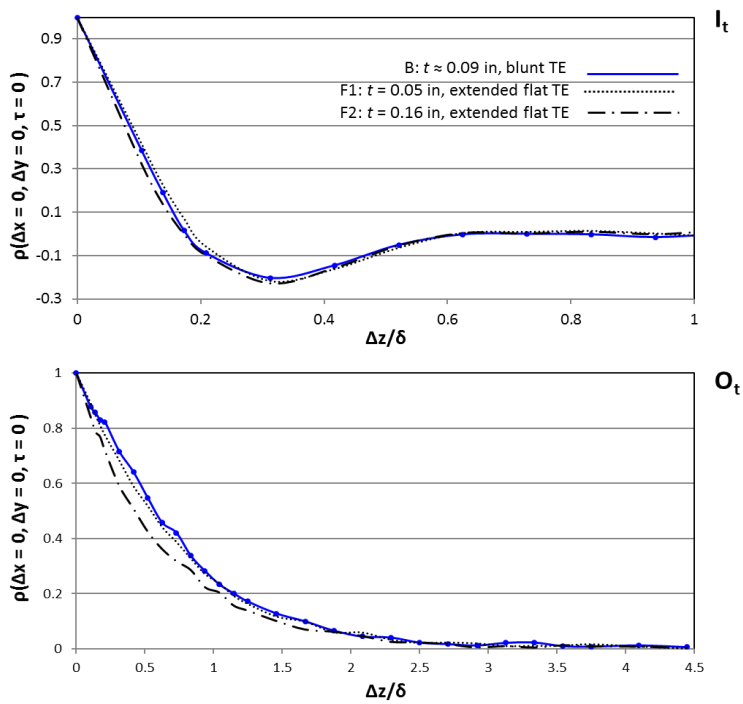

Figure 35. Spanwise correlation of structures in I_t and O_t at trailing edges of flat edged configurations

3.5 Effect of length of a serrated trailing edge on flow structures

Previous studies (Gruber, M et al. (2011)) have shown that serrated trailing edges with length $1\delta < 2h \leq 4\delta$ are the most effective at noise reduction, with the best performance at largest lengths. They also showed that any further increase in length does not increase the effectiveness of the serration. To explore the effect of length on the flow structures near the

المنارة للاستشارات
www.manaraa.com

trailing edge, 3 configurations, L1W2, L2W4 and L3W1 (refer to table 1 in section 2.2.2) were used at α = 5°. They have the same width λ = 0.5δ. Their lengths are 2h = 1.4δ, 2.9δ and 4.3δ respectively. They cover the spectrum of serrations that usually reduce noise under similar flow conditions. Contour data taken with L2W4 as shown in section 3.3 narrowed the field of interest to structures in I_t and O_t near the root and r_s-tip of the serration. Therefore, wake profiles, streamwise and spanwise correlation data of structures in I_t (≈ 0.25δ) and O_t ≈ (0.9δ) at the root, r_s-tip and tip positions were used in this analysis. The results were compared with data at the trailing edge of the reference configuration B at α = 5°.

Figure 36 shows the wake profile and power spectral density at y_s locations of maximum turbulence intensity (in I_t and I_b) measured at the r_s-tip location. The mean velocity and turbulence intensity profiles show that the wake rises with increase in length, a result of mixing and the wake deficit reduces with increase in length, a result of wake development. The spectra in I_t remains about the same between configurations. In I_b, the longest modifier (L3W1) shows a decrease in peak intensity and an increase in decay rate across frequency.

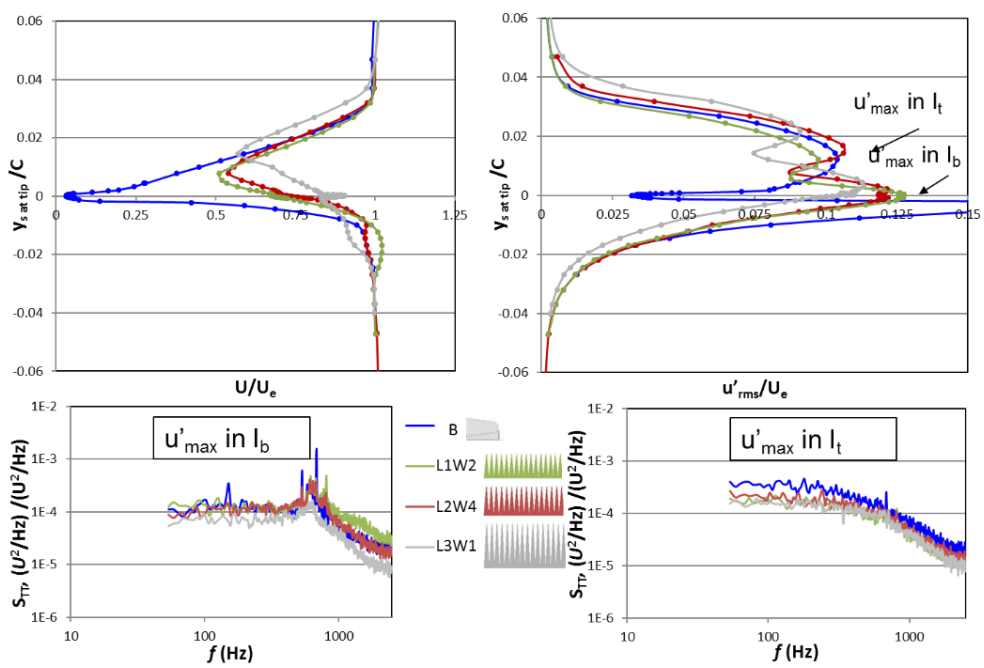

Figure 36. Wake profiles measured at r_s-tip of serrations of different lengths

المنارة للاستشارات
www.manaraa.com

XT plots at I_t near the root, r_s-tip and tip of the three configurations were generated and are shown in figure 37(a to c) respectively. All serrations in this range of 2h show increasing flow structure speeds with respect to the reference trailing edge B. There is a general trend of increase in convective speeds of flow structures in I_t (region 1 and 2) with an increase in serration length (near the tip location, a maximum length (L2W4) with respect to increasing speed might be present). This confirms the earlier finding that a decrease in wake deficit that corresponds to convective flow structures decreases noise. The configuration with maximum length L3W1 has the least wake deficit and the highest convective speeds and is also known from independent work (Gruber, M et al. (2011)) to be effective in noise reduction. It is also worth noting that the effect of 2h on flow structures is through its dependence on δ more than its dependence on λ.

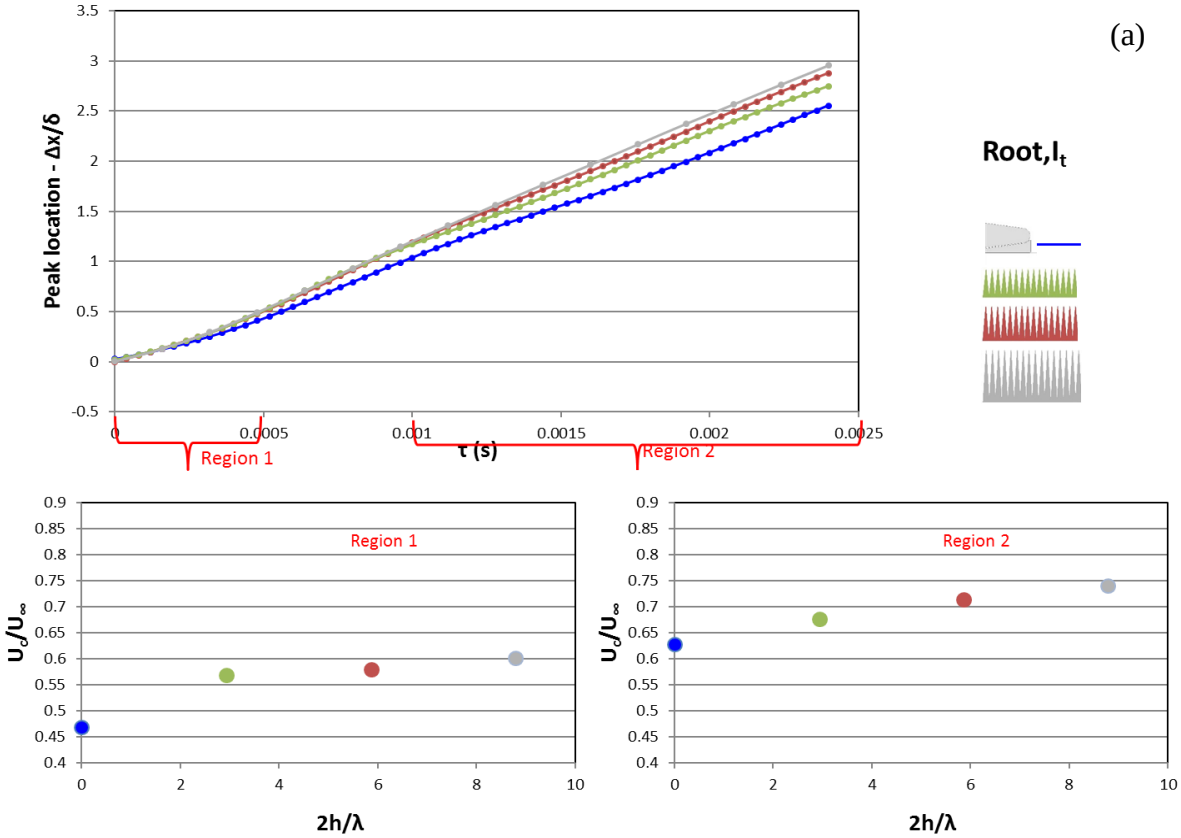

Figures 37(a). Effect of length of serrations on convective speeds of structures in I_t near the root

المنارة للاستشارات
www.manaraa.com

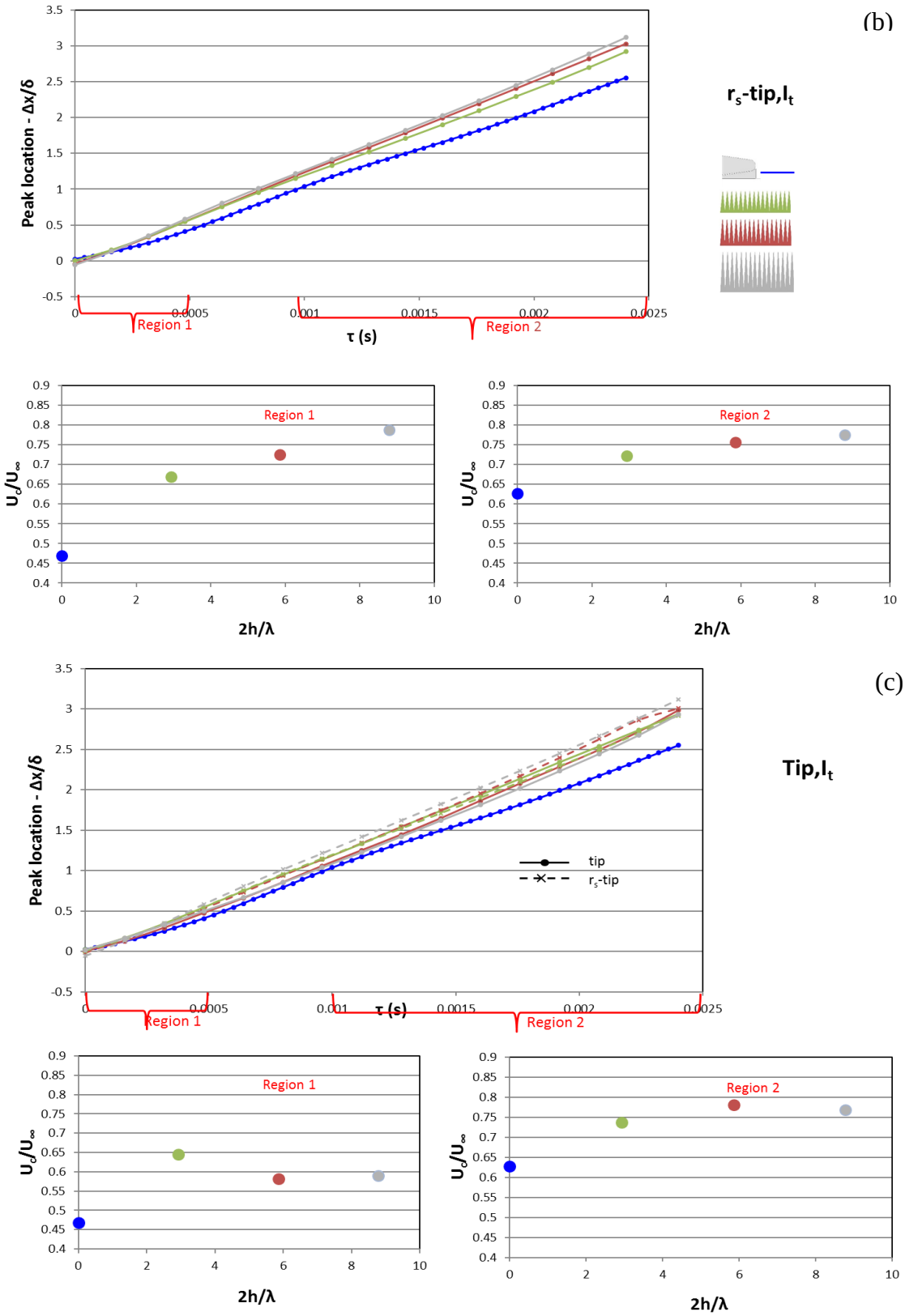

Figures 37(b and c). Effect of length of serrations on convective speeds of structures in I_t near r_s-tip and tip positions respectively

المنارة للاستشارات
www.manaraa.com

The speeds of the flow structures in region 1 and 2 in I_t at the r_s-tip positions are almost the same. This is to be expected from the lack of a bounding solid surface at this location. Figure 37(c) contains the XT plots of structures at both the r_s-tip and tip positions on the same graph. It can be seen that structures at the r_s-tip location move faster than those at the tip. The same was observed for all serrations. This difference in speeds of structures in the x-direction could affect their behavior along the z-direction forming a three dimensional flow feature near the serration. Figure 38 shows the difference in speeds between r_s-tip and tip locations for all the three configurations. In region 1, it increases with increasing length. In region 2 a trend cannot be determined at this point.

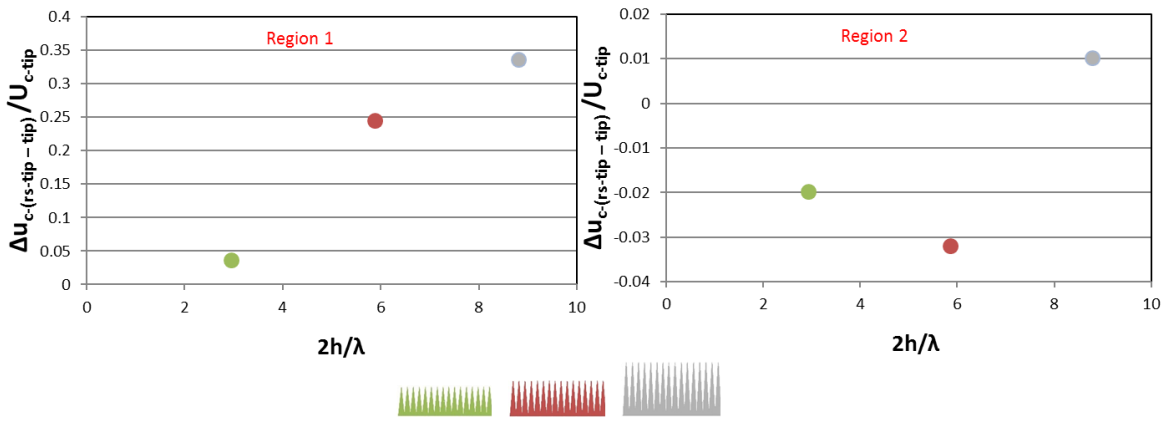

Figure 38. Difference in convective speeds of structures in I_t at r_s-tip and tip positions for serrations of different lengths

The streamwise correlation plots at increasing τ for the reference trailing edge B and the longest trailing edge L3W1 are shown in figure 39. These measurements were taken in I_t at the r_s-tip and tip positions respectively. It is possible to notice the absence of the region of weak absolute disturbances at the r_s-tip position and a decrease in size of the absolute disturbances at the tip. In general, the region of weak absolute disturbances becomes small.

المنارة للاستشارات
www.manaraa.com

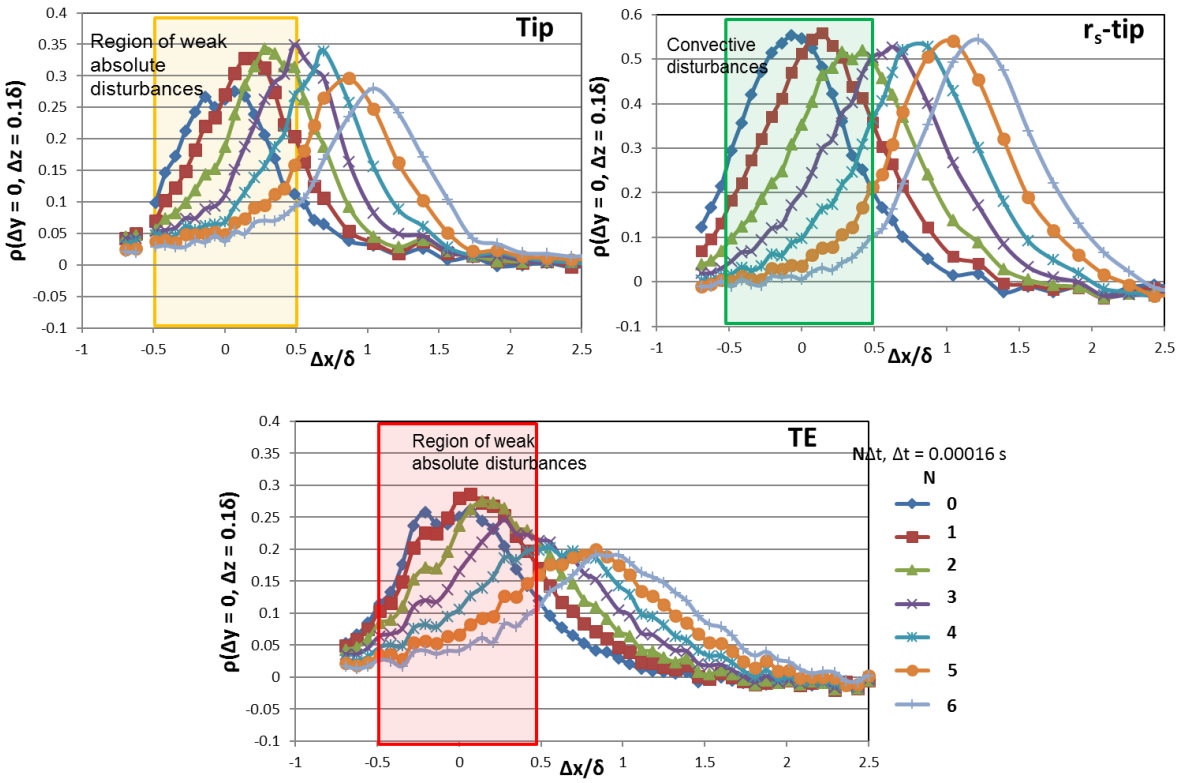

Figure 39. Evolution of structures in the streamwise direction in I_t near the tip, r_s-tip of L3W1 and trailing edge of B

The streamwise cross correlation of structures in O_t are shown in the appendix (figures a5 and a6). They show a similar trend as the structures in I_t, but move consistently faster. The spanwise cross-correlation curves in O_t near the r_s-tip location at increasing time delay τ for configurations L1W2 and L3W1 are shown in figure 40. They can be compared against those in the O_t near the trailing edge of configuration B. With increasing τ, ρ does not take negative values near the point of reference (at location of S, $\Delta z = 0$) for configuration L3W1 unlike the short trailing edge L1W2 and the reference configuration B which have the same trend in the spanwise direction and with evolution of time.

المنارة للاستشارات
www.manaraa.com

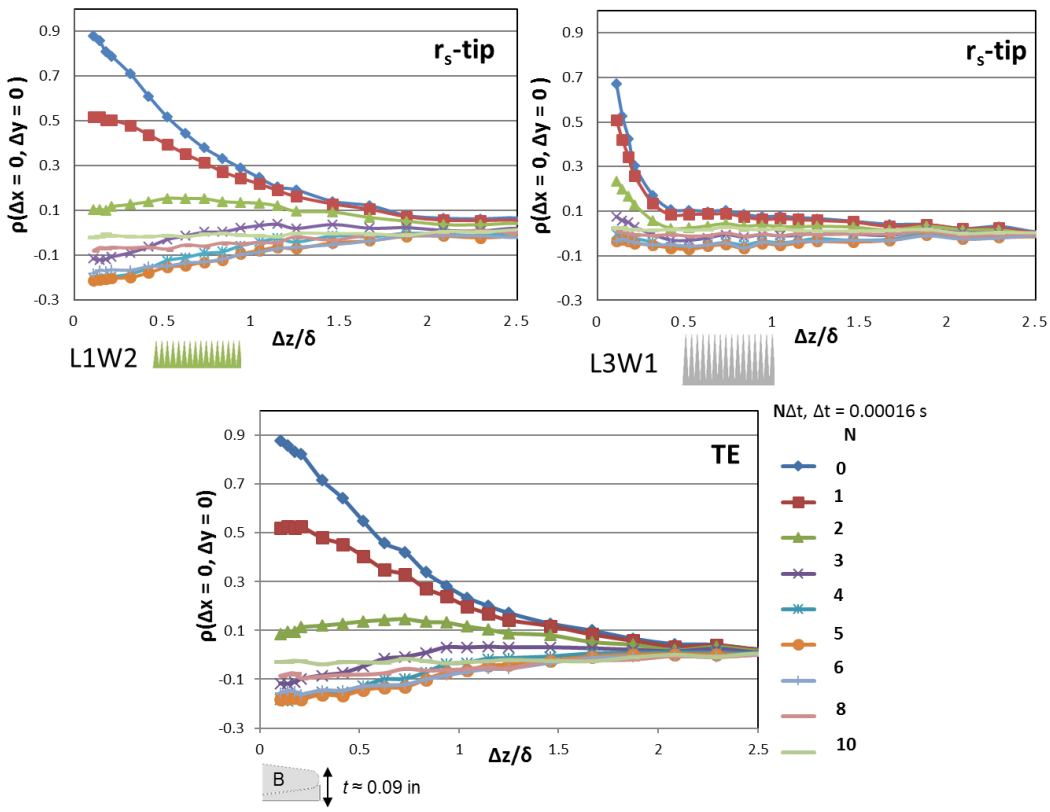

Figure 40. Evolution of structures in the spanwise direction in O_t near r_s-tip of L1W2, L3W1 and trailing edge of B

To quantify how the serrations interact with the structures in the spanwise direction, exponential curves and sixth order polynomials were fit to the first six to eight points on the spanwise correlation curves of structures in O_t and I_t respectively at $\tau = 0$. The half-width (defined as twice the spanwise distance at which the value of ρ is 0.5) of these structures were estimated and plotted against a measure of sharpness of the serrations $2h/\lambda$. This was repeated for the root, r_s-tip and tip locations. They are shown in figures 41(a), (b) and (c) respectively. Gauss curves were fit to the data in O_t at the root location. It can be seen that the correlation of structures slightly expands in size in the spanwise direction near the root for all serrations with respect to the reference configuration B. The same can be seen in I_t at r_s-tip. In O_t at r_s-tip and in I_t and O_t at the tip, a drastic decrease in spanwise correlation of structures with increasing length 2h is observed. This effect is more prominent with

المنارة للاستشارات
www.manaraa.com

structures in the O_t region. The three dimensional structure organizes itself from root to tip and is more organized for the longer serration.

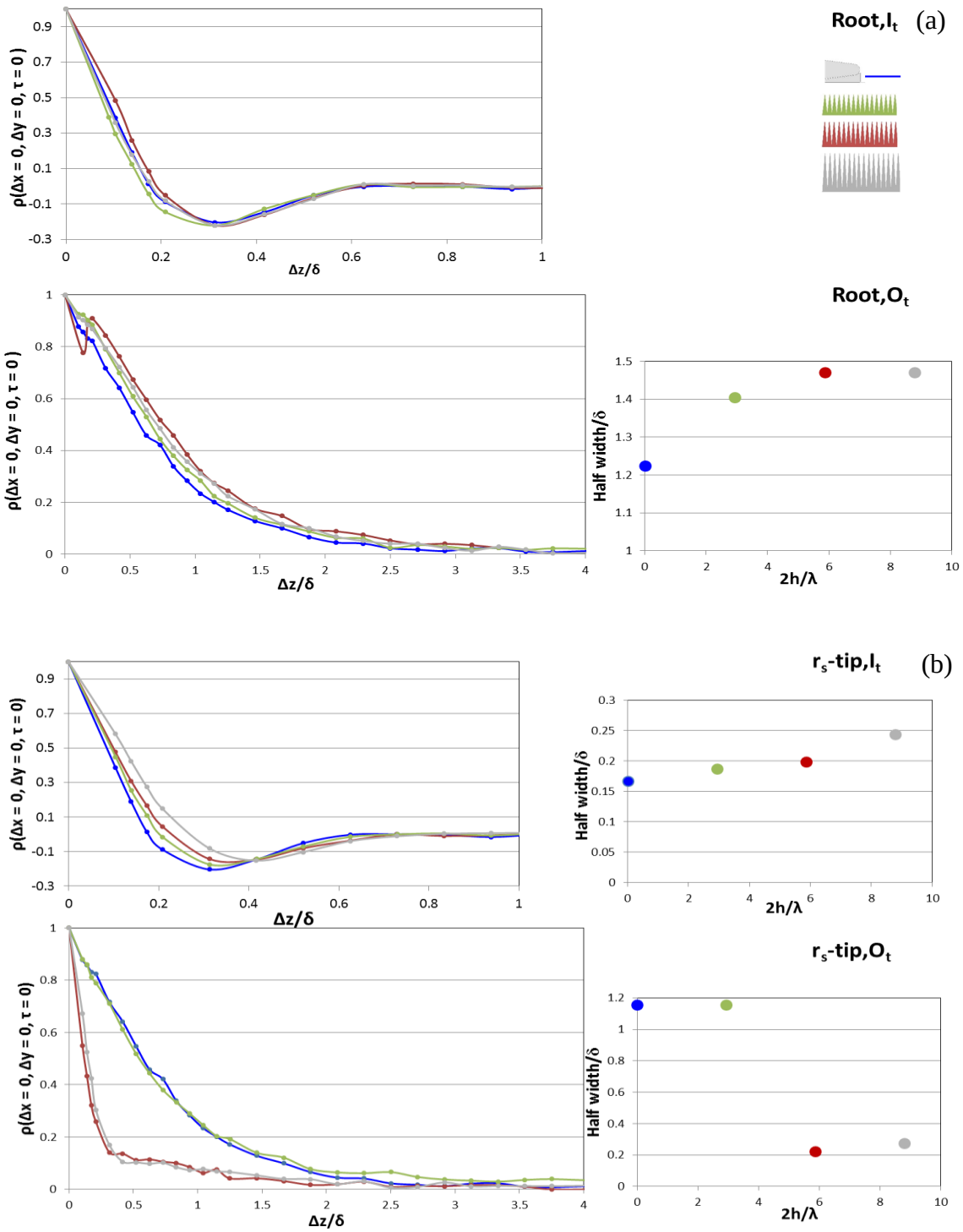

Figures 41(a and b). Spanwise correlation and half width of structures in I_t and O_t at the root and r_s-tip positions respectively (varying 2h)

المنارة للاستشارات
www.manaraa.com

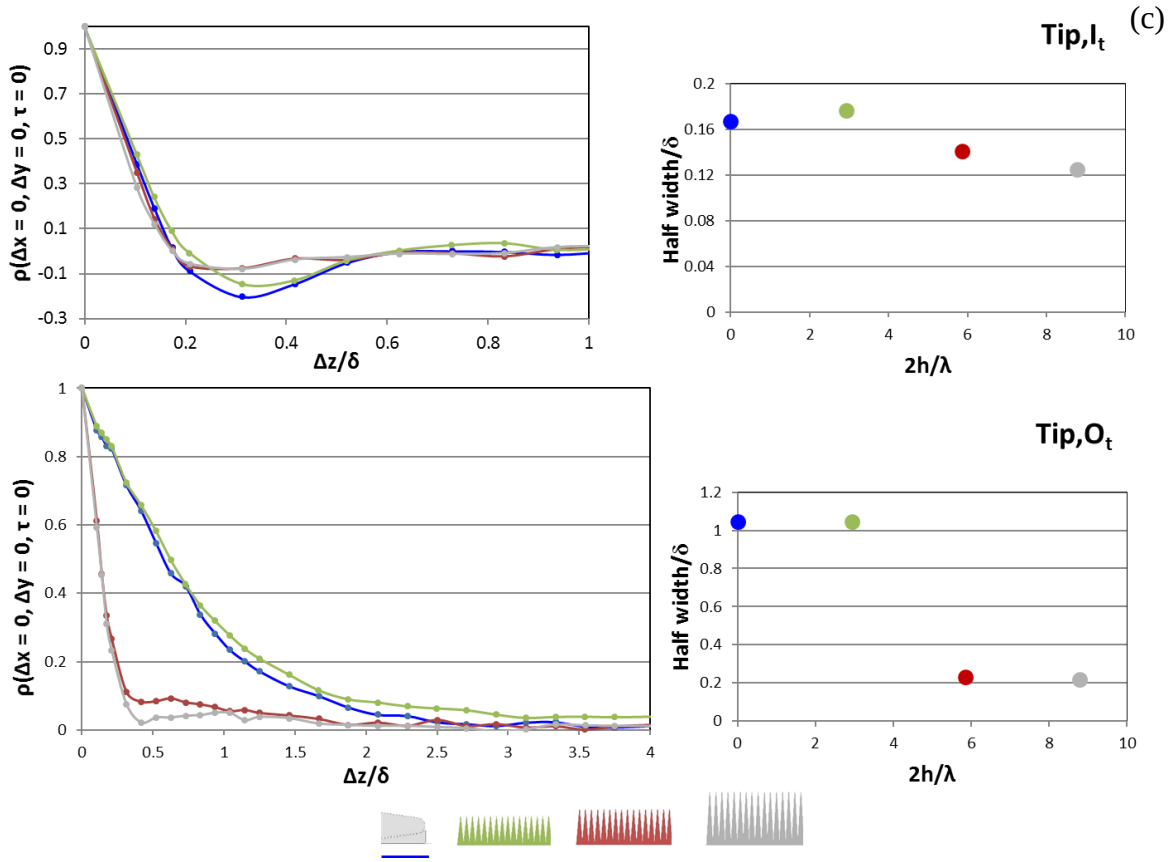

Figures 41(c). Spanwise correlation and half width of structures in I_t and O_t at the tip (varying 2h)

From the above results it is possible to see an association of increase in convection speed of structures in the lower region I_t near the serration to the increase in spanwise decay rate (or decorrelation) of structures in the outer region O_t towards the tip. The longer the serration, more significant this effect. We have already seen the effect of increase in convection speed on TE noise reduction. The findings above strongly indicate that long serrations, the most effective in noise reduction work by a related mechanism of minimizing the presence of absolute disturbances and increasing the spanwise decay of flow structures near the trailing edge.

المنارة للاستشارات
www.manaraa.com

3.6 Effect of width of a serrated trailing edge on flow structures

Previous studies (Gruber, M et al. (2011), Howe, M. S (1991)) have shown that sharp serrated trailing edges with serrated angle $\varphi = \tan^{-1}(\lambda/4h) < 45°$ (figure 7) are generally good noise reducers. Gruber experimentally showed that though sharp serrations (small λ) reduce noise, the effectiveness with respect to λ may be through λ's dependence on 2h and not δ. With a knowledge of the effect of convective flow structures in I_t and the spanwise decay of structures in O_t on TE noise reduction, we hoped to explore the effect of the width of a serration on the flow structures near the trailing edge and therefore better understand its effect on TE noise. The configurations L1W1 and L1W2; L2W1, L2W2, L2W3, L2W4, L2W5 and L2P2 (refer to table 1 in section 2.2.2) were used at $\alpha = 5°$ for the same. L1W1 and L1W2 have the same length $2h \approx 1.45\delta$ and the L2 configurations have the length $2h \approx 2.9\delta$. The configurations with largest width λ take the notation W1. L1W1 is a poor reducer of noise and L2W4 is an efficient reducer of noise. The configuration L2P2 has a plan area ratio of 25% while all the other triangular serrations have an area ratio of 50%. Wake profiles, streamwise and spanwise correlation data of structures in I_t ($\approx 0.25\delta$) and O_t ($\approx 0.9\delta$) at the root, r_s-tip and tip positions were used in this analysis. The results were compared with data at the trailing edge of the reference configuration B at $\alpha = 5°$.

Figure 42 shows the wake profile at the r_s-tip location of configurations B, L2W1, L2W2, L2W3, L2W4 and L2W5. The mean velocity and turbulence intensity profiles show that the wake rises for all configurations. L2W1, L2W2 and L2W3 have the least wake deficit and highest rise in wake. This might suggest that L2W1 has the highest speed of convective structures in I_t and could in turn have the highest spanwise decay rate of structures in O_t. From previous results in this study this could also indicate that it is the best noise reducer

المنارة للاستشارات
www.manaraa.com

even though experiments by Gruber (2011) show otherwise. Spanwise and streamwise data that were taken explain this discrepancy.

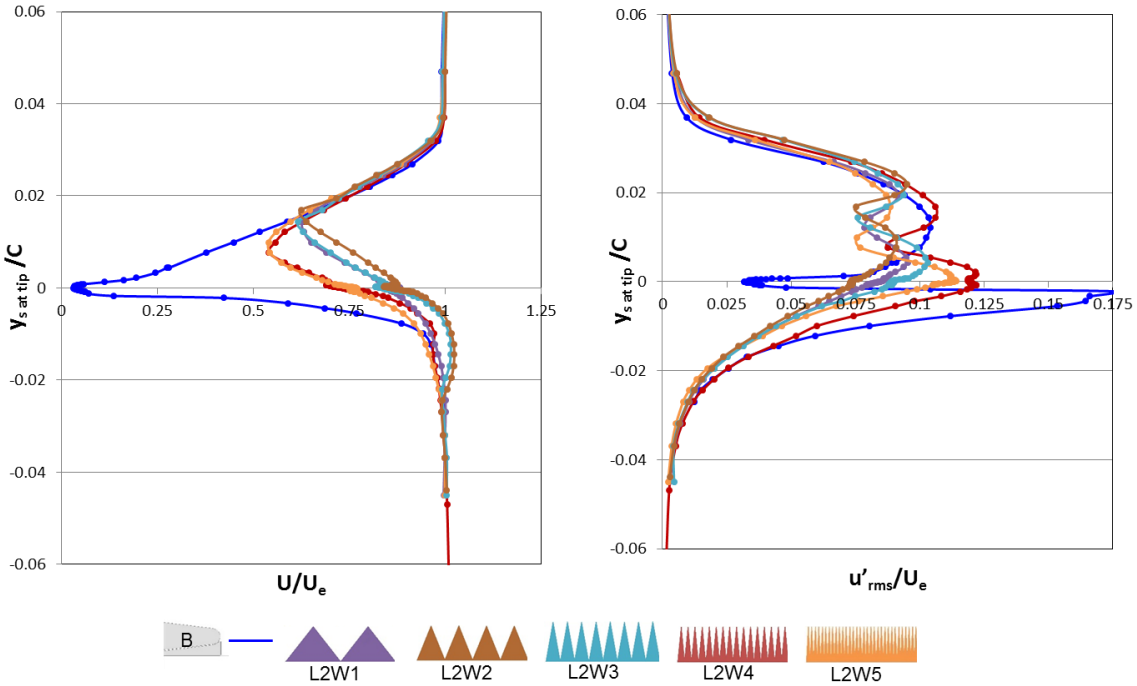

Figure 42. Wake profiles measured at r_s-tip of serrations of different widths

XT plots of structures and their corresponding convective speeds at I_t near the root, r_s-tip and tip of the various configurations were generated and are shown in figures 43(a to c) respectively. At the root (figure 43(a)) of the plot showing convection speeds in region 1, there seems to be a width corresponding to L2W4 w.r.t minimum convective speed (comparing L2s). The convective speed is a maximum at this same width in region 2. The same is noticed at the tip location (figure 43(c)). At r_s-tip, the width of L2W4 barely corresponds to a minimum convective speed in regions 1 and 2. The effect is more visible for configurations of larger length L2 than L1. The width of configuration L2W4 appears as a point of maximum or minimum with respect to convective speed and therefore is of interest to us.

المنارة للاستشارات
www.manaraa.com

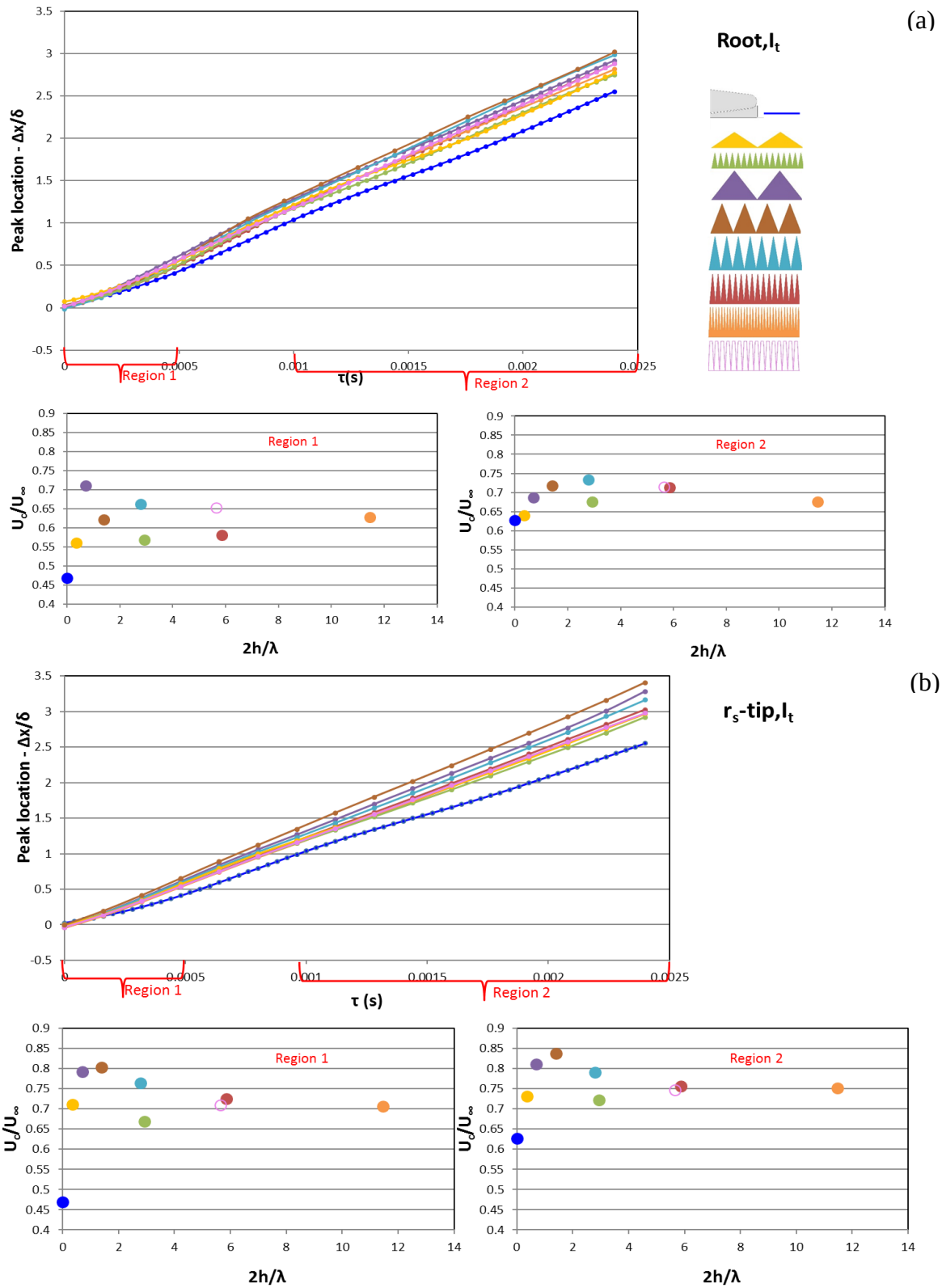

Figures 43(a and b). Effect of width of serrations on convective speeds of structures in I_t near root and r_s-tip positions respectively

المنارة للاستشارات
www.manaraa.com

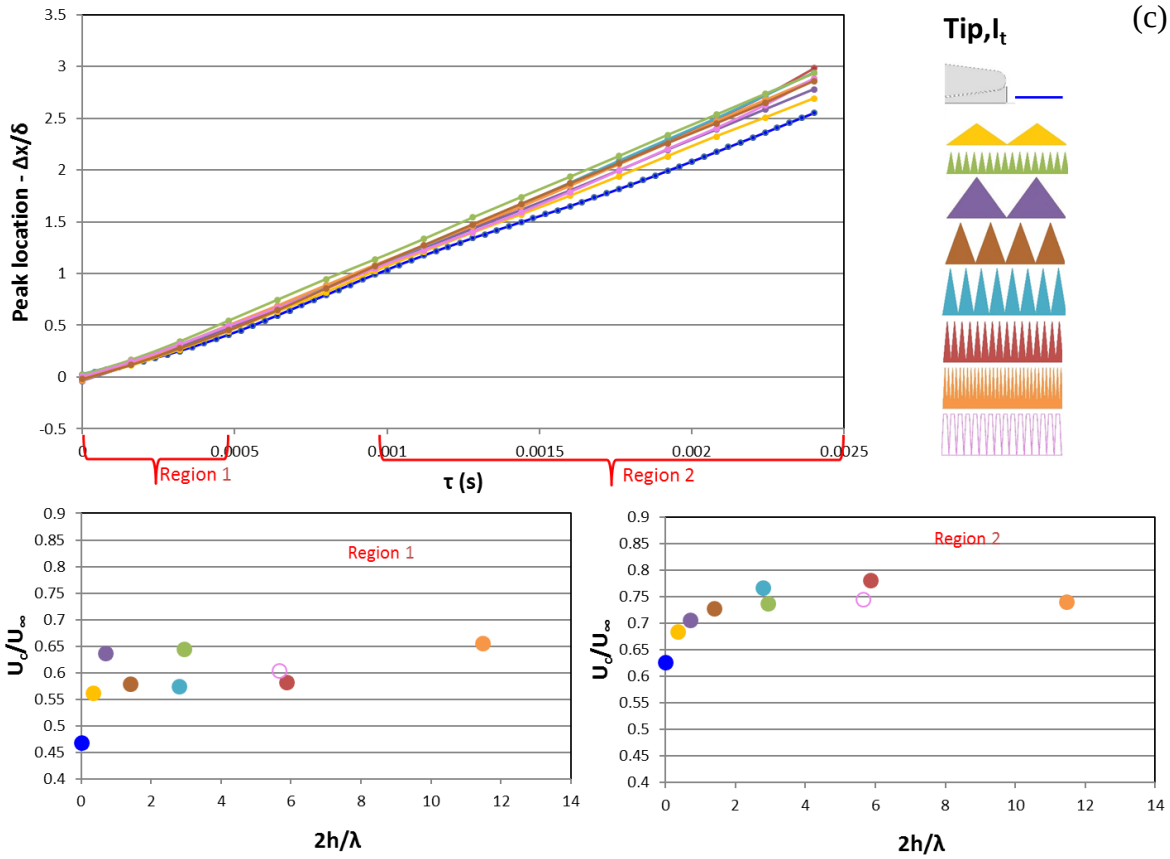

Figures 43(c). Effect of width of serrations on convective speeds of structures in I_t near the tip

Figure 44 shows the difference in speeds of structures between r_s-tip and tip locations at region 1 and 2. In region 2, decreasing width decreases the difference in speeds and reaches a minimum value at L2W4. This minimum width could correspond to an optimal difference in speeds in region 1. It should also be noted that the convective speeds are all consistently higher than the reference configuration B. We predict that for serrations of large values of 2h, the effect of decreasing width is to decrease the difference in speeds between the r_s-tip and tip in region 2 and maintain a difference in region 1; there also exists a width at which the difference in speed is a minimal in region 2 and optimal in region 1. This could be the

المنارة للاستشارات
www.manaraa.com

serration of best width for a given large 2h for the purposes of noise reduction. The spanwise correlation manifests this effect clearly.

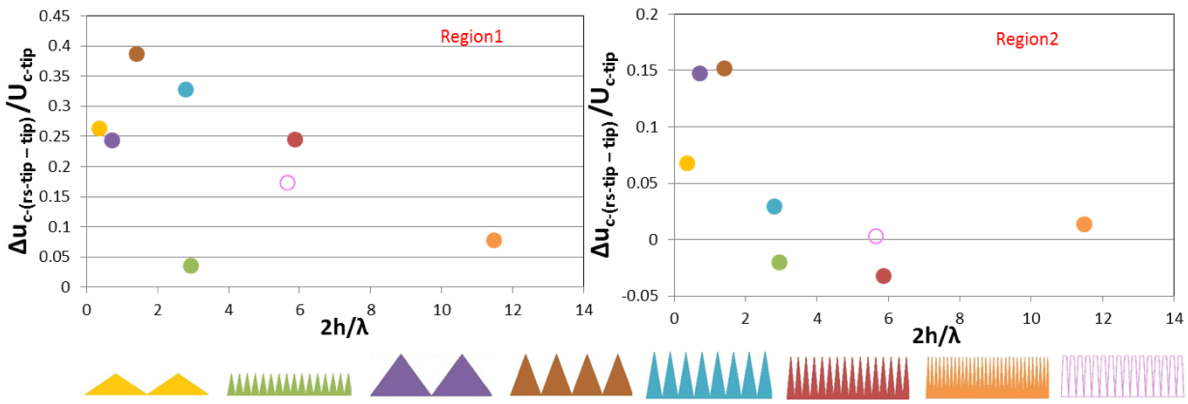

Figure 44. Difference in convective speeds of structures in I_t at r_s-tip and tip positions for serrations of different widths

Figures 45(a to c) show the spanwise correlation curves of structures in I_t and O_t at $\tau = 0$ at the root, r_s-tip and tip locations respectively. Exponential curves and sixth order polynomials were fit to the first six to eight points on spanwise correlation curves of structures in O_t and I_t. The half-width of these structures were estimated and plotted against a measure of sharpness of the serrations 2h/λ. This was repeated for the root, r_s-tip and tip locations. Gauss curves were fit to the data in O_t at the root location.

المنارة للاستشارات
www.manaraa.com

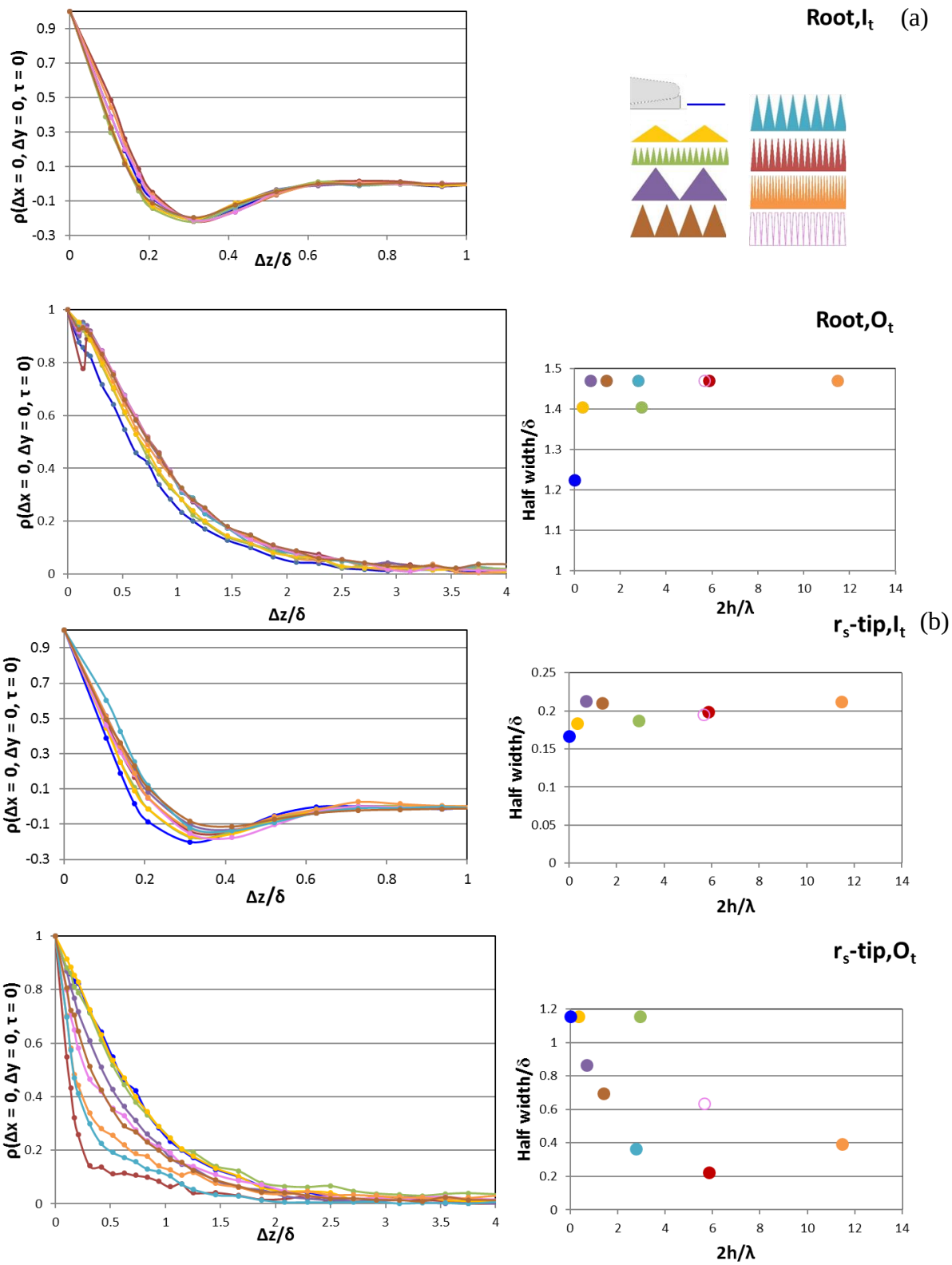

Figures 45(a and b). Spanwise correlation and half width of structures in I_t and O_t at the root and r_s-tip positions respectively (varying λ)

المنارة للاستشارات
www.manaraa.com

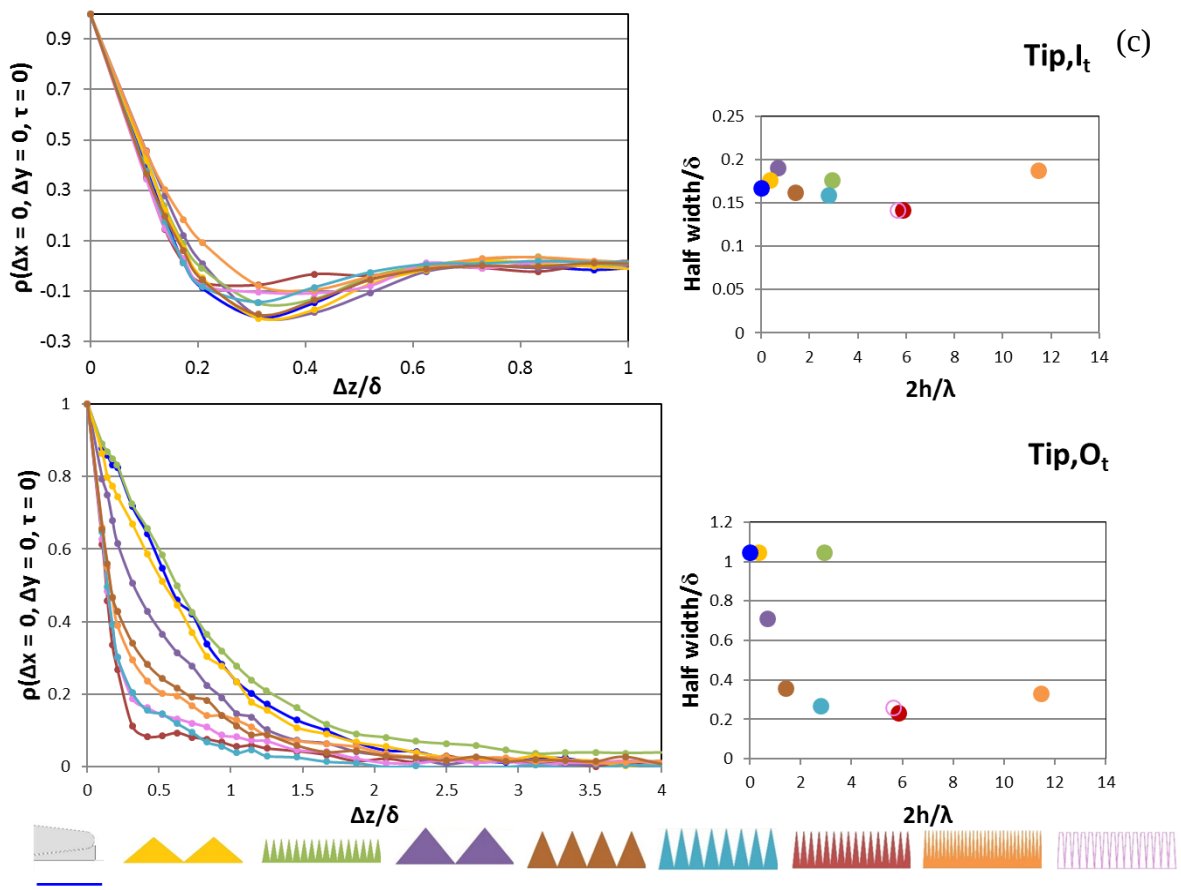

Figures 45(c). Spanwise correlation and half width of structures in I_t and O_t at the tip (varying λ)

It can be seen from the half-width values that the correlation of structures slightly expands in size in the spanwise direction near the root for all serrations with respect to the reference configuration B, with longer serrations resulting in larger structure correlation. The length is shown to influence the structures more than the width at the root location. The structures in I_t at the r_s-tip location might have a minimum half-width with decreasing λ at L2W4. The structures in I_t at the tip and O_t at r_s-tip and tip all attain a definite minimum value of half width at a small λ corresponding to L2W4. This is the same configuration that appeared as a point of maximum or minimum with respect to convective speed in regions 1 and 2 of the XT plots as shown before. The reduction of width for short serrations does not

المنارة للاستشارات
www.manaraa.com

seem to affect the half width of flow structures in any way. Following these observations, we can certainly say that for a given length of serrations $1\delta << 2h \leq 4\delta$, there exists a minimum width that maximizes spanwise decay of structures and optimizes the convective speed of structures in the streamwise direction. These findings help us understand how the width of a serration affects flow structures corresponding to TE noise. It is known that sharp serrations (small λ and large 2h) reduce noise. Our results could help identify the best value of λ with respect to large 2h ($1\delta << 2h \leq 4\delta$) that constitutes an effective noise reducing serration. They also show a dependence of h with respect to λ and vice-versa. It is worth noting that the effect of λ on flow structures is through its dependence on 2h more than its dependence on δ.

Figure 46(a) shows configuration L3W1 on the plot of spanwise half-width of structures in O_t at the r_s-tip and tip locations for all configurations used. It falls on the curve close to the minimum half-width value that our results show can be achieved using serrations of length $1\delta << 2h \leq 4\delta$. Figure 46(b) shows L3W1 on the plot of difference in convective speeds of structures in I_t between r_s-tip and tip positions for all configurations used. It falls on the curve close to the minimum value in region 2 and takes the value ≈ 0.35 in region 1. In light of our results as described in the previous paragraphs, we suggest that for $2h = 4.3\delta$, there exists a width $\lambda \neq 0.5\delta$, but $\approx 0.7\delta$ ($4.3\delta / 5.86$) that could maximize spanwise decay and optimize streamwise convective speeds of structures thereby reducing trailing edge noise. This check reinforces the prediction that for a given large value of 2h, it is possible to find the best λ that we think will be an effective noise reducer. The complex interaction of flow structures with respect to 2h, λ and δ as described above could also explain some of the discrepancies (– an increase in noise power level of trailing edge noise at high frequencies) that Gruber (2010, 2011) noticed with the increase in 2h and decrease in λ.

المنارة للاستشارات
www.manaraa.com

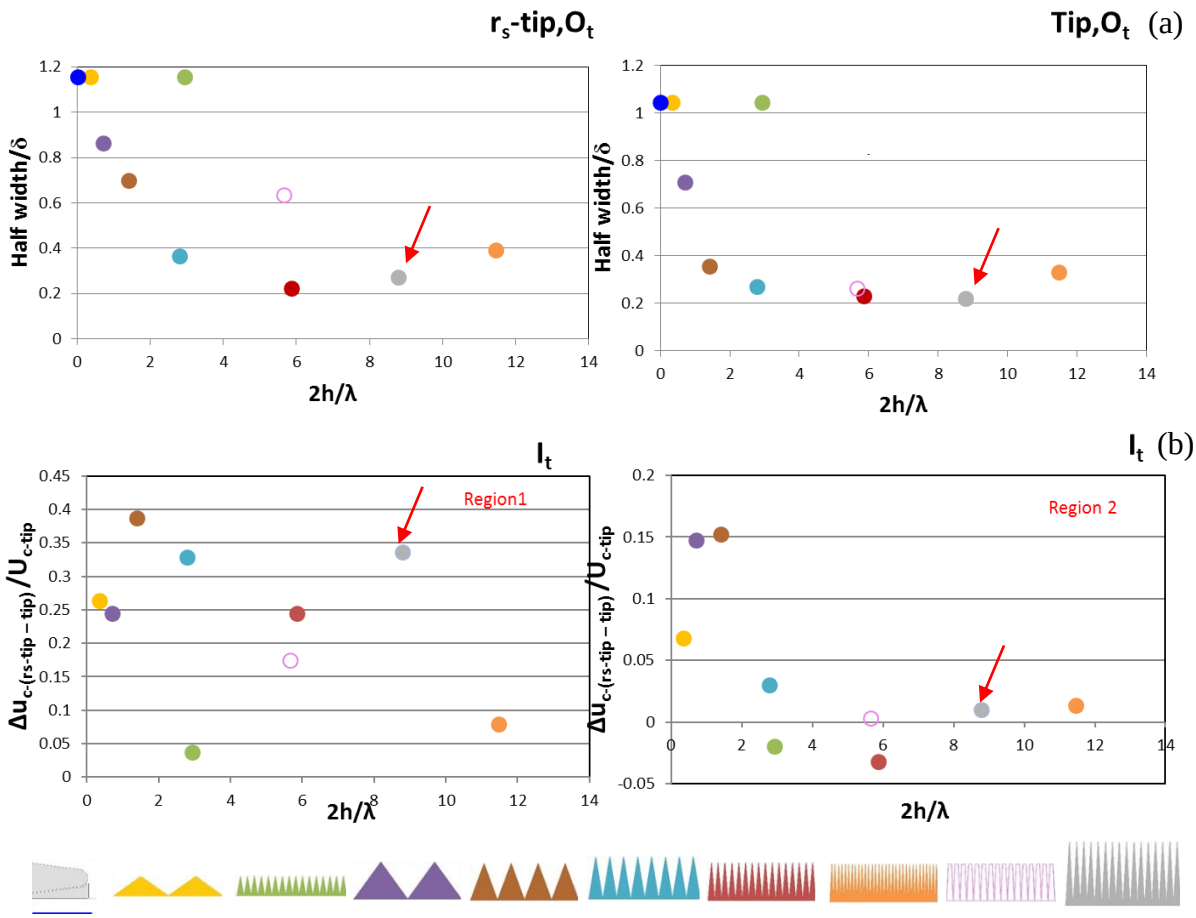

Figure 46. (a) Half width of structures in O_t at the r_s-tip and tip positions respectively. (b) Difference in convective speeds of structures in I_t at the r_s-tip and tip positions

The configuration L2P2 does not perform well in terms of convective speeds or spanwise decay of structures and is therefore a poor reducer of TE noise. The shape of the serrated trailing edge is of importance in noise reduction.

المنارة للاستشارات
www.manaraa.com

XT plots of structures at O_t near r_s-tip and tip of the various configurations are shown in figures a7 and a8 respectively in the appendix. Boundary layer profiles at the root and wake profiles at r_s-tip and tip respectively of all serrated TE configurations are shown in figures a9(a) to a9(c) respectively. Similarly, the convective speeds at the two regions of interest in the XT plots at I_t near the root, r_s-tip and tip respectively are shown in figures a10(a) to a10(c); the half-width of structures in O_t at $\tau = 0$ at the root, and I_t at $\tau = 0$ at r_s-tip and tip locations respectively are shown in figures a11(a) to a11(c).

المنارة للاستشارات
www.manaraa.com

CHAPTER 4

SUMMARY AND CONCLUSIONS

4.1 Summary

The flow-mechanisms responsible for generation and reduction of TE noise were investigated on a NACA 0012 airfoil. Focus was given to the study of flow structures in the turbulent boundary layer that might be involved with broadband trailing edge noise (TBL-TE noise). Experiments in a low-speed low turbulence wind tunnel were performed at a chord Reynold's number of ~850,000 and Mach number of 0.1. Hot-wire anemometry with two traversing hot-wires (S and T) were used as the main sensor for unsteady velocity measurements.

Preliminary studies were performed at $\alpha = 0°$ to establish a fully developed turbulent boundary layer at the trailing edge. A trailing edge configuration that was considered to be "sharp" in nature (Sh) was used at $\alpha = 0°$. Two-point spanwise correlation data obtained at various y-distances in the turbulent boundary layer at the trailing edge classified the boundary layer into three main regions of interest: the inner-top region ($I_t : 0 \leq y_s/\delta < 0.8$) that was located in the log-law region of the boundary layer, the outer-top region ($O_t : 0.8 \leq y_s/\delta < 1$) located in the outer region of the boundary layer and the potential region ($P_t : y_s/\delta > 1$) that extends outside the boundary layer into the inviscid region of the flow. I_t and O_t were chosen for further investigation to focus on flow structures in the boundary layer. Contour-correlation data in the spanwise plane with respect to structures in these two regions were taken. The structures in I_t decayed to zero very quickly ($\approx 0.6\delta$) in the spanwise direction approximately as a strongly damped sinusoid. Structures in O_t decayed as Gaussian curves to

المنارة للاستشارات
www.manaraa.com

zero at around $\Delta z = 5\delta$. The flow structures in these two regions were anti-correlated with respect to each other. Two-point streamwise line and contour correlation data with respect to structures in I_t and O_t near the trailing edge were obtained. They showed a short zone near the trailing edge in I_t with "weak absolute disturbances". This zone seemed to constitute of absolute disturbances of small amplitude superimposed on slow-moving disturbances in the x-direction. Further downstream of this zone the disturbances were convective in nature ($U_c \approx 0.65U_\infty$), although of a slow speed. The structures in O_t comprised of purely convective disturbances ($U_c \approx 0.8U_\infty$)

An angle of attach $\alpha = 5°$ was used to approximate the behavior of a real airfoil. The turbulent boundary layer generated at this angle of attack closely resembled problems of practical interest. The suction side consisted of a fully turbulent boundary layer with fluctuating velocity components that were broadband in nature. The pressure side exhibited velocity perturbations in the boundary layer that were tonal in nature. A modified trailing edge (B) that was characterized as "blunt" was used as the reference configuration at $\alpha = 5°$. Spanwise correlations in the turbulent boundary layer or near wake at the trailing edge revealed three regions of interest on the suction side: I_t, O_t and P_t and two regions of interest on the pressure side: I_b and O_b. Spanwise contour data, streamwise line and contour correlation data showed that the regions I_t and O_t on the suction side exhibited similar properties to those at $\alpha = 0°$. Structures in I_b were weakly absolute in nature for a short zone close to the trailing edge and transitioned to slowly convective disturbances further downstream. They also exhibited properties of highly-energetic vortex shedding, correlated over a large span. To limit the study to TBL-TE interaction noise, investigation of flow structures was confined to I_t and O_t on the suction side of the airfoil model. The turbulent

المنارة للاستشارات
www.manaraa.com

boundary layer and properties of the flow-structures in these two regions of interest were chosen as the baseline for later comparison with serrated trailing edges.

The first serrated TE modifier that was tested was designated L2W4 of length $2h = 2.86\delta$ and $\lambda = 0.49\delta$ at $\alpha = 5°$. Previous independent studies (Gruber, M et al. (2011)) have experimentally shown that a serrated trailing edge of given dimensions was effective at reducing trailing edge noise under similar flow conditions. Wake profiles at the r_s-tip (figure 7) location showed a decrease in wake deficit accounted to the development of turbulent wake and a rise in wake accounted to mixing with flow from the pressure side. Streamwise and spanwise contour data were taken with respect to structures in I_t and O_t at the root and r_s-tip of the serration. Changes in the streamwise direction with respect to structures in I_t were observed. The zone of weak absolute disturbances near r_s-tip was absent and the structures near the root in the zone of weak absolute disturbances moved with a greater speed than those near the trailing edge of the reference configuration. This effect was more prominent with structures in I_t than those in O_t. The spanwise correlation contours of structures in I_t near r_s-tip revealed the presence of a three dimensional structure near the serration. The structure was periodically correlated in the spanwise direction over intervals that scaled with the width of the serration. The evidence suggested that the presence of the weak absolute instability and its interaction with the trailing edge could be a major flow mechanism associated with trailing edge noise. The new three dimensional structure could influence trailing edge noise reduction. To rigorously quantify these changes, convection plots and spanwise line correlation data of structures in I_t and O_t near the root, r_s-tip and tip locations were obtained and the corresponding convection speeds and spanwise half width of structures respectively

المنارة للاستشارات
www.manaraa.com

were estimated for serrated trailing edges of various lengths and widths. Results from Gruber (2010, 2011) were used to choose “good” and “bad” trailing edge noise modifiers.

The effect of trailing edge thickness on flow structures associated with noise was investigated. It is already known that thick trailing edges generate higher tonal and broadband noise. It was conjectured that a relationship exists between the absolute disturbances in I_t near the trailing edge and trailing edge noise. Four flat trailing edge configurations with various rounded thicknesses were used in this part of the study (table 1). It was found that the smallest wake deficit was associated with a transition of disturbances from absolute to convective in the I_t region near the trailing edge. This logically happens for the thinnest trailing edge. Sharpness changes an unsteady wake to an unsteady mixing layer (figure 34). Thus, a relation was established between absolute disturbances and trailing edge noise. The presence of these disturbances was conjectured to be a major source of noise. Changing the nature of these flow structures to that of convective disturbances could be used to reduce noise.

A total of nine serrated TE modifiers were used (table 1). Three serrated TE modifiers L1W2, L2W4 and L3W1 of same width $\lambda = 0.49\delta$ and lengths 2h ranging from 1.4δ to 4.3δ were used to study the effect of length of serrations on flow structures affecting trailing edge noise. Previous studies (Gruber, M et al. (2011)) showed that serrations with lengths in the range $1\delta < 2h \leq 4\delta$ were generally effective at noise reduction though an increase in noise at high frequencies for large h and small λ was noticed. They also stated that increase in h was associated with a general decrease in TE noise radiation. Wake profiles at r_s-tip locations of serrations showed a rise of wake and a reduction in wake deficit with an increase in length. It was observed that flow structures in I_t at the root, r_s-tip and tip locations increased in

المنارة للاستشارات
www.manaraa.com

convective speed by a maximum of 28%, 70% and 35% respectively in region 1 (zone of weak absolute disturbances) with respect to the reference TE configuration B. In region 2 (convective disturbances) they increased by 18%, 24% and 22% respectively. The maximum increase was associated with the longest trailing edge. A simultaneous decrease in the spanwise half width length of structures in O_t near r_s-tip and tip was also observed with the least half width length associated with the longest serration. Previous work (Howe, M. S (1978), Amiet, R. K (1975), Howe, M. S (1991)) theoretically show that trailing edge noise is directly proportional to the spanwise correlation length of vertical velocity fluctuations in the turbulent boundary layer. From the predicted effect of absolute disturbances on trailing edge noise in this study and with a pre-existing knowledge of the effect of 2h and half width on trailing edge noise, we may expect that an increase in the length of serrations transitions the characteristics of the turbulent wake/boundary layer from absolute to convective while simultaneously decreasing spanwise length of structures and this combined effect could lead to a reduction of trailing edge noise.

To investigate the effect of λ on flow structures, 6 trailing edge configurations of length $2h \approx 2.9\delta$ (L2s) and two configurations of length $\approx 1.4\delta$ (L1s) were used. Previous work (Gruber, M et al. (2011), Howe, M. S (1991)) states that sharp trailing edges (large 2h and small λ) are generally effective noise reducers (ignoring discrepancies at high frequencies). From our data, it was found that λ was dependent on δ, through its association with 2h. A decrease in width corresponded with a general decrease in spanwise half width of structures towards the end of the serration. This effect was more prominent in the O_t region near r_s-tip and tip. The half width decreased only up to a minimum value and then increased with decreasing width. It achieved a minimum value of half width at configuration L2W4

المنارة للاستشارات
www.manaraa.com

suggesting that this serration is most effective at de-correlating structures. It is also to be noted that this trend was observed only in long serrations (L2s). The short serrations L1s did not exhibit any changes with respect to the spanwise half width length. The convective speed of structures near all serrations increased with respect to the baseline configuration. For a given length $2h \approx 2.9\delta$, the relation with respect to convective speeds with decreasing λ was more complex. Nevertheless, it can be said that L2W4 was the point of maxima or minima with respect to convective speeds measured at various key locations of the serration (I_t, O_t near root, r_s-tip and tip). To obtain a favorable effect from decreasing width for a given large 2h, evidence suggests that it might be necessary to optimize the convective speed of structures in I_t. The values of half width and convective speeds of flow structures with respect to $2h/\lambda$ of all serrations collapsed onto a curve that levelled off close to the values of L2W4 ($2h/\lambda \approx 5.86$). In light of this, we predict that for a given value of 2h, $1\delta << 2h \leq 4\delta$, there exists a width λ ($2h/\lambda \approx 5.86$) that could maximize spanwise decay and optimize streamwise convective speeds of structures thereby reducing trailing edge noise (figures 46(a) and (b)). To confirm the first half of this finding, the half width and convective speed of L3W1 (longest serration $2h = 4.3\delta$) were added to the curves half width/δ versus $2h/\lambda$ and U_c/U_∞ versus $2h/\lambda$ respectively defined by the serrations of length $2h \approx 2.9\delta$. The values fell on the curves close to L2W4. These results might shed light into the discrepancies predicted by Gruber at high frequencies. They also help us understand the relation between length and width of a serration. This study also increases our understanding of how serrations affect flow-structures that are associated with trailing edge noise.

المنارة للاستشارات
www.manaraa.com

4.2 Conclusions

There is a zone of weak absolute disturbances in I_t near the trailing edge that could be a major source of trailing edge noise. Experiments showed that the effect of reduction of trailing edge thickness accompanied by a reduction in wake deficit transitions this zone into regions of convective disturbances. Results from independent studies (Henderson, B et al. (2004), Brooks, T. F et al. (1989), Hutcheson, F.V and Brooks, T. F (2004)) reinforced the prediction that absolute disturbances in I_t could be a major source of trailing edge noise.

Previous studies (Gruber, M et al. (2011)) have experimentally shown that an increase in serration length reduces trailing edge noise. Results from this study show that the effect of an increase in serration length is to decrease the presence of absolute disturbances while increasing the convective speed of flow structures in the streamwise direction in general. It also simultaneously results in an increase in spanwise decay of flow structures near the serration. Evidence indicates that this combined effect results in the reduction of trailing edge noise.

The effect of decreasing width of serrations indicates the existence of a width for a given large serration length that most effectively reduces noise. The characteristics of the three dimensional flow structure that forms near a serration plays an important role in noise reduction. A decrease in width for a given large serration length corresponds to a decrease in spanwise correlation of structures up to a given value of width. A further decrease in width results in an increase in correlation length. A similar trend was observed for convective speeds of flow-structures near the serrations. Evidence from this study and results from

المنارة للاستشارات
www.manaraa.com

independent work (Gruber, M et al. (2011)) suggests that the width of a serration is to be chosen to maximize spanwise decay while optimizing convective speed of structures.

4.2 Future work

Simultaneous acoustic measurements made with these serrations could definitively confirm our findings. The effect of absolute instabilities on noise needs to be further explored, and we expect that its impact on noise reduction will be significant. Serrations with much larger and smaller values of 2h ($1\delta \geq 2h > 4\delta$) can be investigated for various λ. Finally, other TE modifiers like flexible brushes and porosity that alter the rigid nature of the trailing edge itself should be examined. Further results will expand the design space for practical and effective trailing edge noise reducing modifiers.

المنارة للاستشارات
www.manaraa.com

REFERENCES

Amiet, R. K. 1975. Acoustic radiation from an airfoil in a turbulent stream. *Journal of Sound and Vibration. Vol 41, Issue 4.*

Amiet, R. K. 1976. Noise due to turbulent flow past a trailing edge. *Journal of Sound and Vibration. Vol 47, Issue 3.*

Blake, W. K. 1986. Mechanics of flow-induced sound and vibration, volume II: complex flow-structure interactions. *Academic Press.*

Brooks, T. F and Hodgson, T. H. 1981. Trailing edge noise prediction from measured surface pressures. *Journal of Sound and Vibration. Vol 78, Issue 1.*

Brooks, T. F, Pope, D. S and Marcolini, M. A. 1989. Airfoil self-noise and prediction. *Tech.Rep. 1218 NASA Reference Publication.*

Chase, D. M. 1972. Sound radiated by turbulent flow off a rigid half-plane as obtained from a wavevector spectrum of hydrodynamic pressure. *The Journal of the Acoustical Society of America. Vol 52, Issue 3B.*

Chong, T. P, Joseph, P. F. 2013. An experimental study of airfoil instability tonal noise with trailing edge serrations. *Journal of Sound and Vibration. Vol 332.*

Chong, T. P, Vathylakis, A. 2015. On the aeroacoustic and flow structures developed on a flat plate with a serrated sawtooth trailing edge. *Journal of Sound and Vibration. Vol 354.*

Choudhari, M. M et al. 2002. Aeroacoustic experiments in the Langley low-turbulence pressure tunnel. *Tech.Rep. NASA TM-2002-211432.*

Clark, I. A et al. 2014. The noise generating and suppressing characteristics of bio-inspired rough surfaces. *20th AIAA/CEAS Aeroacoustics conference.*

Clark, I. A et al. 2015. Bio-inspired trailing edge noise control. *21st AIAA/CEAS Aeroacoustics conference.*

Cohen, J and Wygnanski, I. 1987. The evolution of instabilities in the axisymmetric jet. Part 1. The linear growth of disturbances near the nozzle. *Journal of Fluid Mechanics. Vol 176.*

Cohen, J and Wygnanski, I. 1987. The evolution of instabilities in the axisymmetric jet. Part 2. The flow resulting from the interaction between two waves. *Journal of Fluid Mechanics. Vol 176.*

المنارة للاستشارات

www.manaraa.com

Corcos, G. M. 1963. The structure of the turbulent pressure field in boundary-layer flows. *Journal of Fluid Mechanics. Vol 18.*

Crighton, D. G. 1975. Basic principles of aerodynamic noise generation. *Progress in Aerospace Sciences. Vol 16, Issue 1.*

Curle, N. 1955. The influence of solid boundaries upon aerodynamic sound. *Proceedings of the Royal Society. Vol 231, Issue 1187.*

Dassen, T et al. 1996. Results of a wind tunnel study on the reduction of airfoil self-noise by the application of serrated blade trailing-edges. *National Aerospace Laboratory NLR-TP-96350.*

Dowling, A.P and Ffowcs Williams, J. E. 1983. Sound and sources of sound.

Ffowcs Williams, J. E and Hall, L. H. 1970. Aerodynamic sound generation by turbulent flow in the vicinity of a scattering half plane. *Journal of Fluid Mechanics. Vol 40, Issue 4.*

Fiedler, H. E et al. 1998. Three-dimensional mixing layers and their relatives. *Journal of Experimental Thermal and Fluid Science. Vol 16.*

Finez, A et al. 2010. Broadband noise reduction with trailing edge brushes. *16th AIAA/CEAS Aeroacoustics conference.*

Fink, M. R. 1975. Experimental evaluation of theories for trailing edge and incidence fluctuation noise. *AIAA Journal. Vol 13, Issue 11.*

Gaster, M. 1975. A theoretical model of a wave packet in the boundary layer on a flat plate. *Proceedings of the Royal Society. Vol 347.*

Geyer, T, Sarradj, E and Fritzsche, C. 2010. Measurement of the noise generation at the trailing edge of porous airfoils. *Journal of Experimental Fluids. Vol 48.*

Glegg, S. A. L, Devenport, W. J, Spitz, N. 2009. Application of proper orthogonal decomposition to trailing-edge noise. *AIAA Journal. Vol 47, Issue 6.*

Gruber, M and Joseph, P.F. 2011. On the mechanisms of serrated airfoil trailing edge noise reduction. *17th AIAA/CEAS Aeroacoustics Conference.*

Gruber, M., Joseph, P, Chong, T. P. 2010. Experimental investigation of airfoil self noise and turbulent wake reduction by the use of trailing edge serrations. *16th AIAA/CEAS Aeroacoustics Conference. Vol 2.*

Henderson, B, Kinzie, K and Haskin, H. 2004. The effect of nozzle trailing edge thickness on jet noise. *10th AIAA/CEAS Aeroacoustics conference.*

المنارة للاستشارات

www.manaraa.com

Herr, M, Dobrzynski, W. 2005. Experimental investigations in low-noise trailing edge design. *AIAA Journal. Vol 43, Issue 6.*

Herr, M. 2007. Design criteria for low-noise trailing edges. *13th AIAA/CEAS Aeroacoustics conference.*

Howe, M. S. 1978. A review of the theory of trailing edge noise. *Journal of Sound and Vibration. Vol 61, Issue 3.*

Howe, M. S. 1988. The influence of surface rounding on trailing edge noise. *Journal of Sound and Vibration. Vol 126, Issue 3.*

Howe, M. S. 1991. Aerodynamic noise of a serrated trailing edge. *Journal of Fluids and Structures. Vol 5.*

Howe, M. S. 1991. Noise produced by a sawtooth trailing edge. *The Journal of the Acoustical Society of America. Vol 90, Issue 1.*

Howe, M. S. 1999. Trailing edge noise at low Mach numbers. *Journal of Sound and Vibration. Vol 225, Issue 2.*

Huerre, P and Monkewitz, P. A. 1990. Local and global instabilities in spatially developing flows. *Fluid Mechanics. Vol 22.*

Hutcheson, F. V and Brooks, T. F. 2004. Effects of angle of attack and velocity on trailing edge noise. *42nd AIAA Sciences meeting.*

Jaworski, J. W and Peake, N. 2013. Aerodynamic noise from a poroelastic edge with implications for the silent flight of owls. *Journal of Fluid Mechanics. Vol 723.*

Jaworski, J. W and Peake, N. 2013. Parametric guidance for turbulent noise reduction from poroelastic trailing edges and owls. *19th AIAA/CEAS Aeroacoustics conference.*

Kamruzzaman, M et al. Wind turbine aerodynamics and aeroacoustics at University of Stuttgart - An overview of research and development.

Kamruzzaman, M et al. 2011. Comprehensive evaluation and assessment of trailing edge noise prediction based on dedicated measurements. *Journal of Noise Control Engineering. Vol 59, Issue 1.*

Kanevce, G and Oka, S. 1973. Correcting hot-wire readings for influence of fluid temperature variations. *DISA information, pages 21–24.*

Khorrami, M. R and Choudhari, M. M. 2003. Application of passive porous treatment to slat trailing edge noise. *NASA/TM-2003-212416.*

المنارة للاستشارات

www.manaraa.com

Kit, E et al. 2007. On the periodically excited plane turbulent mixing layer, emanating from a jagged partition. *Journal of Fluid Mechanics. Vol 589.*

Koch, W. 1985. Local instability characteristics and frequency determination of self-excited wake flows. *Journal of Sound and Vibration. Vol 99, Issue 1.*

Lee, H and Kang, S. H. 2000. Flow characteristics of transitional boundary layers on an airfoil in wakes. *Journal of Fluids Engineering. Vol 122, Issue 3.*

Lighthill, M. J. 1952. On sound generated aerodynamically I. General theory. *Proceedings of the Royal Society. Vol 211, Issue 1107.*

Lighthill, M. J. 1954. On sound generated aerodynamically II. Turbulence as a source of sound. *Proceedings of the Royal Society. Vol 222, Issue 1148.*

Lutz, T, et al. 2007. Design and wind-tunnel verification of low-noise airfoils for wind turbines. *AIAA Journal. Vol 45, Issue 4.*

Mack, L. M. 1969. Boundary-layer stability theory. *Jet Propulsion Laboratory, NASA, NAS 7-100.*

Marasli, B, Champagne, F. H and Wygnanski, I. J. 1991. On linear evolution of unstable disturbances in a plane turbulent wake. *Physics of Fluids. Vol 3, Issue 4.*

Moreau, D. J, Brooks, L. A and Doolan, C. J. 2012. The effect of boundary layer type on trailing edge noise from sharp-edged flat plates at low-to-moderate Reynolds number. *Journal of Sound and Vibration. Vol 331, Issue 17.*

Nedić, J and Vassilicos, J. C. 2015. Vortex shedding and aerodynamic performance of airfoil with multiscale trailing-edge modifications. *AIAA Journal. Vol 53, Issue 11.*

New, T. H. 2009. An experimental study on jets issuing from elliptic inclined nozzles. *Journal of Experimental Fluids. Vol 46.*

New, T. H. 2010. Effects of notch geometry and sharpness on turbulent jets issuing from indeterminate-origin notched nozzles. *European Journal of Mechanics B/ Fluids. Vol 29.*

Nichols, J. W et al. 2012. Large-eddy simulation for supersonic rectangular jet noise prediction: effects of chevrons. *18th AIAA/CEAS Aeroacoustics Conference.*

Oerlemans, S et al. 2001. Experimental demonstration of wind turbine noise reduction through optimized airfoil shape and trailing-edge serrations. *National Aerospace Laboratory NLR-TP-2001-324.*

المنارة للاستشارات

www.manaraa.com

Rahman, A. A et al. 1987. On temperature compensation in hot-wire anemometry. *Journal of Physics E Scientific Instruments. Vol 30, Issue 3.*

Rienstra, S. W. 1981. Sound diffraction at a trailing edge. *Journal of Fluid Mechanics. Vol 108.*

Sagrado, A. G and Hynes, T. 2012. Wall pressure sources near an airfoil trailing edge under turbulent boundary layers. *Journal of Fluids and Structures. Vol 30.*

Sharma, A and Lele, S. K. 2011. Sound generation due to unsteady motion of a cylinder. *Physics of Fluids. Vol 23.*

Singer, B. A, Lockard, D. P and Kenneth, S. B. 2000. Computational aeroacoustic analysis of slat trailing-edge flow. *AIAA Journal. Vol 38, Issue 9.*

Spitz, N. 2005. Prediction of trailing edge noise from two-point velocity correlations. *Masters of Science Thesis. Virginia Polytechnic Institute and State University.*

Tanner, M. 1972. A method for reducing the base drag of wings with blunt trailing edge. *Aeronautical Quarterly, Vol. 23.*

Wlezien, R. W and Kibens, V. 1986. Passive control of jets with indeterminate origins. *AIAA Journal. Vol 24, Issue 8.*

Wolf, A et al. 2015. Trailing edge noise reduction of wind turbine blades by active flow control. *Wind energy. Vol 18.*

Wolf, W. R, Azevedo, J, F and Lele, S. K. 2012. Convective effects and the role of quadrupole sources for aerofoil aeroacoustics. *Journal of Fluid Mechanics. Vol 708.*

Wygnanski, I et al. 2011. The application of boundary layer independence principle to three-dimensional turbulent mixing layers. *Journal of Fluid Mechanics. Vol 675.*

Zhou, M. D and Wygnanski, I. 2001. The response of a mixing layer formed between parallel streams to a concomitant excitation at two frequencies. *Journal of Fluid Mechanics. Vol 441.*

المنارة للاستشارات

www.manaraa.com

APPENDIX A

FIGURES

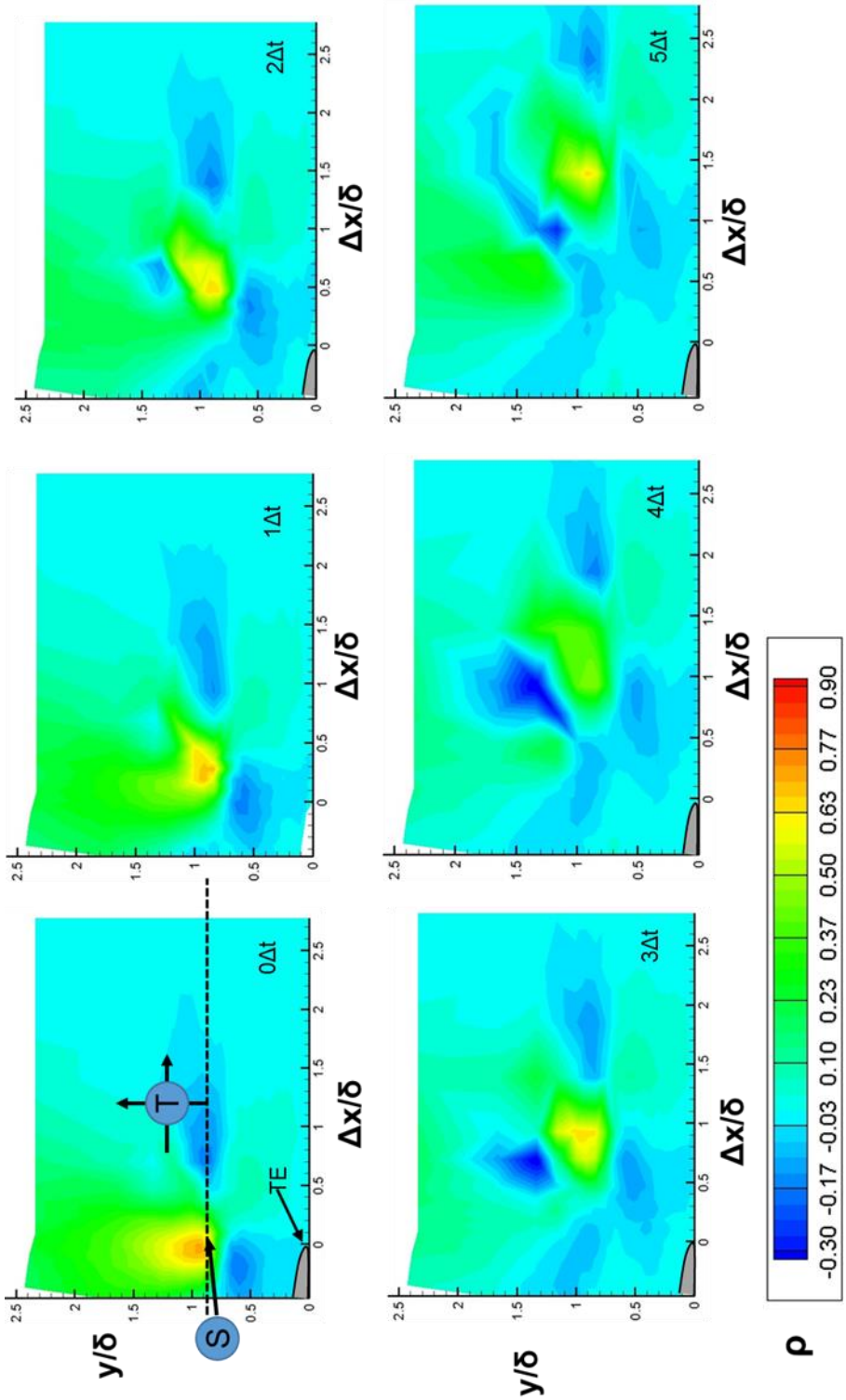

Figure a1. Streamwise correlation of structures in O_t. S is at x/C = 1, Δt = 0.00016 s, α = 0°

المنارة للاستشارات
www.manaraa.com

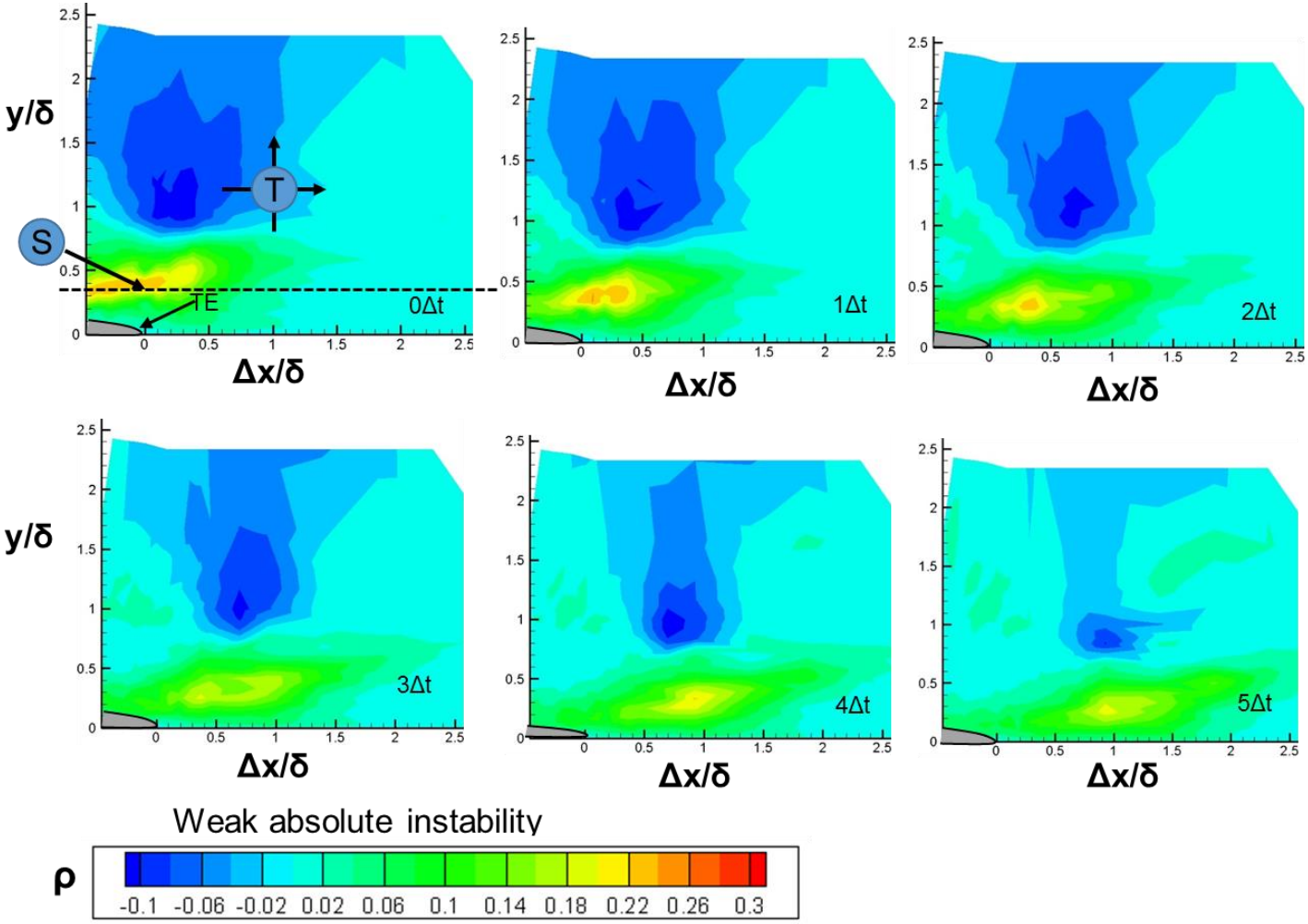

Figure a2. Streamwise correlation of structures in I_t. S is at x/C = 1, Δt = 0.00016 s, α = 0°

المنارة للاستشارات
www.manaraa.com

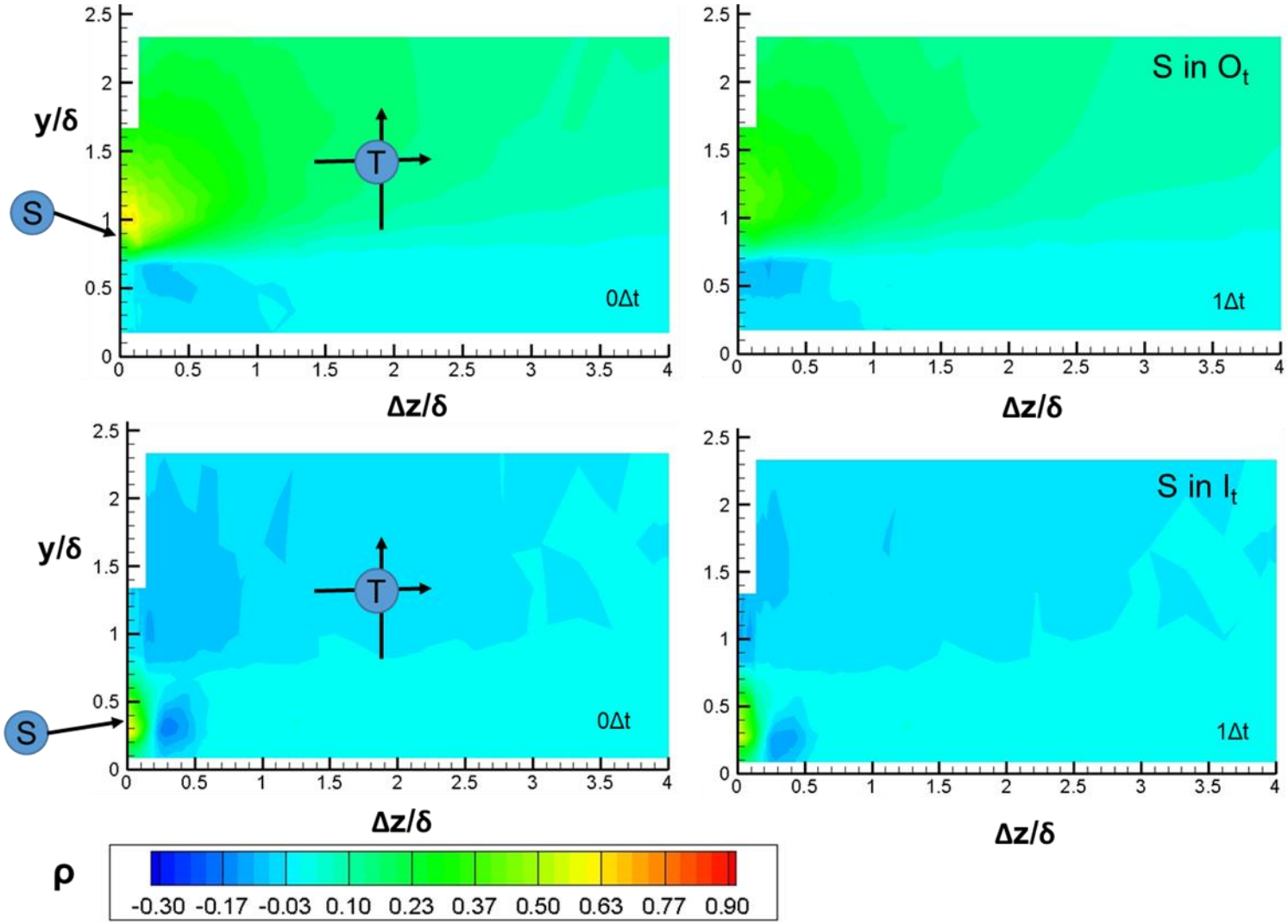

Figure a3. Spanwise correlation of structures in O_t and I_t. S is at x/C = 1, Δt = 0.00016 s, α = 0°

المنارة للاستشارات
www.manaraa.com

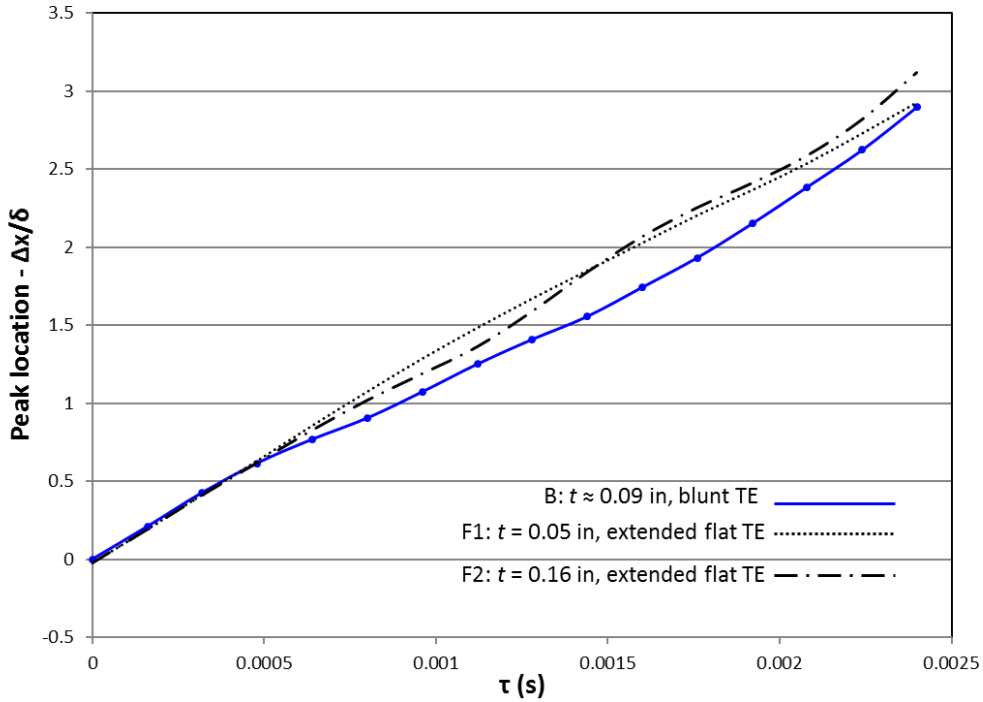

Figure a4. XT plot of structures in O_t at trailing edge of flat edged configurations

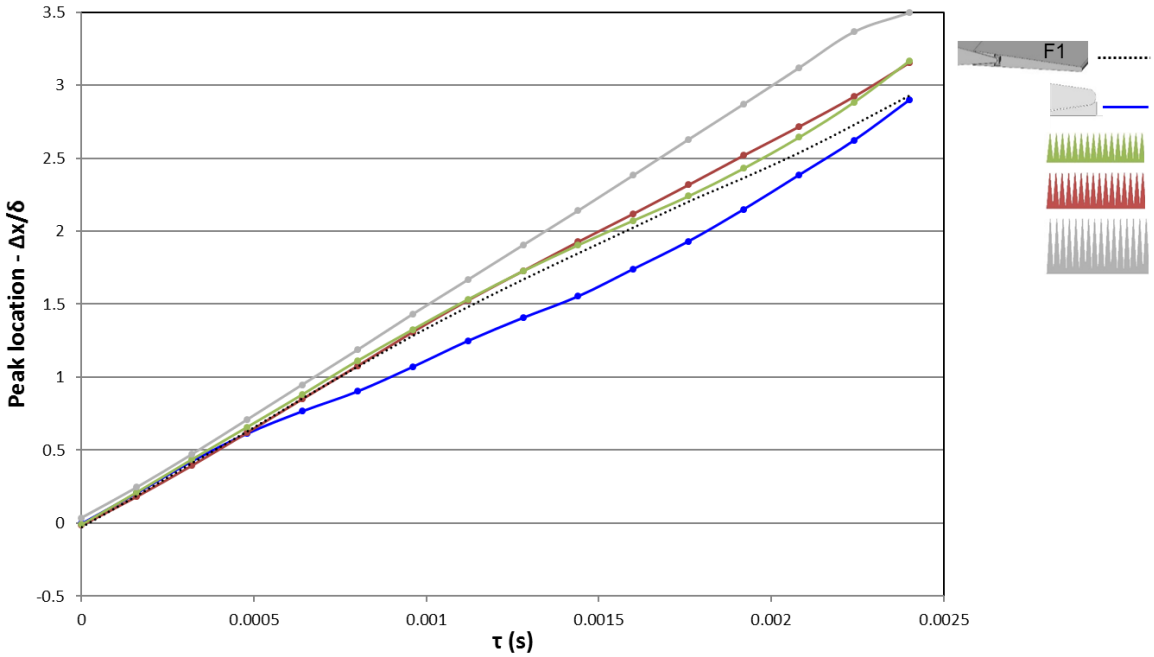

Figure a5. XT plot of structures in O_t at r_s-tip of serrations of different lengths

المنارة للاستشارات
www.manaraa.com

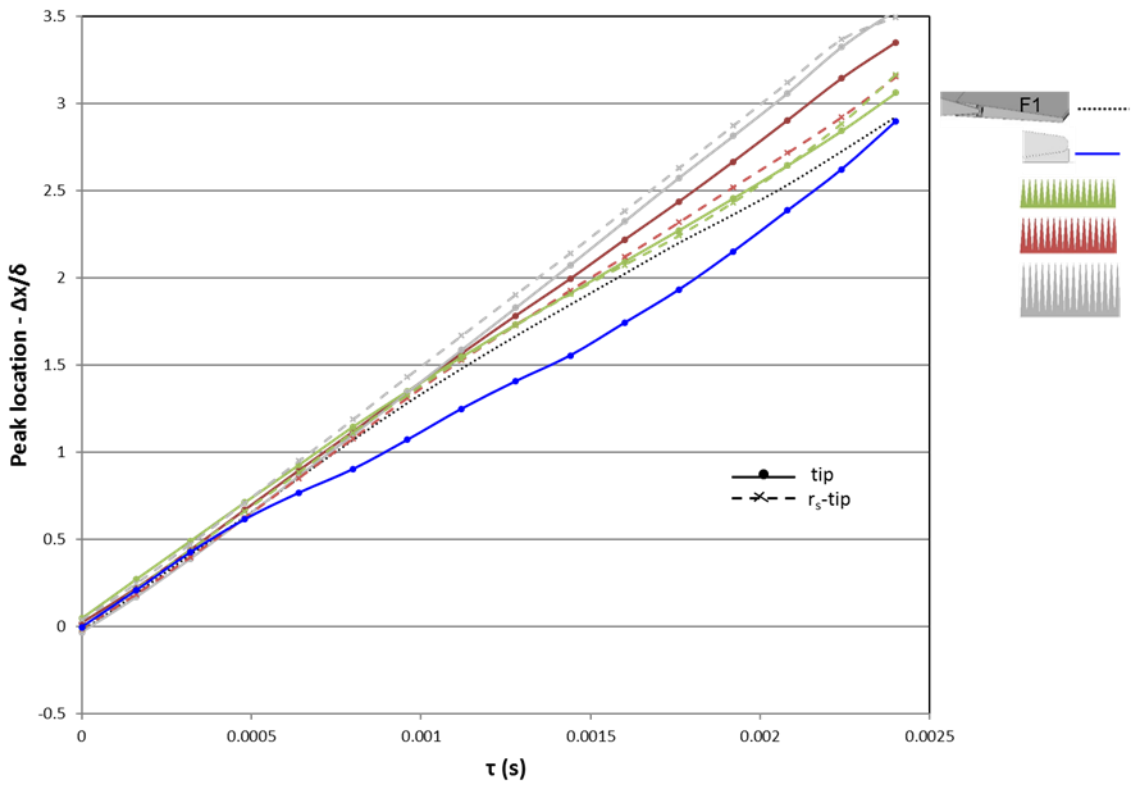

Figure a6. XT plot of structures in O_t at r_s-tip, tip of serrations of different lengths

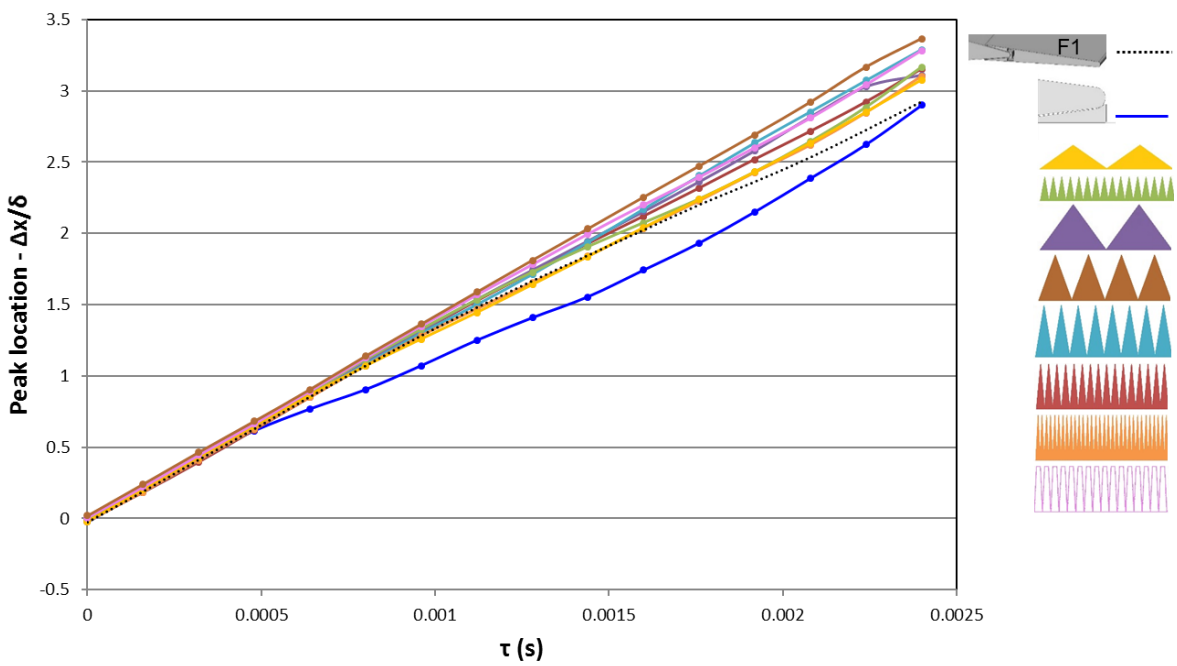

Figure a7. XT plot of structures in O_t at r_s-tip of serrations of different widths

المنارة للاستشارات
www.manaraa.com

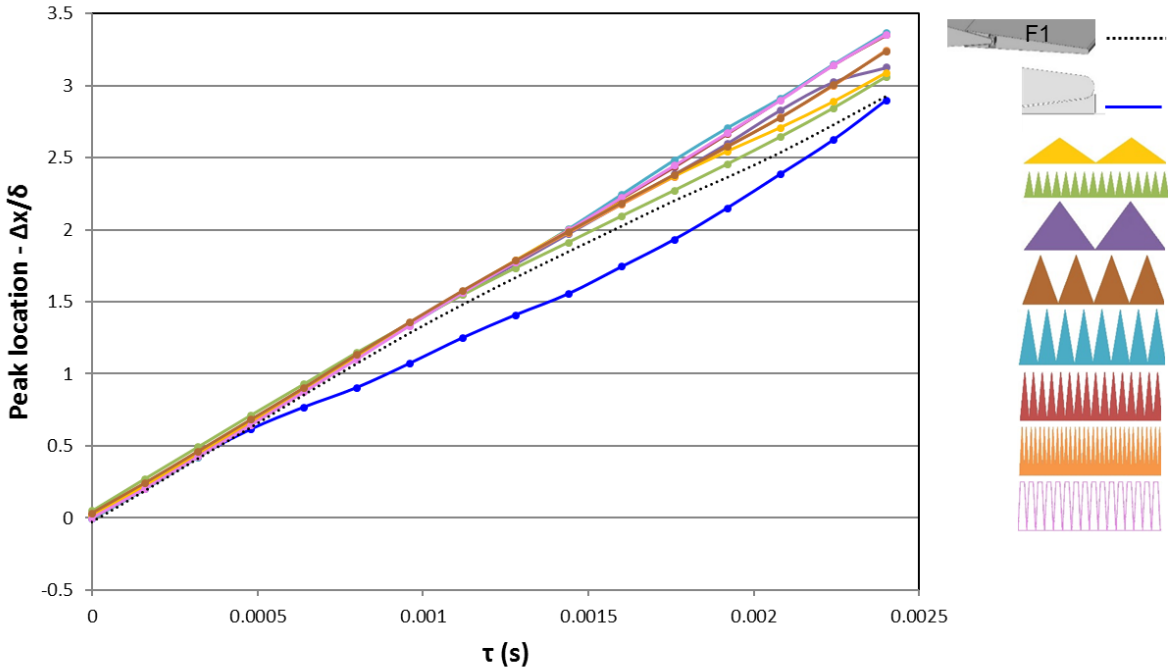

Figure a8. XT plot of structures in O_t at tip of serrations of different widths

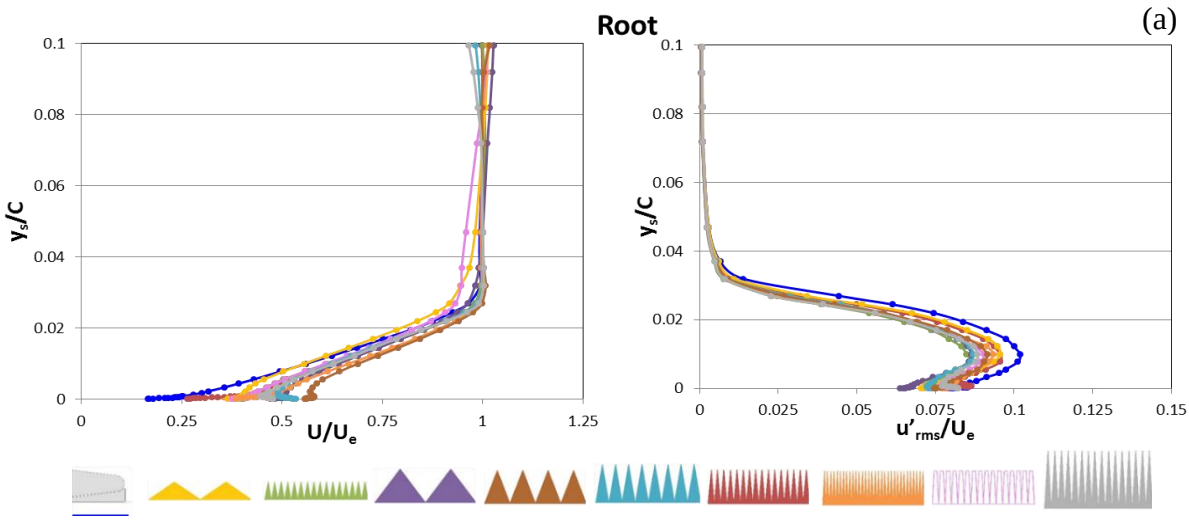

Figure a9. (a) Boundary layer profiles at root of all serrated TE configurations

المنارة للاستشارات
www.manaraa.com

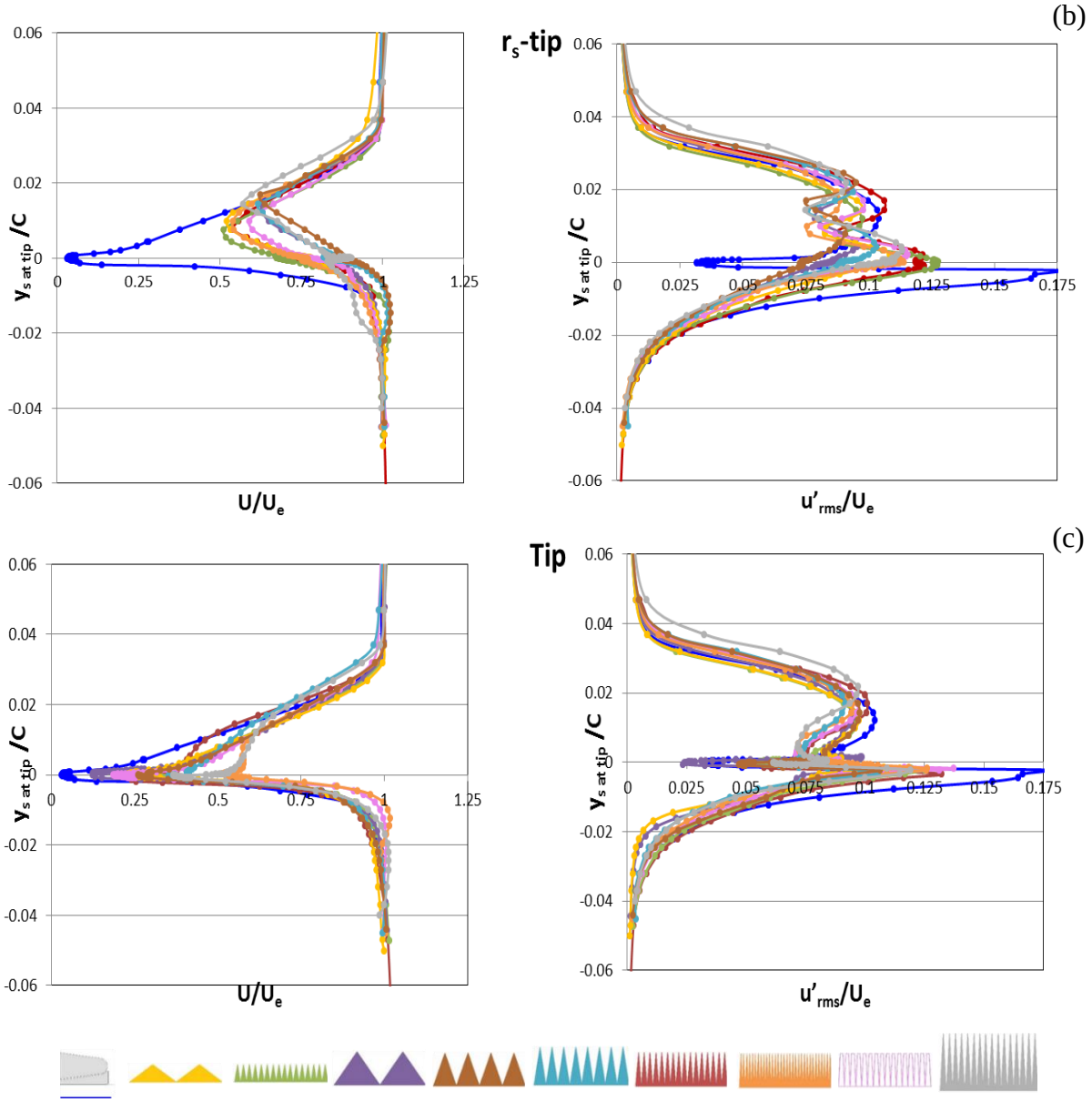

Figure a9. (b) Wake profiles at r_s-tip of all serrated TE configurations. (c) Wake profiles at tip of all serrated TE configurations

المنارة للاستشارات
www.manaraa.com

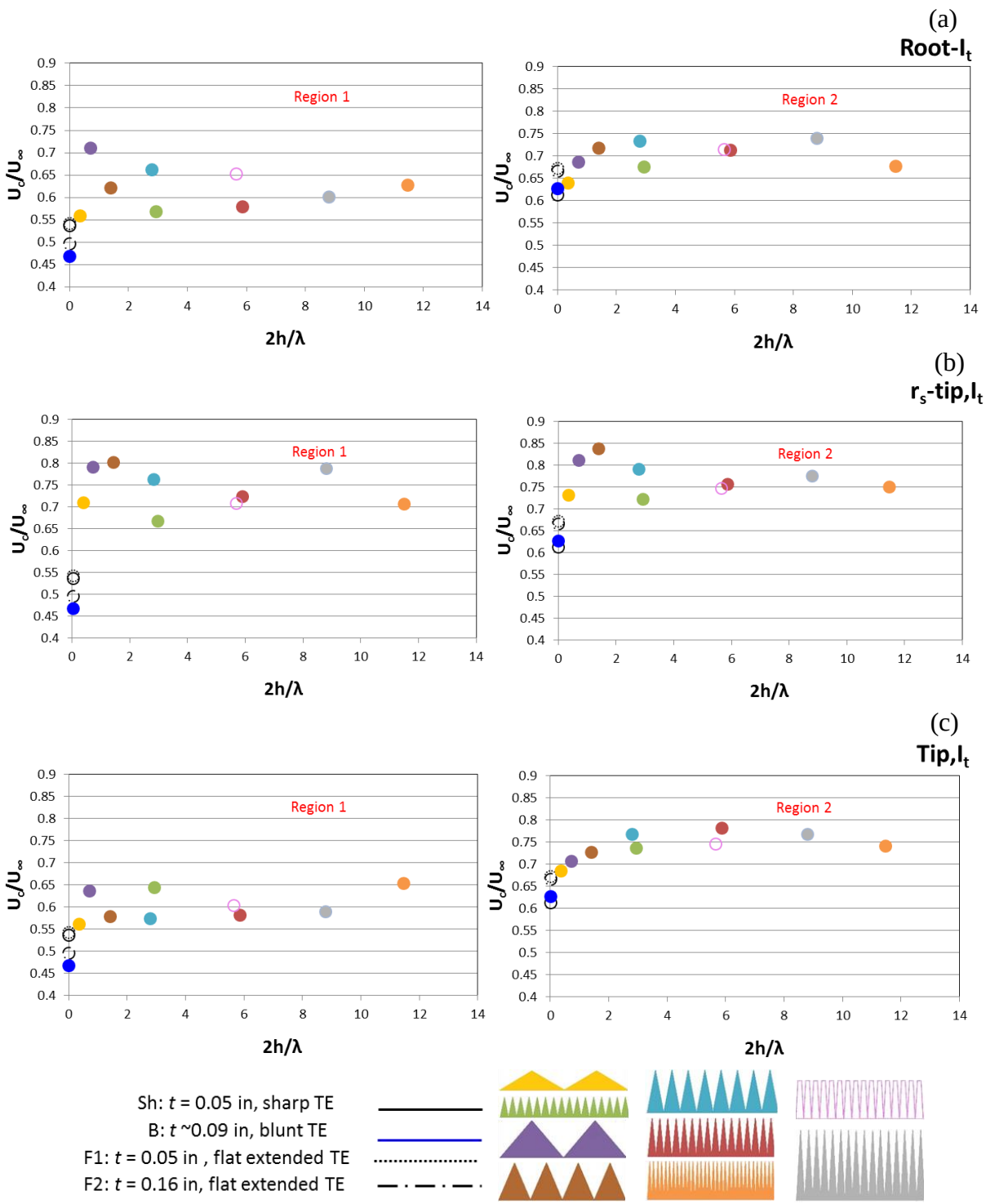

Figure a10. Convective speed of structures in I_t (region 1 and 2) near (a) root, (b) r_s-tip, (c) tip for all serrated TE configurations compared with flat TE configurations

المنارة للاستشارات
www.manaraa.com

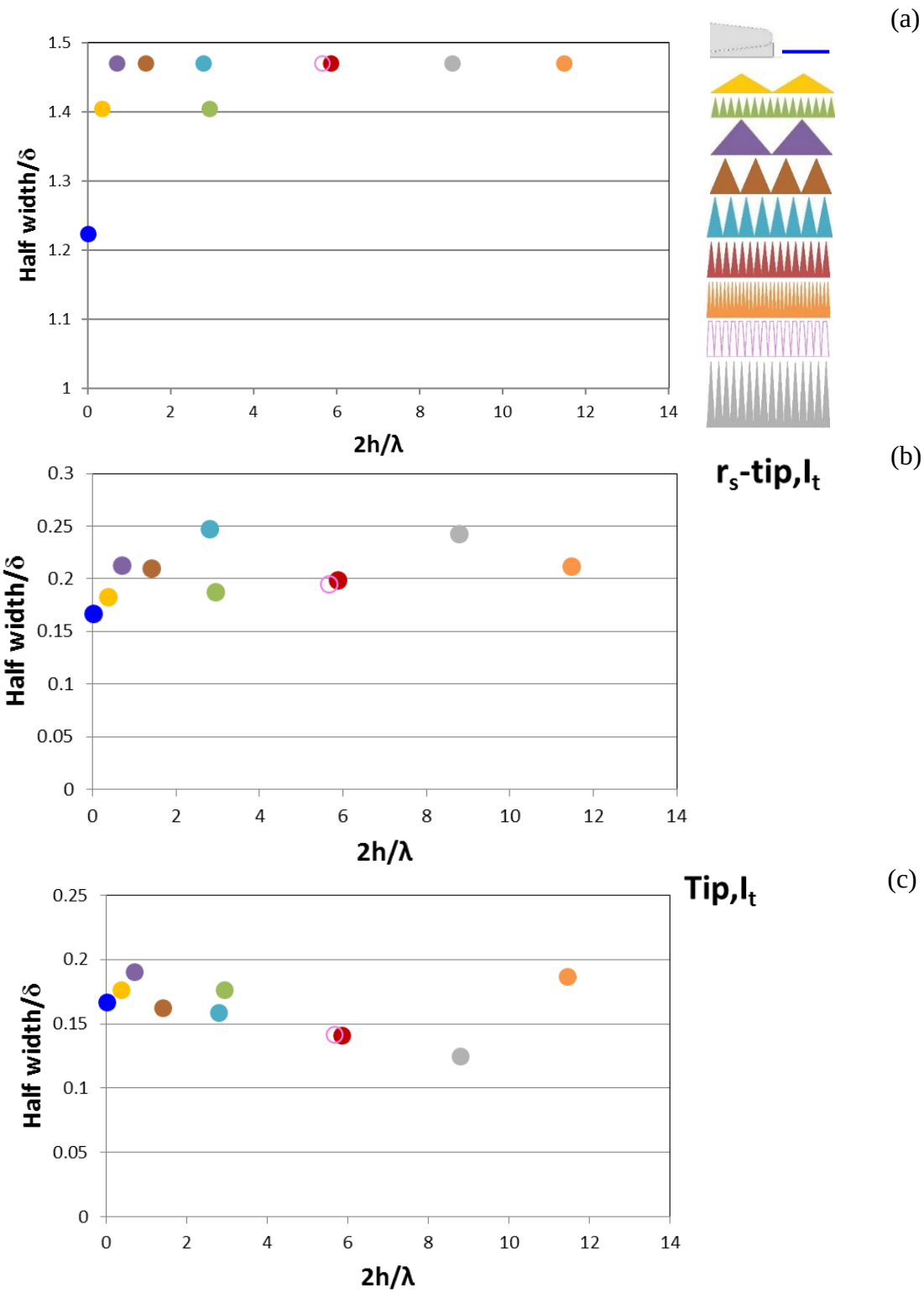

Figure a11. Half width of structures in (a) O_t near root, (b) I_t near r_s-tip, (c) I_t near tip for all serrated TE configurations

المنارة للاستشارات
www.manaraa.com

APPENDIX B

ERROR ANALYSIS

The total error or uncertainty of a measurement consists of the sum of the bias error and the precision error. The bias error results from lack of accuracy in measurement technique (example: drift of instruments used over time) and precision error is mainly from the instruments used. The precision limit of all instruments used were found to be negligible and therefore made no contribution to the overall uncertainty of a measured variable. It is assumed that experimental measurements are normally distributed and therefore the number of samples and ensemble averages used in the experiment were increased to reduce precision error associated with the variable. The main contribution to uncertainty is the bias error.

Unsteady velocity ***U*** is the primary variable used in this study. The significant source of error associated with this variable is the hot-wire resistance drift over time. This was minimized by re-calibrating the hot-wire periodically. The estimated uncertainty associated with mean velocity U is ± 5% with ± 1% at low speeds. The other contributors are the errors from static pressure measurements at low speeds and curve fitting of U to e. The uncertainty associated with velocity fluctuations u' is ± 1%. The results for U and u'_{rms} are given in terms of non-dimensionalized quantities (U/U_e and u'_{rms}/U_e) and therefore the error here due to hot-wire resistance drift decreases drastically. The cross-correlation coefficient ρ has very minimal bias error as the estimated value is non-dimensionalized by the u'_{rms} measured locally at a given location.

There is a scatter of ± 8% associated with values of convective speed (U_c/U_∞) and spanwise half width of flow structures estimated in I_t for various serrated trailing edges. This

المنارة للاستشارات
www.manaraa.com

is accounted to the exact value of the y-position used in I_t to estimate these variables. The y or y_s-positions used for I_t and O_t are ≈ 0.25δ and 0.9δ respectively near the root, r_s-tip and tip. We have already seen how the spanwise and associated streamwise characteristics of flow structures change drastically from I_t to O_t. We have also seen the shape and size of the wake/boundary layer change near different serrated trailing edges. Therefore, a minimal change in the chosen y-position of S in I_t is expected to affect the value of the results, even though the trend between serrations is maintained.

To minimize errors caused by the hot-wire itself to the flow feature of interest, the hot-wire probe holder was placed at an angle of 5º to 25º with respect to incoming flow U_∞. An accelerometer was used to monitor the hot-wire probe vibration. Steps were taken to minimize its impact on the flow and the unsteady velocity measured by the hot-wires as described in section 2.2.6. The length of the hot-wire sensor was small enough to resolve turbulence structures of interest.

The other errors associated with the measurements are the blockage errors due to the airfoil and the traverse system. Their contribution to cross-correlation data may be assumed to be a minimal. As lift and drag data were not used to formulate results in this study, these errors did not contribute to the final conclusions. Blockage due to the traverse was minimized by adding fairings. The traverse was kept at a minimum distance of 9 in at all times from the trailing edge or serration tip so as to minimize its effect on flow-structures nearby. It was located as close to the trailing edge as possible along the y-direction (~centered around the trailing edge) to minimize the effects of asymmetry caused by the traverse in the wake. The hot-wire and traverse system locations with respect to the trailing edge and serrations were

المنارة للاستشارات
www.manaraa.com

maintained a constant throughout the study so that any errors due to blockage on the results would be minimized.

The hot-wire positions were periodically zeroed at the trailing edge/tip to avoid cumulative error in position. They were also zeroed locally near the airfoil surface ($y_s = 0$) as needed. The x and z-position accuracies of T are limited to ≈ 0.015 in. The y-position accuracies of T and S are ≈ 0.005 in and ≈ 0.01 in respectively. The precision of the traverses however is very high and are specified in section 2.2.4. This reduces the relative error between any two points that follow the first location in a given sweep on the grid. A digital encoder attached to the traverses reduces the overall error associated with grid positions of the hot-wires.

المنارة للاستشارات
www.manaraa.com